AN INVESTIGATION TO DETECT DELAMINATION IN COMPOSITE LAMINATED PLATES UNDER DYNAMIC LOADING

A Thesis

presented to

the Faculty of California Polytechnic State University,

San Luis Obispo

In Partial Fulfillment

of the Requirements for the Degree

Master of Science in Aerospace Engineering

by

Jason Christopher Starnes

June 2015

COMMITTEE MEMBERSHIP

TITLE:	An Investigation to Detect Delamination in Composite Laminated Plates Under Dynamic Loading
AUTHOR:	Jason Christopher Starnes
DATE SUBMITTED:	June 2015
COMMITTEE CHAIR:	Faysal Kolkailah, Ph.D. P.E., Professor of Aerospace Engineering
COMMITTEE MEMBER:	Kurt Colvin, Ph.D., Professor of Industrial and Manufacturing Engineering
COMMITTEE MEMBER:	Dianne DeTurris, Ph.D., Professor of Aerospace Engineering
COMMITTEE MEMBER:	Eltahry Elghandour, Ph.D., Lecturer of Engineering

ABSTRACT

An Investigation to Detect Delamination in Composite Laminated Plates Under Dynamic Loading

Jason Christopher Starnes

In recent years composites have progressively been used for large-scale structures such as aircraft, ships, ground vehicles, and wind turbine blades. Traditional Nondestructive Evaluation (NDE) techniques have various limitations in assessing the performance of the large-scale composite structures. For instance, many techniques have the ability to measure either global or local properties but cannot measure both simultaneously. Nondestructive vibration detection techniques present a potential solution for evaluating both local and global large-scale composite structures, which are largely based on the fact that damage in a structure influences its dynamic characteristics such as modal parameters and Frequency Response Functions (FRF).

This study investigates locating delamination in composite laminate plates under dynamic loading utilizing accelerometers during dynamic response as an alternative structural health monitoring method in composite structures. The test specimens were manufactured using unidirectional carbon fiber/epoxy creating 11 cross-ply composite laminate plates with $[0,90,0,90]_s$ orientation. Delaminated regions were placed at one inch increments, horizontally along the specimen.

During testing, one side of each composite laminate plates were clamped using a custom fabricated fixture, cantilevered leaving the remaining edges free. An Unholtz-Dickie shake system excited the specimens. Dynamic response measurements using teardrop style piezoelectric accelerometers were taken along the surface face of each specimen, individually located along a 3 X 10 grid. Each response was compared collectively to examine any acceleration differences and damping between specimens. Finite element Modeling (FEM) ensured correlation of the flexural bending mode shapes between theoretical, analytical, and experimental. It was found that, the comparison between the results of the theoretical, Finite Element Analysis, and experimental data were in good agreement and delamination can be detected.

ACKNOWLEDGMENTS

People do not care how much you know until they know how much you care.

– Theodore Roosevelt

I want to especially thank Dr. Faysal Kolkaila for accepting me as a graduate student in such short of time and Dr. Eltahry Elghandour for his patience. To my fellow graduate students, thank you for assistance, collaboration, and support through this journey. Brad Schab specifically, thank you for all the help and time you extended me in aiding with writing MatLAB codes. Cody Thompson and his facilities student employees for masterfully manufacturing precision vibration fixtures and hosting little séances to get equipment running. And last but not least my committee for their assistance and expertise.

The author would like to thank his parents for their individual support and encouragement along this journey. And finally, his wife, Heather—the most important person behind the scenes—for her dedication in supporting this graduate student through the highs and lows of higher education and navigating to a successful thesis. I want to also mention my daughter, in hopes she too will discover a fine appreciation in understanding that higher education opens doors to places unknown. Hard work pays off, even in the midst of sacrifice.

TABLE OF CONTENTS

Page

LIST OF TABLES

LIST OF FIGURES

LIST OF EQUATIONS

Equation Page

CHAPTER 1

1. INTRODUCTION

The following sections provide a general overview of composite material, focusing on delamination, delamination detection, and structural health of such material. Structural dynamics is also reviewed and applications in composites in detecting delamination's is presented. A brief literature review of previous and current research efforts are also examined. Finally, the objective of the research is defined and the scope of the research is addressed.

1.1. Overview of Composite Laminate Materials

Composite materials consist of two or more constituent materials joined together that create laminated properties that differ from their individual material properties. Of these composites, the fibers are the principal load-carrying members, and the matrix or resin material keeps the fibers together; acts as a load-transfer medium between fibers; and protects the fibers from being exposed to the environment. Often fiber-reinforced composite materials for structural applications are often made in the form of a thin layer called lamina.[1]

The use of composite laminate materials in various types of engineering structures (e.g., aerospace, automotive, medical prosthetic devices, and electronic circuit boards) have become more important in the design and construction of manufactured engineering products; especially in aerospace. Aircraft parts made from composite laminate materials, such as fairings, spoilers, and flight controls, were developed during the 1960s for their weight

savings over aluminum parts.[2] There are new generations of large aircraft from The Boeing Company and Airbus to name a few that are designed with all composite fuselage and wing structures.

1.2. Types of Composite Materials

Since the advances in composite materials there are two types of composite materials; man-made and natural. Man-made components of composite materials consist of fibers, resins, curing stages, and core materials.

1.2.1. Fibers

All composite fibers generally start with spooled unidirectional continuous raw fibers. The individual fiber is called a filament and sometimes identified as a an individual glass fiber.[2] When filaments are bundled into something that represents a textile strand, they are commonly referred to as tows, yarn, or roving. Yarns are known to be twisted fiberglass stands, while Kevlar® yarn is not. Tows and roving do not have a twist, but are rather a single grouping of filament or fiber ends in a single direction consisting of 20-end or 60-end glass roving.[2] Roving products typically utilize mandrels for filament winding and then resin cure to final configuration.

Carbon fibers can also be found as a tape, fabric, or a weave (knitted or stitched) as shown in Figure 1-1. Tape fibers are usually known as unidirectional prepreg that is impregnated with resins, typically thermosets. Fabrics offer more flexibility than strait unidirectional tapes, thus are commonly used for more

complex shapes. Fabrics are found in raw (dry) or prepreg states with more options during the manufacturing stages. Fabrics are generally woven structural fabrics and are usually constructed with reinforcement tows, strands, or yarns interlocking, as if they were knitted like a sweater.

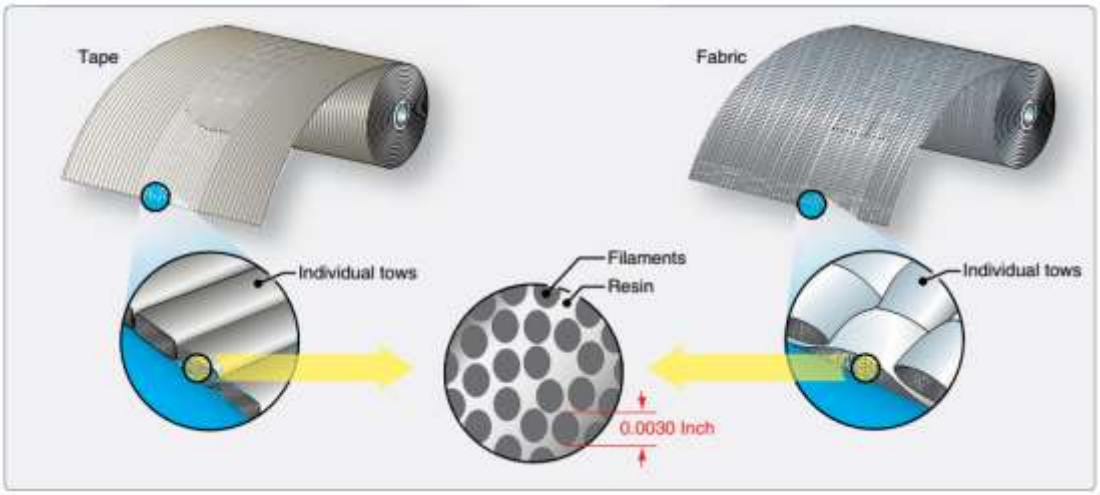

Figure 1-1 Types of tape and fabric products.[2]

Plain or satin weaves are more common fabric styles. Plain weave construction is manufactured from each fiber alternating over and then under each intersecting strand (tow, bundle, or yarn). The fiber strand count is equal in both warp (longitudinal) and fill (transverse) directions for most plain weave fabrics.

Satin weaves have less crimp and are easier to distort than a plain weave.[2] The fiber bundles traverse both in warp and fill directions changing over/under position less frequently than a plain weave and can be varied to increase or decrease fabric weight. Figure 1-2 shows different styles of fabrics.

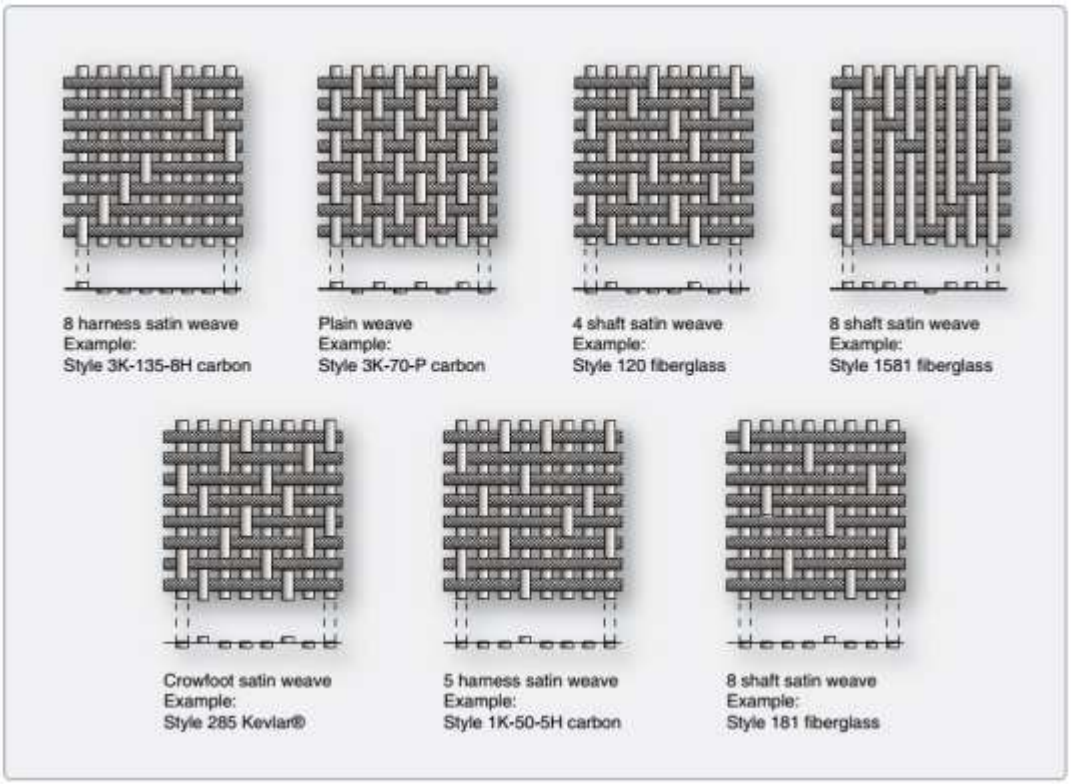

Figure 1-2 Different styles of fabric weave.[2]

Knitted or stitched (nonwoven) fabrics are very similar to unidirectional tape with similar mechanical advantages. The fiber placement of nonwoven fabrics is as if it was a plain or satin weave, but does not have the over/under turns of woven fabrics. The fibers are held in place by stitching with fine yarns or threads after preselected orientations of one or more layers of dry plies as shown in Figure 1-3.[2] Some common stitching yarns are polyester, aramid, or thermoplastics.

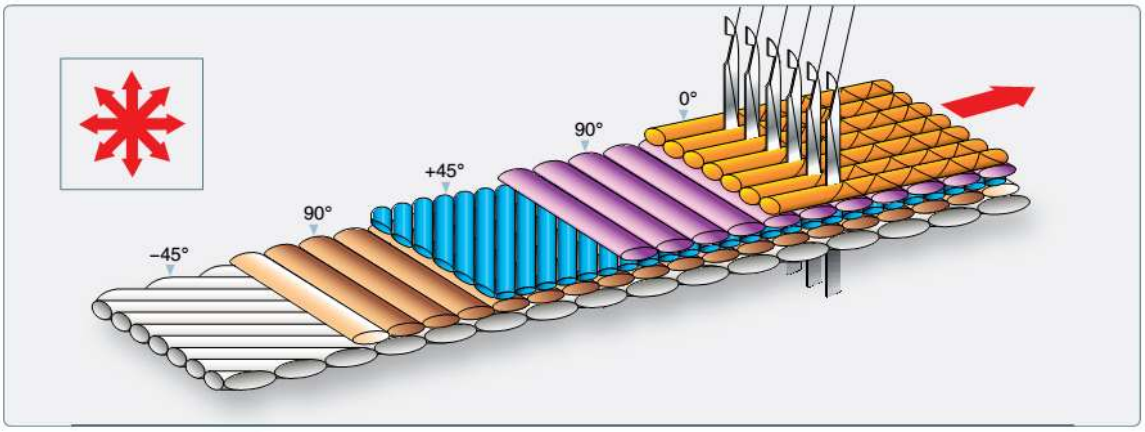

Figure 1-3 Unidirectional nonwoven fabric weave style.[2]

The common fiber materials are fiberglass, Kevlar®, carbon/graphite, ceramic, and boron. Each material has its advantages and disadvantages, as well as specific uses. For instance, fiberglass (E-, S-, and S2-glass) is used for fairings, radomes and wing tips and is advantages due to their low cost, chemical and galvanic corrosion resistance, and nonconductive electrical properties. Kevlar® or Aramid fibers are known for impact resistance, but are weak in compression, hard to drill and cut, and have high water absorption (hygroscopy). Service reports have indicated that some parts made from Kevlar® absorb up to 8 percent of their weight in water.[2] Carbon/graphite are typically used for structural applications due to their high strength and corrosion resistance, except when used in contact with metallic structures. Carbon/graphite is also disadvantageous due to high cost and low conductivity during lightning strikes, where coating and copper meshes are used for protection.

As for the more exotic materials, boron tape is used in repairs typically due to its corrosion resistance, high strength, and thermal expansion properties.

However, boron tape lacks in weight saving, flexibility during layups, is expensive, and hazardous to personnel. Ceramic fibers are used in high-temperature application and can reach to upwards of 2,200 degrees Fahrenheit.[2]

1.2.2. Resins

The resin or matrix materials are polymers that are used in prepreg materials, adhesives, bonding agents, and for the general manufacturing process. These polymers are generally referred to as thermosets or thermoplastics. Thermosets are the most diverse and widely used due to their cured characteristics. Thermoplastics may be softened by heat and can be dissolved in various organic solvents.

Thermosetting Plastics do not soften appreciably under heat but may char and blister. Once the plastic becomes hard, additional heat will not change it back into a liquid as it would with a thermoplastic. The most common thermosets used with composite materials are polyesters, vinyl ester, phenolic, epoxy, polyimides, polybenzimidazoles (PBI), ,and bismaleimides (BMI).

Thermoplastic materials can be softened repeatedly by an increase of temperature and hardened by a decrease in temperature. Thermoplastic materials are not used as a resin based material for most composite laminate structures. Some common thermoplastics used with composite materials are semicrystalline thermoplastics, Amorphous thermoplastics, and Polyether Ether Ketone (PEEK).

1.2.3. Curing Stages

Composite laminate materials use a chemical reaction to cure and are described as three curing stages (A, B, and C), which are defined in Table 1-1.

Table 1-1 Curing stages of resin.[4]

Stages	Description
A	The components of the resin (base material and hardener) have been mixed but the chemical reaction has not started. The resin is in the A stage during a wet layup procedure.
B	The components of the resin have been mixed and the chemical reaction has started. The material has thickened and is tacky. The resins of prepreg materials are in the B stage. To prevent further curing the resin is placed in a freezer at 0 °F. In the frozen state, the resin of the prepreg material stays in the B stage. The curing starts when the material is removed from the freezer and warmed again.
C	The resin is fully cured. Some resins cure at room temperature and others need an elevated temperature cure cycle to fully cure.

1.2.4. Core Materials

Though core materials are not used in the research presented, it should be noted as one of the major components in composite manufacturing. The main premise is that core material can make materials stiffer and stronger without cost of weight. A typical example of the use of core materials advantages are shown in Figure 1-4.

	Solid Material	Core Thickness t	Core Thickness 3t
	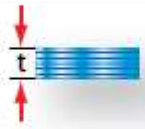	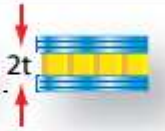	
Thickness	1.0	7.0	37.0
Flexural Strength	1.0	3.5	9.2
Weight	1.0	1.03	1.06

Figure 1-4 Strength and stiffness of honeycomb sandwich material compared to solid material.[2] The values for thickness and flexural strength rows are multipliers if the overall thickness is double and quadrupled. The weight row shows the added weight when the thickness is doubled and quadrupled. The values are unitless.

Core materials are generally honeycomb, foam, and balsa wood. Balsa wood has a density of less than one-half of the density of conventional wood products and has a considerably higher density than the other types of structural cores.[2]

Most honeycombs are anisotropic; that is, properties are directional. The most common core material used for aircraft honeycomb structures is aramid paper (Nomex® or Korex®).[2] Other Honeycomb materials are fiberglass, kraft paper, thermoplastics, aluminum, steel, special metals such as titanium, aramid paper, carbon, and ceramic; and each have their own special use.

Foams are typically heavier and not as strong as honeycomb. Foams are usually used in homebuilt and lighter aircraft to give strength in areas that need structural stability. Common foams are polystyrene, phenolic, polyurethane, polypropylene, polyvinyl chloride (PVC), and polymethacrylimide (Rohacell).

1.3. Advantages and Disadvantages of Composite Materials

Composite material systems result in a performance unattainable by individual isotropic materials. They offer the advantage of a flexible design that can be tailored to any design requirement. The primary advantages of composite laminate materials are their high strength, low weight, stiff structures, thermal expansion, and decent corrosion resistance. Figure 1-5 graphically shows some of the material advantages of composite materials compared to common isotropic materials.

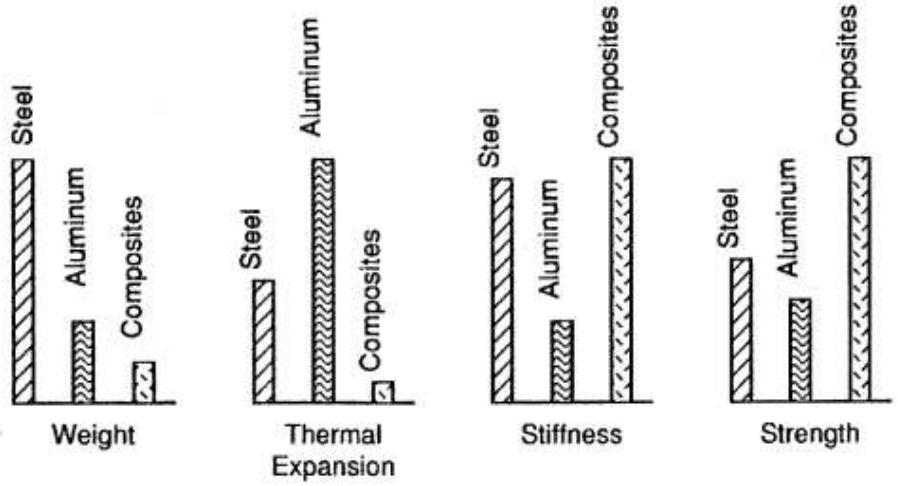

Figure 1-5 Relating different characteristics of steel, aluminum and composite materials.[3]

With great structural integrity there comes a great cost to composite materials. Machining with special tools, the manufacturing process of laying up through numerous techniques, and storage of the material can become costly for any company. Along with manufacturing, repairs to composite materials does not come as easy as repairing metallic, homogeneous materials. Repairs costs

quickly increase based on labor costs, material, and cure and patch times. There are also environmental strains on such materials, like water for instance. Water, fluids, or dirt can become trapped in cavities in built up areas created by honeycomb structures and in unknown voids in the material causing rapid structural degradation.

1.4. Composite Structures

When designing and manufacturing advanced composite structures, it is essential to select optimal ply orientation to provide efficient structural stiffness and weight. The part might require 0° plies to react to axial loads, ±45° (common) plies to react to shear load, and 90° plies to react to side loads.[4] A good example of critical ply orientation is during repair, ply orientation and ply sequence is key and if it does not mirror the manufactured layup sequence the product could be deemed inoperable.

For directional fibers, unidirectional materials run in one direction, such as pre-impregnated tapes. They hold their strength and stiffness in only the direction of the fibers. Bidirectional materials or plain weave fabric run in two directions, typically 90° apart. Bidirectional plies have strength in both directions, but not necessarily the same strength. The plies of a quasi-isotropic layup are stacked in a 0°, –45°, 45°, and 90° sequence or in a 0°, –60°, and 60° sequence.[2] Quasi-isotropic plies simulate properties of an isotropic materials such as aluminum or titanium. Figure 1-6 illustrates unidirectional, bidirectional and quasi-isotropic lay-ups.

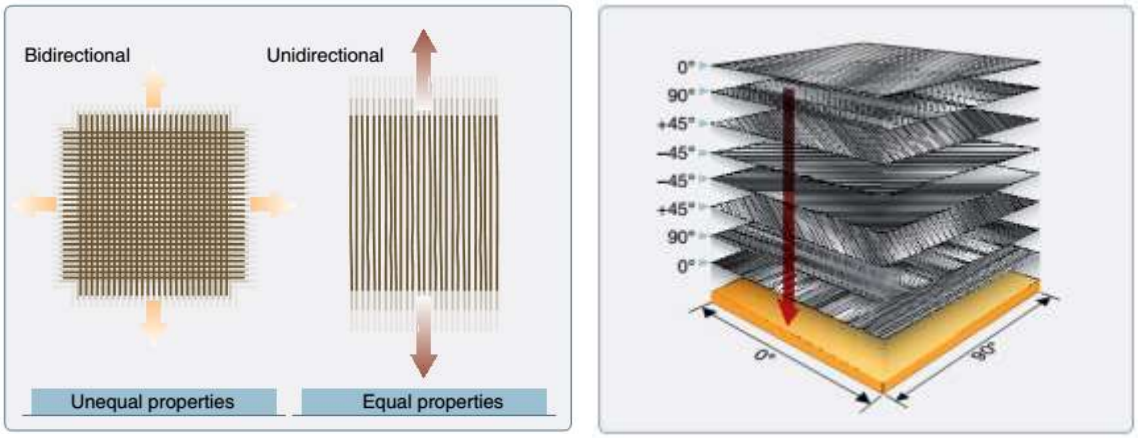

Figure 1-6 Unidirectional, bidirectional and quasi-isotropic (far right image) lay-up examples.[2]

With the understanding of how advanced composite materials depend directly to ply orientation, it should easily be understood that the strength design requirements are a function of the applied load direction. When determining a structures shape and design use, the type of composite layup can affect the operational use of end products.

Composite materials can also improve successful products, such as rocket motors (Atlas V) allowing rocket to lift heavier payloads, expand efficiently, and overall have a higher performance. Another example is the carbon-fiber body BLU-129 small diameter bomb, which usually has an iron body. The munitions carbon-fiber body disintegrates rather than fragments (like iron) reducing the risk of collateral damage.[10]

1.5. Structural Dynamic Response

Typically, dynamic responses are represented by Frequency Response Functions (FRF), which are measured from an excitation force (input) and acceleration responses (output) of the structure. A basic method to obtain natural or resonant frequencies (synonymous in this case) is to choose the peak frequencies values of a FRF. Natural frequencies are related to the global properties of a structure, since they have the same values regardless of grid point. Local properties of a structure are related to Mode Shape (MS - no load or force on structure dependent) and Operating Deflection Shapes (ODS – load or force on structure dependent) and are dependent on the test location. ODS can have units of amplitude, displacement, velocity, or acceleration and is used in conjunction with the transient response. Mode shapes are unitless, but can be represented by Hertz, echoing the natural frequency values. Acquiring modal data such as natural frequencies and MS requires modal analysis using the data near the resonant points in FRF; as used in this study.

Generally, it is sufficient enough to consider only the first 3 or 4 modes of most geometries, since the higher modes are quickly dampen out. The first natural frequency is the most critical and can impose the most immediate damage to most equipment faster than that of modes 2 or 3. Modes 2 and 3 refer to the fatigue and life cycles that something may see through operation.

The ‘mode shapes’ represent the different responses of a system, which show the deformed shapes of the system. The fundamental (or first mode)

frequency always corresponds to the mode shape with the lowest frequency.[9] Mode shapes for modes 2 and 3 have very general sinusoidal shapes. General bending mode shapes can be found in Figure 1-7.

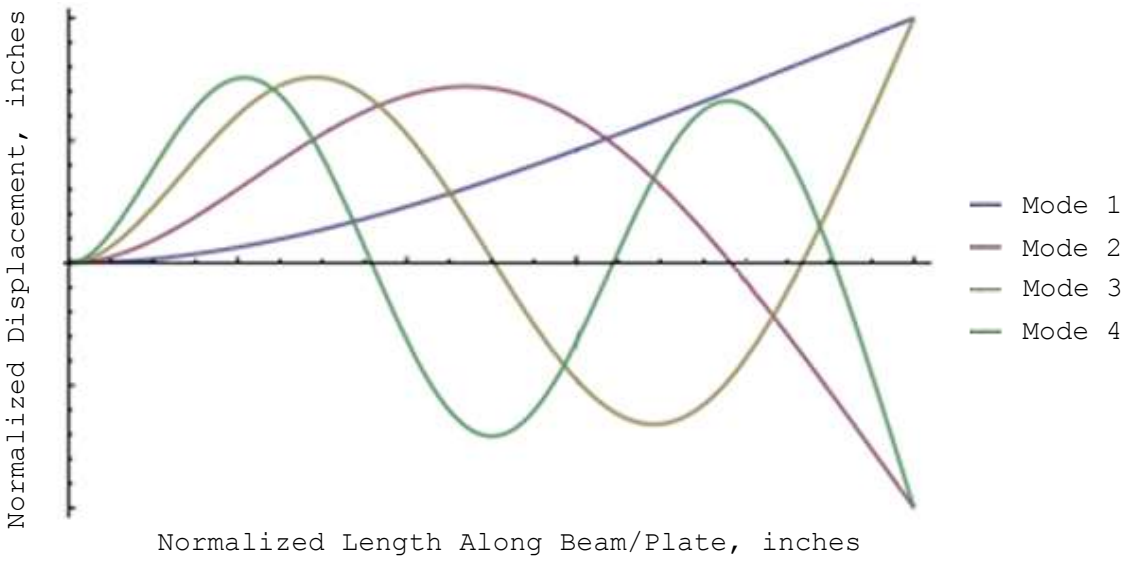

Figure 1-7 General bending mode shapes for each natural frequency.[40]

Frequency of a system, or of an applied force, is a measure of the rate at which the system vibrates.[9] The motion is generally sinusoidal in nature and has a displacement, velocity or acceleration related to the amplitude. During shaker table excitations, the amplitude is usually the peak acceleration seen by the response.

Damping refers to the loss of mechanical energy in a system. As energy is taken out of the system through the damping, the amplitude of the response reduces until the motion eventually ceases.[9] Dampening can also be represented as a widening the response peak. The amount of damping will

determine the duration of the response, thus if the test article is stiff, there will be higher resonance and faster dampening.

1.6. Overview of Manufacturing Defects in Composite Laminate Material

Manufacturing defects can be large enough to be visible with the naked eye, to as small as an individual fiber. To determine the impact a defect may have on a structure, the understanding of the structural use and the fiber direction must be considered. Thus, not all defects must be repaired depending on their structural use and load bearing requirements in the design.

Most manufacturing defects include delamination, resin starved or resin rich areas, blisters, air bubbles, wrinkles, voids, or even thermal decomposition. Manufacturing damage includes anomalies, such as porosity, microcracking, and delamination's resulting from processing discrepancies[2] and relates directly to manufacturing defects. The source of manufacturing defects range from improper cure and processing cycles to tool drops and contamination.

This research focuses mainly on delamination, which is formed on the layers in the laminate interfaces. Under certain conditions, delamination's or debonds can grow when subjected to repeated loading (cyclic) and can cause catastrophic failure when the laminate is loaded in compression.[4]

1.6.1. Causes of Delamination

Delamination's may form from matrix cracks that grow into the interlaminar layer or from low-energy impact.[2] During the manufacturing process, delaminated

laminates can begin to form from dust between layers, left or forgotten bagging and backing material to prepreg materials, forgotten tools in between ply's, and resin starved areas.

Other considerations for causes of delamination can be found during post process manufacturing. The use of drill motors with a hydraulic dash pod or other type of feed control are preferred because they restrict the surging of the drill as it exits the composite materials; thus reduces breakout damage and delaminations.[2] Likewise, composite materials are conductive, thus using an electric drill may cause short circuits in equipment.[2] Drill bits and other process tools with carbide or diamond coatings are ideal to use because bits that use standard high-speed steel can cause delamination's.

Another critical delamination area is the use of proper fastening systems. Bolts with relatively small footprints or the use of atypical-composite fasteners can cause load paths through the composite laminate skins leading to stress concentrations that develop delamination's over time. Delamination can occur in-service if the laminates are overloaded, subjected to extreme heat, or fatigue over time.

1.6.2. Delamination Detection Methods

Visual inspections cannot find internal flaws in composite laminates, as where most delamination's occur. However, visual inspection is the primary inspection method for all composite laminate materials, except when known, internal damage is relevant. Thus, nondestructive inspection equipment and advanced

inspection techniques are typically used to detect defects. The most common inspection methods to detect delamination are expressed in Table 1-2.

Table 1-2 Comparison of NDI test equipment.[2]

Method of Inspection	Type of Defect							
	Disbond	Delamination	Dent	Crack	Hole	Water Ingestion	Overheat and Burns	Lightning Strike
Visual	X (1)	X (1)	X	X	X		X	X
X-Ray	X (1)	X (1)		X (1)		X		
Ultrasonic TTU	X	X						
Ultrasonic pulse echo		X				X		
Ultrasonic bondtester	X	X						
Tap test	X (2)	X (2)						
Infrared thermography	X (3)	X (3)				X		
Dye penetrant				X (4)				
Eddy current				X (4)				
Shearography	X (3)	X (3)						

Notes: (1) For defects that open to the surface
(2) For thin structure (3 plies or less)
(3) The procedures for this type of inspection are being developed
(4) This procedure is not recommended

1.6.2.1. Audible Sonic Testing (Coin Tapping)

Sometimes referred to as audio, sonic, or coin tap, this technique makes use of frequencies in the audible range (10 Hz to 20 Hz).[2] Coin Tapping is the most common technique used to detect delamination and is a surprisingly accurate method in the hands of experienced personnel.

The method is accomplished by tapping the inspection area with a solid round disk or lightweight hammer-like device and listening to the response of the structure to the hammer, as seen in Figure 1-8.[2] A clear, sharp, ringing sound indicates a well-bonded solid structure, while a dull or thud-like sound indicates a discrepant area. This method is not reliable for structures with more

than four plies.[4] There is an automated tap test, which is more reliable. The automated tap test records a signal from an unflawed area to set its calibration and any deviation from this indicates a flawed area, comparing the acoustic signals.

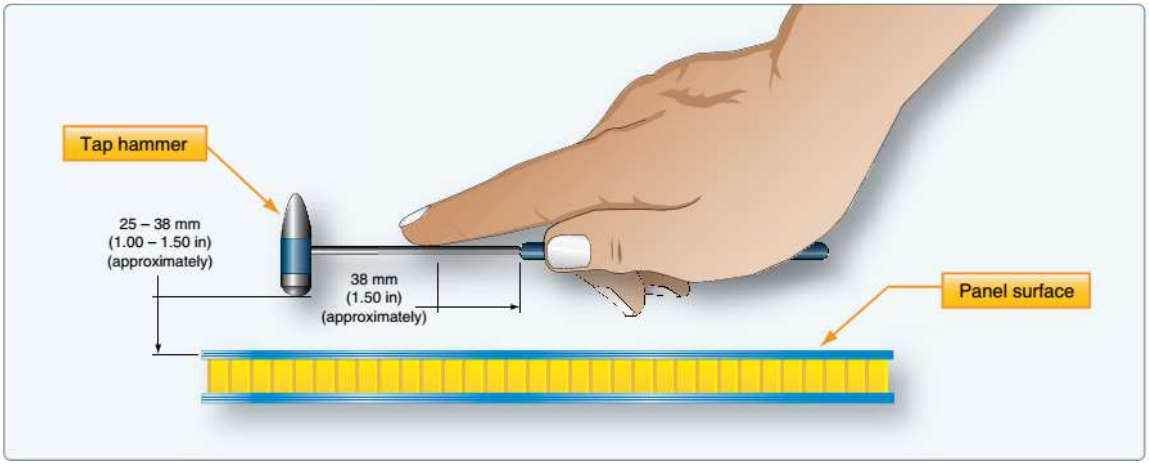

Figure 1-8 Tap test with tap hammer.[2]

1.6.2.2. Ultrasonic Inspection

Ultrasonic inspection has proven to be a very useful tool for the detection of internal delamination's, voids, or inconsistencies. A high frequency (usually several MHz) sound wave is introduced into the part, an ultrasonic wave strikes an interrupting object, the wave or energy is either absorbed or reflected back to the surface. Disrupted or diminished sonic energy is picked up by a receiving transducer and converted into a display on an oscilloscope or a chart recorder. Examples of ultrasonic testing methods can be found in Figure 1-9.

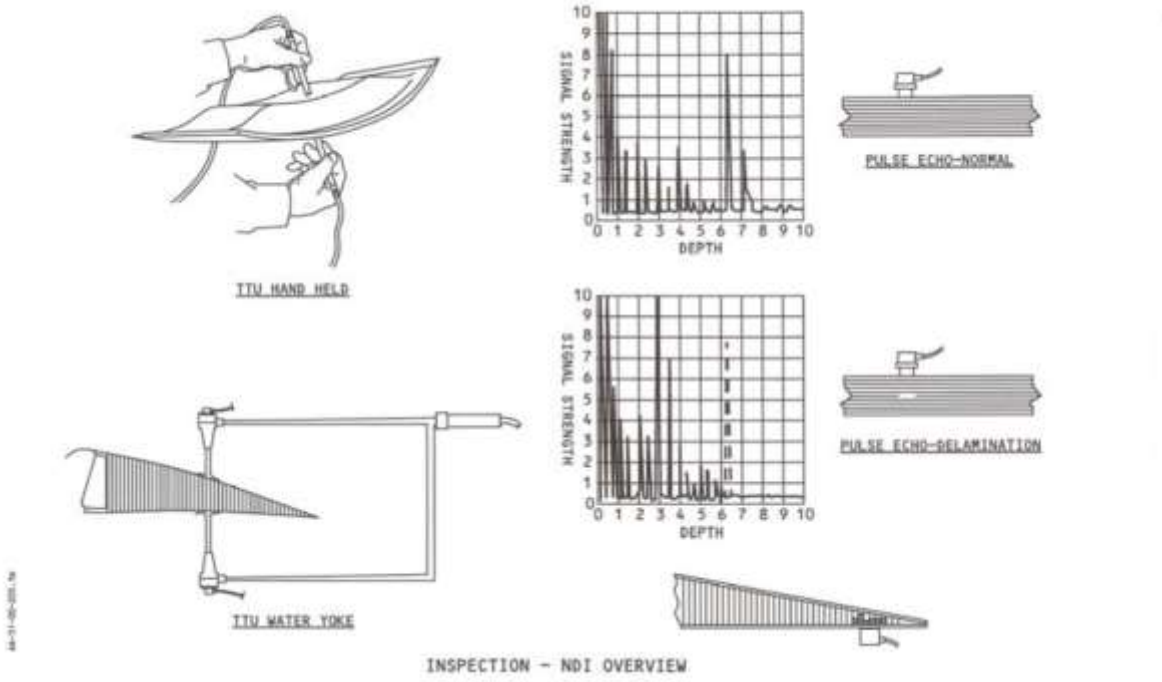

Figure 1-9 Ultrasonic testing methods.[4]

1.6.2.3. Radiography

This inspection method is accomplished by X-raying the part or assembly that is under test while recording the absorption of the rays onto a film sensitive to X-rays. Internal anomalies such as delamination's in the corners, crushed core, blown core, water in core cells, voids in foam adhesive joints, and relative position of internal details can be detected. Problems with this method is it is hard for large portions of aircraft to test, safety to personal is an fundamental concern, and lead shielding is expensive. Typical radiography tools used are NDT x-ray radiography tubes that are portable. They are generally employed by aiming the x-ray portion at the defected area, where the damaged area is

projected on to an external monitor. An example of radiography tools are shown in Figure 1-10.

Figure 1-10 Portable NDT x-ray radiography tubes.[43]

1.6.2.4. Infrared Thermography and Shearography

Though these are still in development they have been used industry. Both methods visually emulate photoelastic testing, which renders single or multiple colored topography on the surface of the test article. Shearography uses lasers to project a fringe pattern on a structure. A change in the pattern demonstrates there is a defect in the test article. This is a typical procedure for surfaces and is not good for internal nondestructive testing.

Infrared thermography uses heat mapped on the skin of an aircraft or production part through external thermal excitation. The disturbance in the material is read using an infrared detection device that visually shows thermal discoloration around the defected area. Shearography and thermography test methods are shown in Figure 1-11.

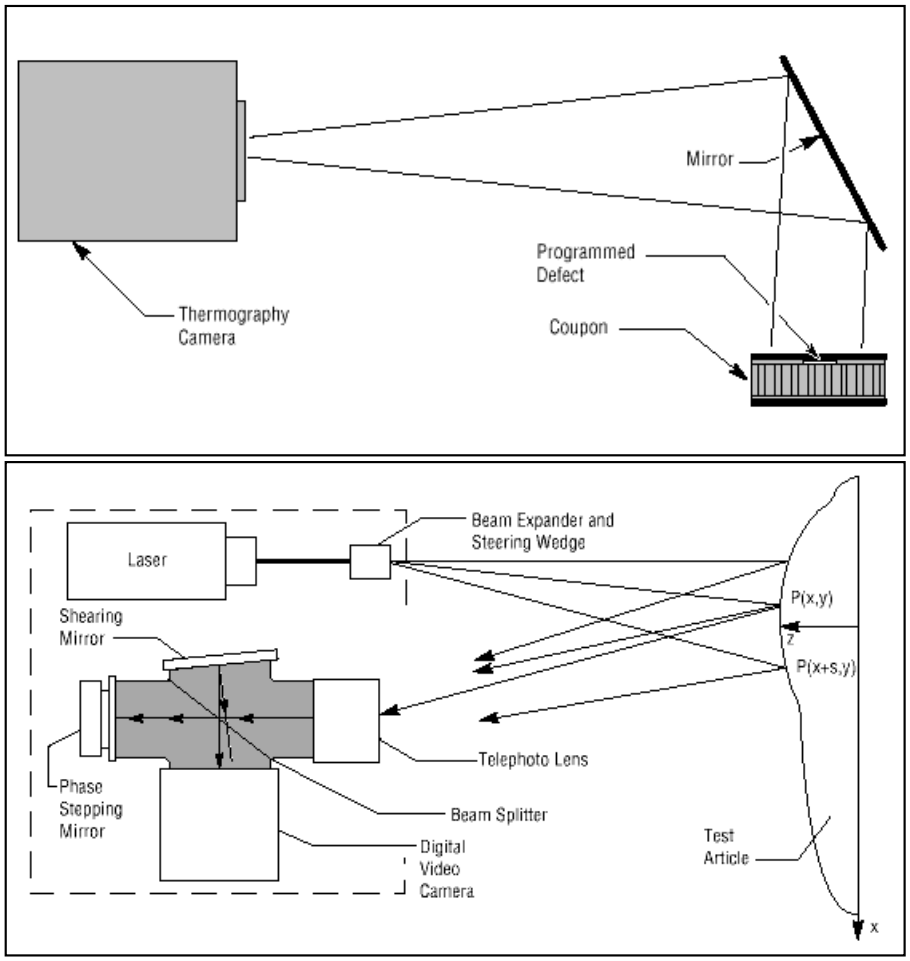

Figure 1-11 TOP, example of Thermography. BOTTOM, example of Shearography.[42]

1.6.3. The Impact Delamination has on Manufacturing

In any manufacturing setting there are quality control measures and process procedures that dictate what is a good or bad production part. Delamination can contribute to costly designs, increasing lead times, failures in compliance, cracks, fatigue, and many other attributes. Causes come traditionally through machine tolerance, improper tools used, tool drop, operator procession, and various others. The improvements in manufacturing has been extensive with newer layup technologies, better drill bits and tools for post processing, tool drop safety, etcetera. The repair of these advanced composite laminate materials requires an in-depth knowledge of composite structures, materials, and tooling.[2]

Things that cause delamination and debonds to be deemed critical may depend on dimensions of delamination; number of delamination's at given locations; location-in the thickness of laminate, free edges, stress concentrations; or load behavior based on tension/compression not being analyzed correctly or laminate ply's not efficiently laid. These items can cost manufacturers significant amounts of money and delays in deadlines. The loss of contracts could be at stake as well.

1.7. Previous Nondestructive Testing and Detection Studies of Composite Laminate Delamination

The number of journals and research papers published in the last two decades attest to the fact that there has been a major effort to develop composite material

systems, and to analyze and design structural components made from composite materials.[1] For finding delamination through free vibration, researchers first concentrated on free modes and followed with constrained modes. To focus on the later, constrained modes were investigated using biomaterial and organic fibers. One of the pioneers of this researcher was Ramkumar [19]. In 1979, he insightfully proposed a model of four Timoshenko beams that were connected at the delaminated edges to form a full composite beam with one complete horizontal width delamination. The results obtained from this research were lower than experimental measurements.

In 1982, Wang [20] advanced Ramkumar analytical solution by introducing coupling between flexural and axial vibration of delaminated segments of the material. Free mode was first examined at this point too. Using an isotropic beam with splits and classical Euler-Bernoulli beam model theory, Wang's natural frequency calculations were in line with experimental results. Wang proved that the coupling effect was the reason for discrepancies between calculated and experimental data that Ramkumar neglected. In the same year, similarly Mujumdar and Suryanarayan [22] used Euler-Bernoulli theory. Similar to Wang, this study utilized four joined isotropic beams, while assuming coupling between bending and axial vibration. Wang analyzed "free mode vibrations" and Mujumdar and Suryanarayan focused on "constrained" modes.

Yin et al. [23] and Chen et al. [24] in 1992 researched vibrations of a delaminated beam with respect to buckling using classical and shear deformable beam theory. They both assumed delamination was of closed form during

motion. In the same year, Shen et al. [25] continued the research, which whom developed an analytical model. The model predicts vibration frequencies and modes of delaminated beams.

In 1994 Han et al. [26] demonstrated the use of finite element models accurately capturing the Timoshenko beam theory. They presented their results though finite element analysis that suitably agreed with other previous solutions. Further, Shu et al. [27] studied constrained mode models for biomaterial beams in 1995 showing promising results.

Lestari et al. [30] examined multiple delamination's of a single beam using classic beam theory in 1999. Their study simulated the open and closed behavior between delaminated layers. In 2001, Krawczuk [29] explored natural frequencies of cantilever beams containing delamination and incorporated formulation methods based on modeled beams and columns.

Della et al. [28, 31, 32, 33, 34 and 35] have scrutinized both "free" and "constrained" modes of delaminated multilayer beams since 1995. They mathematically verified that the slenderness ratio has an impact on the vibration behavior of the beam. The introduction of normalized axial and bending stiffness in their study gave a better indication of vibration behavior of delaminated beams. The coupling between transverse and longitudinal vibration in beams were formulated and investigated, as well. Y. Zou et al. [36] focused on the model-based delamination detection methods using finite elements formulation analysis for composite structures byway of vibrations—progressing research further.

Advancements in simulation software and Finite Element Modeling of defective structures has become more common over the past few years and has been more predominant in research studies. As beams were utilized, plates expanded similarly with common tests. Ousset et al. [16] analyzed the delaminated multi-layer composite plate based on the Mindlin—Reissner plate model. Zak et al. [17] and Ousset et al. developed models of finite elements for beams and plates with boundary delamination. Yoon et al. [18] used MEMS accelerometers to detect delamination by exciting plates with a modal hammer. Their findings comparatively were suggested to be sound.

The present study is similar to Yoon et al. utilizing a grid technique. However, the accelerometers are not adhered to the surface and do not have an array of many test points all seen at once. The present study collects the array individually and will correlates the data to a Finite Element Model to determine sound detection. Yoon et al. used a C-scan system for correlation.

1.8. Scope of Study

The objective of this study was to investigate delamination detection of a dynamically loaded composite structures via accelerometer data. The free vibration of the composite structures was forced with a harmonic, sinusoidal sweep in the vertical direction. Initial fully delaminated areas were individually placed transversely across several horizontal locations or zones along each composite plate specimens. Piezoelectric accelerometers were used to measure the Frequency Response Function (FRF) of the composite structure placed at

several locations along a vertical and horizontal grid surface. Deviations in flexural bending mode shapes, natural frequencies, and differences in amplitudes (Grms) were principle objectives for assessing the delamination locations.

The following chapters discuss the manufacturing methods, experimental test and numerical methodologies, experimental test and numerical results, and a comparison of the study utilizing Finite Element Analysis and control charts.

Chapter 2 discusses the manufacturing methods used to create the experimental composite test specimens, as well as mechanical properties specimens. Composite material test methods and results are discussed with insight into why some material property testing may result in higher percentage errors. Delamination zone manufacturing is discussed as well.

Chapter 3 provides details of the experimental test and methodology in this study. Test methods are discussed formulating how the data will collected.

Chapter 4 exposes the numerical and experimental test results for this study. Analytical and finite element analysis methods concludes this section discussing the uses different software tools.

Chapter 5 highlights the similarities and correlations between the experiment and numerical models. Software tools are displayed through their uses.

Chapter 6 addresses the conclusions of this research and presents the results of all trends with insight to further development.

CHAPTER 2

2. SPECIMENS MANUFACTURING AND TESTING METHODS

The following sections present how each specimen was manufactured and prepared to gather experimental data. Composite material test methods and results are discussed with insight into why some material property testing may result in higher percentage errors. Delamination zone manufacturing is discussed as well.

2.1. Composite Structure Design and Material Used

Desired material would carry characteristics of strength and stiffness without much torsion during a dynamic response if trying to primarily look at flexural bending. If the test article obtains high stiffness, a high resonance or natural frequency will be seen during dynamic response. To achieve higher stiffness more layers of material, weave patterns, fiber materials, and even resin choices can effect stiffness. The use of unidirectional layered plates allows more flexibility in the test article during dynamics responses and varied layup options.

Contribution's to a desirable test articles' dynamic response using unidirectional material allow varying the hand layups pattern to be 0° and 90° symmetric ($[0,90]_s$) over a desired thickness. When varying the pattern at $[0,90]_s$ it allows for good movement for testing due to the desired stiffness. The thickness can be more easily managed and delamination creation is more consistent.

The unidirectional prepreg material used to manufacture each specimen was material from Tencate Advanced Composite Group (TCAC 23510, Lot# 031713-1T2) and was donated to California Polytechnic state University (Cal Poly) by Space Exploration Technologies Corporation (SpaceX) for general academic purposes. The Tencate Advanced Composite Group unidirectional tape consists of M46J (fibers) 12K 200gsm impregnated with TC250 resin system (matrix) with 38 ±3% resin content and has a trade name of M46J/TC250. The thickness of one individual ply of the unidirectional tape measured with calipers having an accuracy of four significant figures read 0.0075 inches thick. It should be noted that the material used surpassed its shelf life and is not certified material due to its expiration date of 18-MARCH-2014.

2.2. Composite Material Properties for Specimen Manufacturing

The ASTM standards used are ASTM D3410[6] for compressive testing and ASTM D3039[7] for tensile testing. ASTM standards are used as a guide to determine the material properties of the material. Since the material has expired, the material is assumed to be an inferior product then when it was a certified material. The manufacturers Poisson's ratio values were used due to the lab not currently having strain gages for the ASTM standard test.

2.2.1. Layup Process

The roll of M46J/TC250 was removed from a freezer at Cal Poly's composite material storage area. The material was allowed to thaw to room temperature,

then rolled out and cut into several 0° and 90°, 12 inch squares sheets, prescribed by ASTM standards for testing. The sheets were layed-up together in one single direction, consisting of three separate plates. The three plates dimensionally achieved 7-8 cut specimens for each test, where the ASTM standard requires 5 to be in agreement to satisfy an accurate test. The three plates each had different thicknesses to support the required test thickness as per the ASTM standards for unidirectional material.

2.2.2. Curing Process

Outer protective film was removed from the uncured composite laminate plates, then placed in-between the two nonporous, Teflon coated sheets. The nonporous, Teflon coated sheets separated the composite laminate from the face of the 12-1/2 inch square metal plates as seen Figure 2-1. The non-porous material keeps the excess epoxy from seeping out onto the metal plates and hardening on them after curing, ruining the plates.[5] The plate curing setup is shown in Figure 2-1.

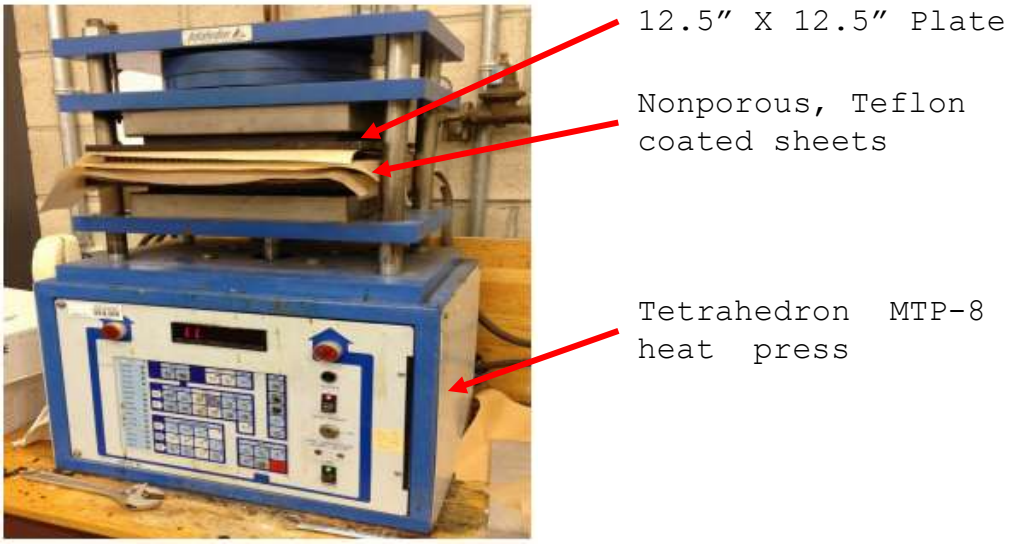

Figure 2-1 Cure cycle setup.

Curing the test specimens was in a Tetrahedron MTP-8 heat press, which has the ability to reach cure temperatures of 600°F with a compression forces of 1000lb. The MTP-8 heat press was developed to create 8 inch square composite plates, which does not generate 6-7 test specimens for one cure cycle. Tooling was later developed for Cal Poly’s Structures’ Lab to create a 12-1/2 inch square plate size, which was utilized for the current test specimens.

The test specimen cure cycle shown in Figure 2-2 began at ambient room temperature and ramped to 190°F at a rate of 3°F/minute. The temperature was held constant for 45 minutes at 190°F. Then the specimen was ramped up again to 265°F at a rate of 3°F/min. Once the test specimen reached the cure temperature of 265°F, it soaked for 120 minutes. At the end of the cure time, the material was ramped down to a temperature of 140°F at a rate of 3°F/minute. The total cure time was roughly 5 hours and 30 minutes. Once the

material and tooling cooled to room temperature, the cure cycle was finished. The test specimen manufacture process was repeated for each ASTM test standard to create 6-7 test specimens.

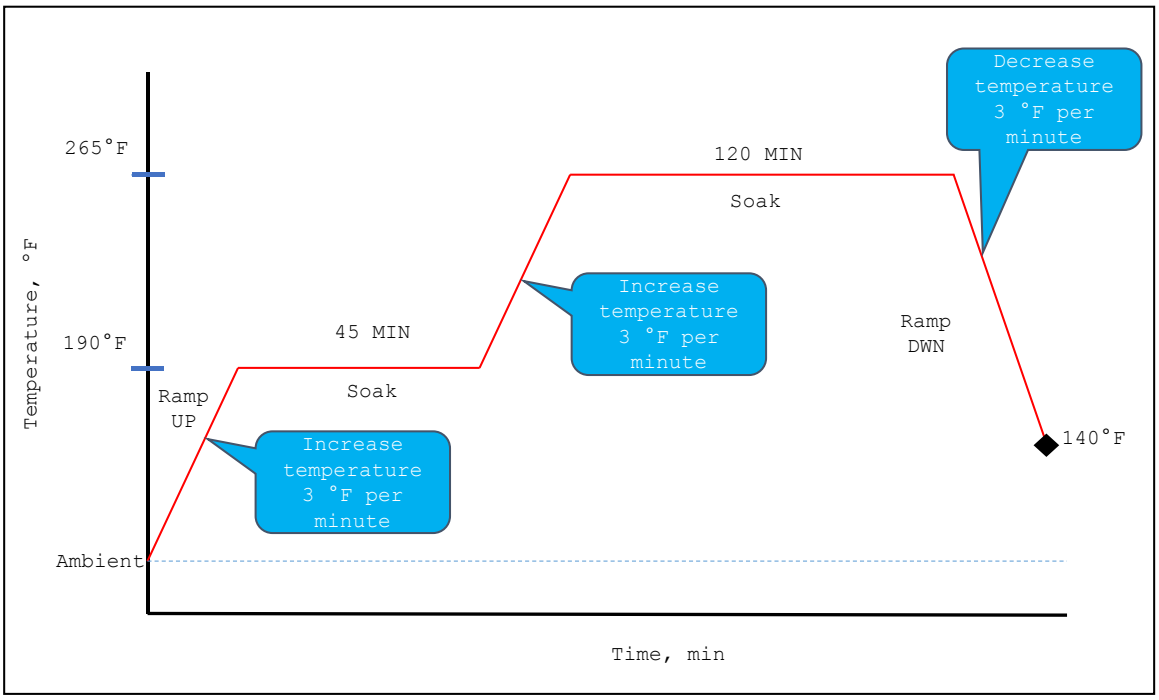

Figure 2-2 Cure cycle for test specimens on the MTP-8.

After curing, the three uncut plates were removed and marked for reference, as shown in Figure 2-3. Each plate is marked with the direction of the plies, the amount of layers, and the average thickness measured with calipers having an accuracy of four significant figures. The plates were then cut into 6-7 test strips in accordance with the ASTM standard size.

Figure 2-3 Three plates, uncut.

2.2.3. Preparing Specimens for Material Properties Testing

Each test specimen had aluminum 5052 tabs adhered to each tip of the specimen, on both sides consisting of four tabs each. The tabs were abraded using course sand paper prior to having the adhesive smeared on each and placed at each tip. Masking tape was used to insure adhesive runoff did not taint the specimens, expressed in Figure 2-4.

The test specimens were finally marked with their individual number on the aluminum tips and on the composite strip surface. This ensured each specimen material to be accounted for if the specimen violently fractures under load, which is common for uniaxial materials. The tabs help protect the specimen tips when pulled or pushed during tensile and compression testing by the Instron 8801 test equipment, shown in Figure 2-5.

Figure 2-4 Test specimen manufacturing process (left) and cured specimens (right).

Figure 2-5 Instron 8801 machine.

The tabs were adhered with 3M two part structural adhesive paste (1614A and 1614B) bonding material. By weight, the ratio of A-to-B used for the structural adhesive was one-to-one and had a 50/50 mixing formula. The adhesive was cured in the Tetrahedron MTP-8 heat press with the same setup as when the laminate plates were cured, utilizing the non-porous sheets and

steel plates. The adhesive cure schedule was 150 degrees Fahrenheit for 1 hour with a steady 100 pounds-force. Once the test specimens were fully cured, they are ready for testing. Figure 2-6 and Figure 2-7 shows the final dimensions of the mechanical properties test specimens for compression and tension.

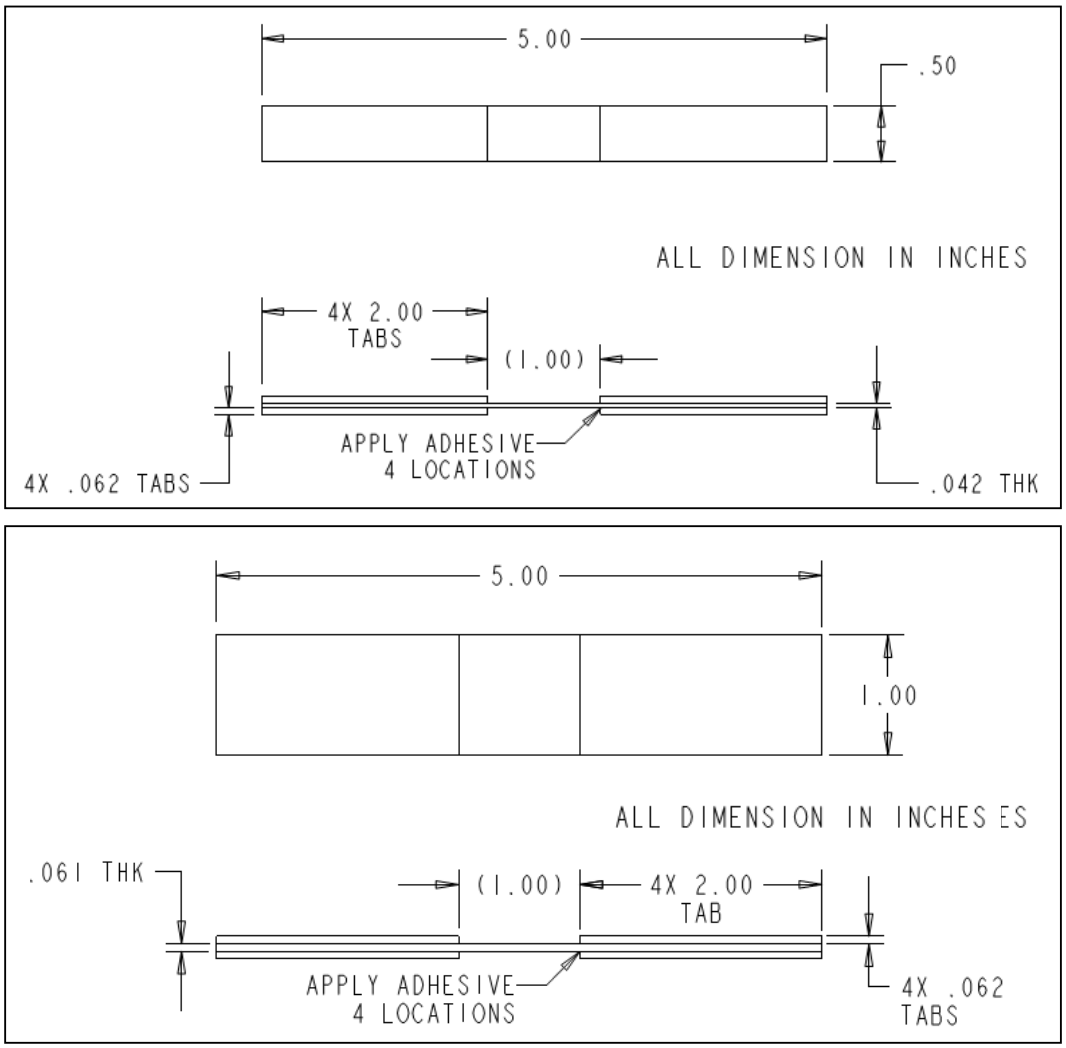

Figure 2-6 Mechanical properties test specimen dimensions for (TOP) compression with fibers (0º) and (BOTTOM) compression across fibers (90º).

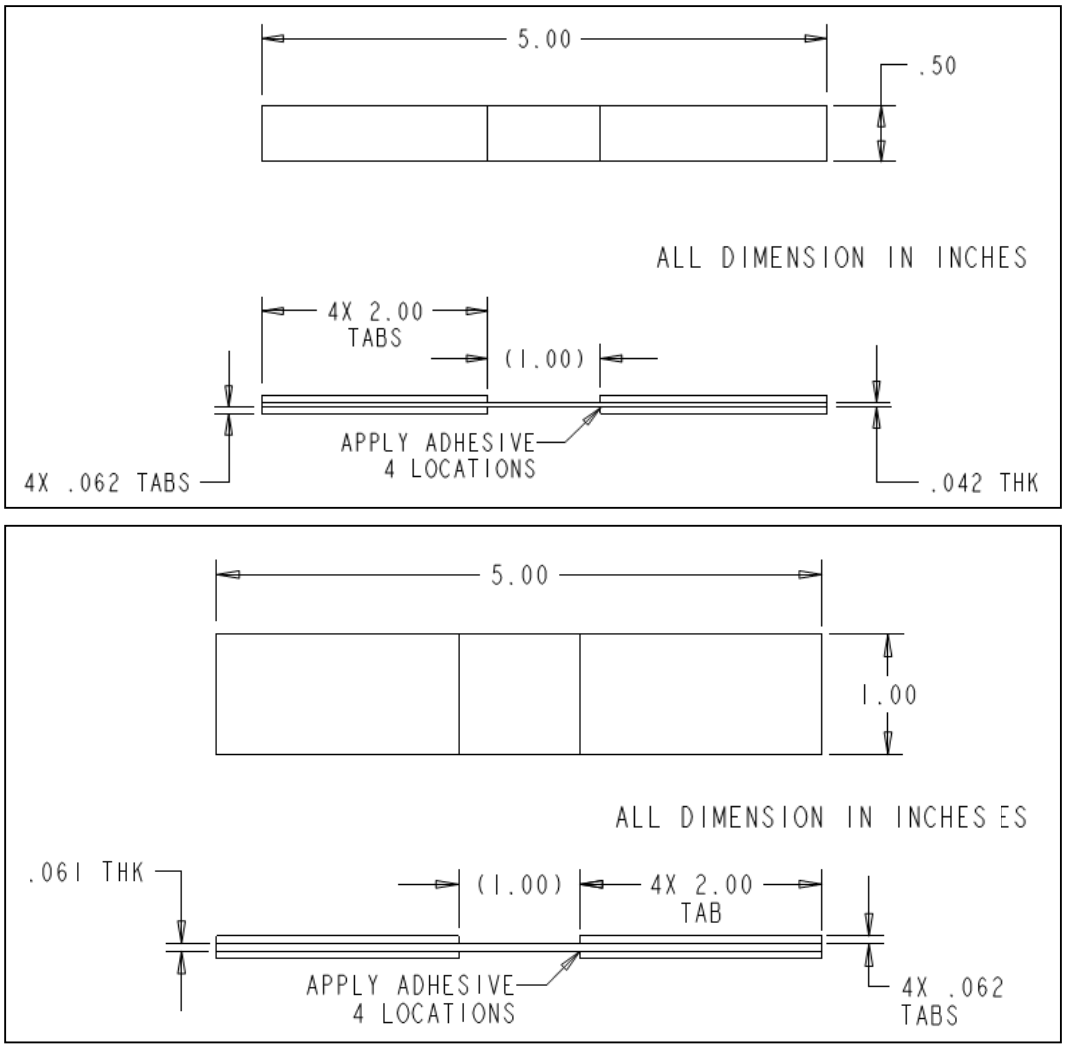

Figure 2-7 Mechanical properties test specimen dimensions for (TOP) tension with fibers (0º) and (BOTTOM) tension across fibers (90º).

2.2.4. Composite Material Properties Results

The mechanical properties of the material were obtained using Cal Polys' structures' lab Instron machine, which generated stress-strain curves. The Instron 8801 software uses the manually inputted dimensions of the material properties specimen and determines the cross-sectional area. As the Instron

8801 machine pulls (tension) or pushes (compression) on the material properties specimens, it divides by the calculated cross-sectional area to determine the maximum tensile/compressive strength.

It should be noted that the strongest materials usually are the most difficult to obtain sound tensile test properties. Axial loading of unidirectional composites present the greatest challenges compared to cross-ply laminates. It is known that the axial tensile and compressive strengths of unidirectional composites are typically higher than the transverse normal and shear strengths. To determine the axial tensile and/or compressive strengths of a unidirectional composite, therefore, the applied loading during the test must be transferred into, and uniformly redistributed within, the test section by shear stresses.[11] Thus, there is the risk that the test specimen might fail in shear before the ultimate axial tensile or compressive stress is reached.[11]

The greatest challenge during tensile/compression testing is gripping the unidirectional composite specimen without introducing unacceptable stress concentrations.[12] Typically the clamps transfer the applied grip strength by shear at the specimens' surfaces into tensile stress. There are strategies to eliminate some of the stress concentrations induced by the grips, generally through adhering tabs to the specimens ends so the shear is through the adhesive and tapering the tabs. The tabs, however, induce a new source of stress concentrations—those associated with the discontinuity created at the gage length ends of the tabs.[12] Other strategies are creating a traditional dog-

bone shaped specimen and specimen of uniform thickness (the tabbed area is built up for strength when clamping).

In summary, clamping force is generally a large issue when testing high-strength unidirectional materials and should be mitigated. Clamping force causes the tensile test to fail before ultimate tensile properties are determined due to stress concentrations in the gripping force. For compression, either shear, end loading, or a combination of the two is induced into the specimen through the wedge grips. The easiest way to eliminate the testing problems for unidirectional testing is to not use tabs or use an industry standard test fixture that addresses these issues head on.[12]

In this study, the specimens' dimensions could not deviate too much from the ASTM standard due to the Instron 8801 machine limitations. Access to adequate tools or resources for post-process manufacturing strategies to create specimens with a more robust geometry, as suggested in the reference articles, was limited. Though the material testing did not deviate from the ASTM standard itself and every effort was made to insure good tensile test data, it is expect that problems may exist with the material properties specimens test results due to the mentioned facts above.

The mechanical properties shown in Table 2-1 compares the tested data with the manufacturers known data. The graphs follow the Table 2-1 showing the stress-strain curves found during testing, Figure 2-8 and Figure 2-9 respectively. The standard deviation found during testing was significantly different. This is most likely due to the testing technique used, outlying results, and the difficulties

of testing unidirectional composite materials. It should be noted that most unidirectional materials do not have a common stress-strain curve. This is due to the fiber orientation causing the tail ends in the yielding area to drop off abruptly, ending at ultimate failure, rather than have a common arching upper register in the ultimate area of plasticity and fracture.

Table 2-1 Mechanical Properties.

Test Method	Direction of Test	Manufacturer Data (psi)	Test Data (psi)	Std Dev From the Mean (psi)	% Error From (Test Data vs Manufacturer Data)
Tensile	σ_{ult}, Longitudinal	2.51E+05	2.72E+05	3.14E+03	8.20%
	σ_{ult}, Transverse	4.50E+04	3.90E+04	2.07E+03	-14.22%
	E_1_Longitudinal	3.40E+07	2.77E+07	1.81E+04	-20.29%
	E_2_Transverse	9.10E+05	8.02E+05	5.28E+03	-12.63%
Compress	σ_{ult}, Longitudinal	1.24E+05	1.20E+05	5.19E+03	-2.96%
	σ_{ult}, Transverse	2.36E+04	2.01E+04	2.55E+03	-16.00%
	E_1_Longitudinal	2.38E+07	2.19E+07	6.46E+03	-8.31%
	E_2_Transverse	6.10E+05	6.95E+05	2.02E+03	13.07%

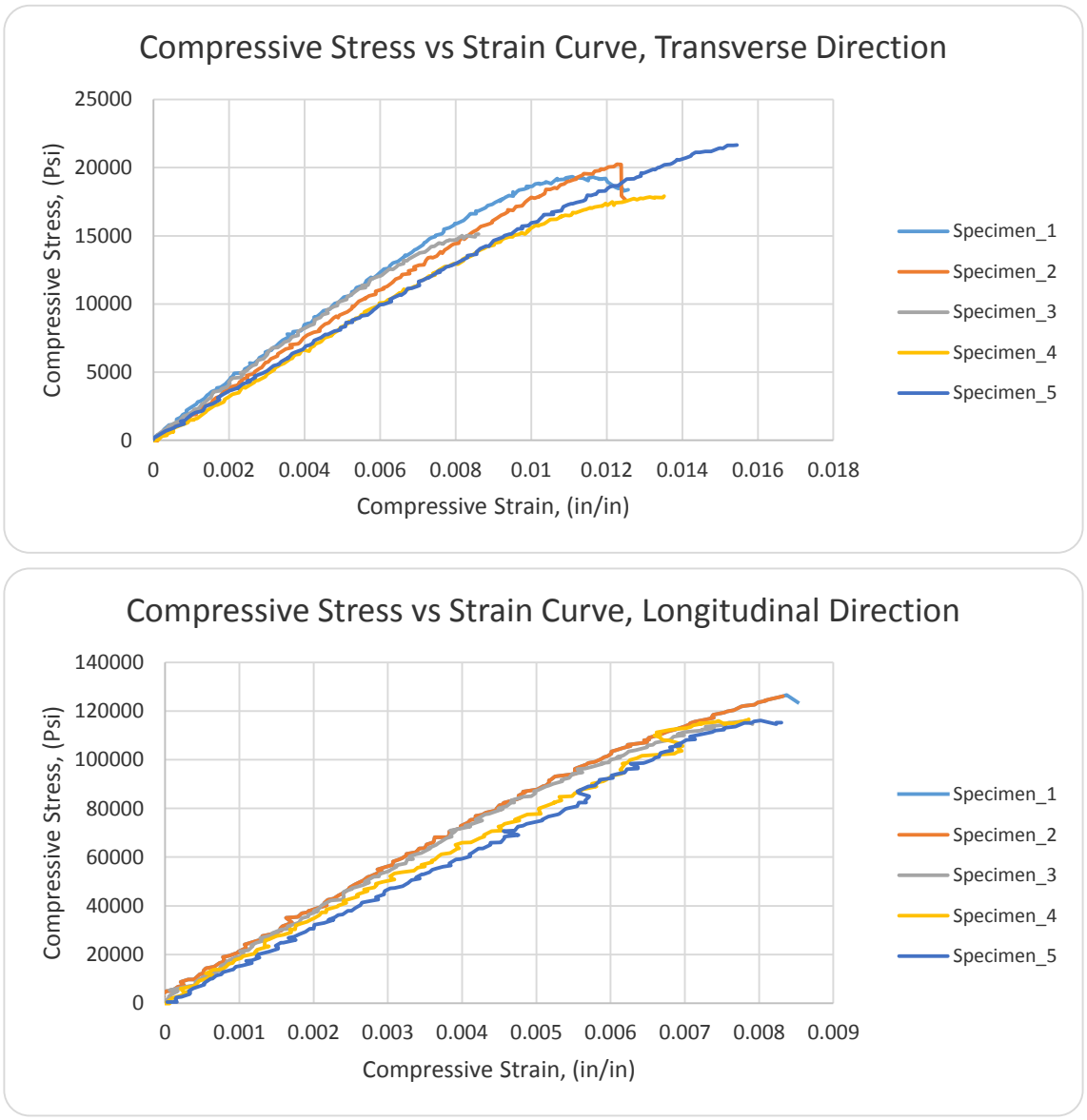

Figure 2-8 Compression curves (inverted for clarity).

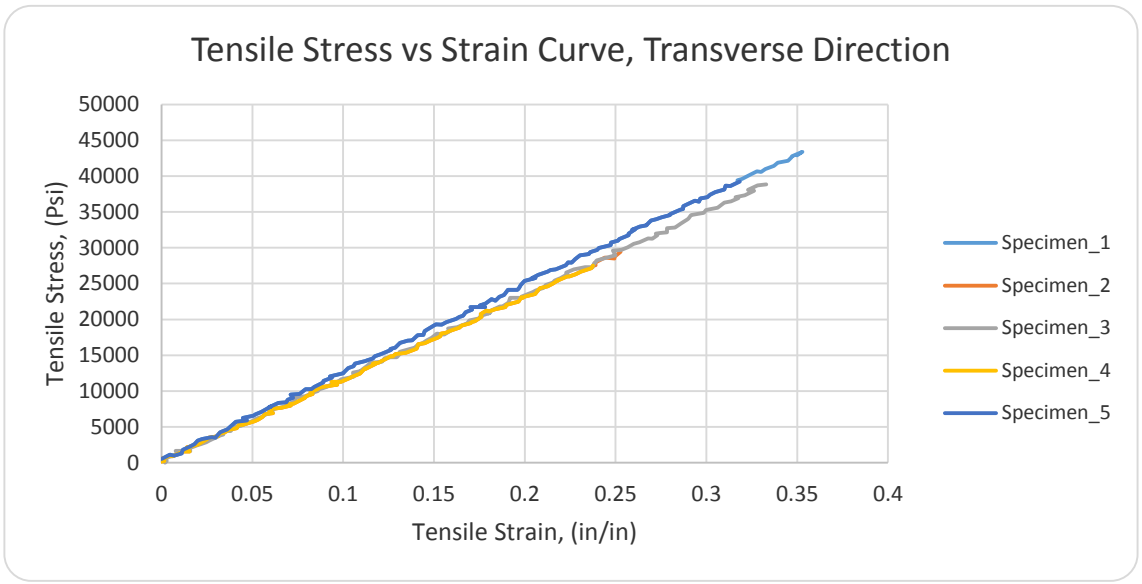

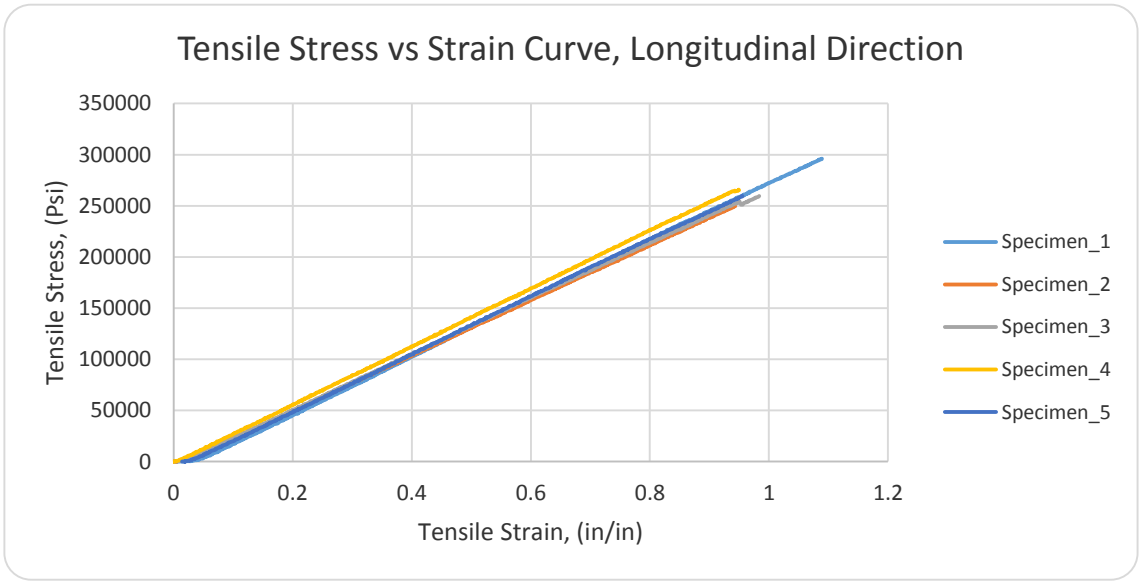

Figure 2-9 Tensile curves.

2.2.5. Fiber Volume Fracture

The ratio of 60:40 fiber to resin ratio is considered optimum.[2] The standard test method for ignition loss (ASTM D2584)[8] helps determine the fiber volume fracture, thus adds guidance in determining the fiber to resin ratio. The test

articles were inserted into a small furnace to burn out the resin, showing a net loss, thus the remaining weight is of the fibers only. From Equation 2-1, the fiber volume fracture was determined.

$$Weight, \% = \left[\frac{(W_1 - W_2)}{W_1}\right] \times 100$$

Equation 2-1 Ignition Mass Loss Calculation.[8]

W_1 represents the initial weight of resin/fibers prior to the furnace, W_2 is the weight of the dry fibers (resin burnt out) after burning in pounds-mass. Burnt resin leaving dry fibers are shown in Figure 2-10. The percentage found is the amount of epoxy that was in the test specimen.

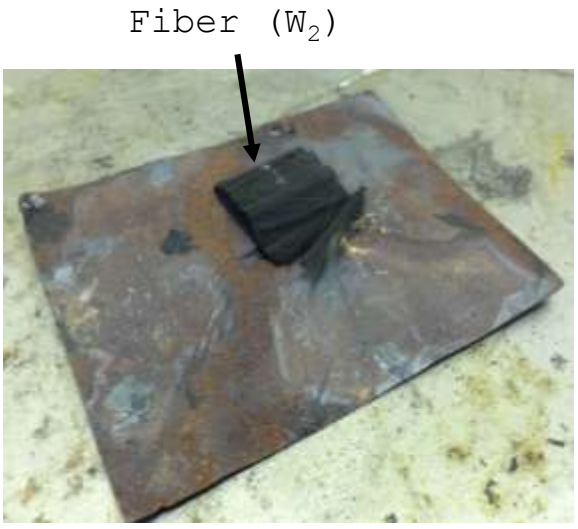

Figure 2-10 Fiber result.

The fiber volume fraction was determined to be 58.5%, which is 5.5% from the manufactures stated value. The found fiber volume fraction correlating closely with standard values for M46J/TC250 fiber volume ratios of 62%.

2.3. Preparing Specimens for Dynamic Testing With/Without Delamination

The M46J/TC250 unidirectional tape was cut into 4 X 14 inch rectangular strips and layed-up in a bi-directional $[0,90,0,90]_s$. This is a laminated plate totaling 8 plies, symmetric about the 90° plane, which eliminates any coupling effect in the plies and is considered a symmetric orthotropic cross-ply laminate. 11 plates total were manufactured having one being a non-delaminated test article as the “control.” The other 10 are delaminated as discussed in further sections of this chapter. The surface was controlled to be as smooth as possible with minimal resin bleed. The surface quality was important to possibly allow multiple tests be done with a verity of test equipment; aiding in test versatility. The hand layup process is shown in Figure 2-11.

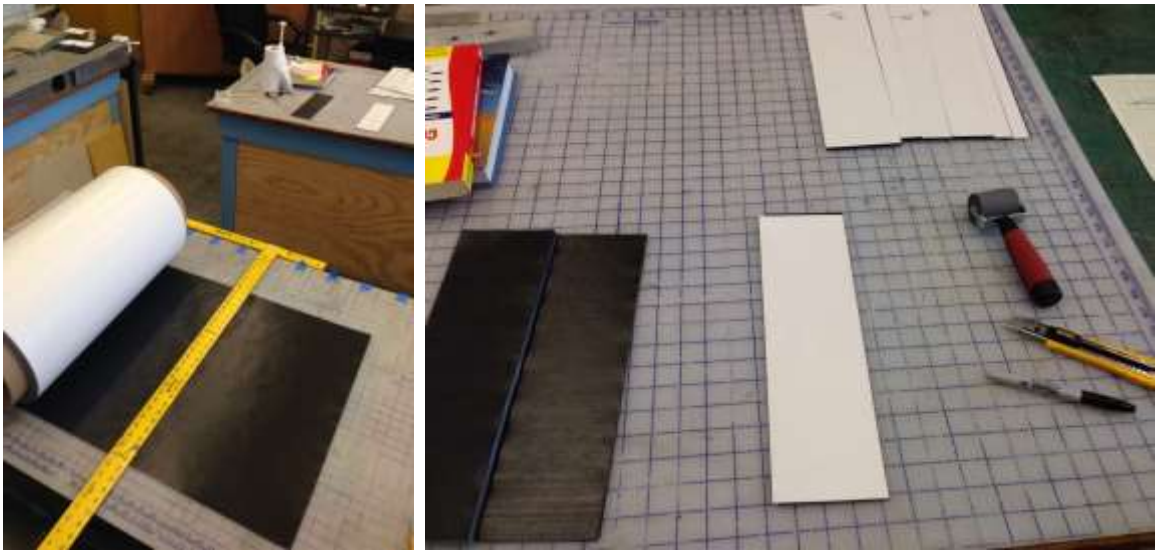

Figure 2-11 Hand layup process.

2.3.1. Layup Process With/Without Delamination

A 1 X 4 inch rectangular, high-temperature, non-porous poly-vac bag was placed at mid-layer of the 10 test articles. The procedure to ensure the bag material was at one inch increments was by using a cheap and effective jig shown in Figure 2-12 and Figure 2-13. The jig helped layout the process for each delaminated area, mark off the clamping zone for the vibration fixture, and aid in the post-manufacturing-process of cutting off the salvage area of each plate to their final dimensions. Figure 2-14 shows the post cure layup.

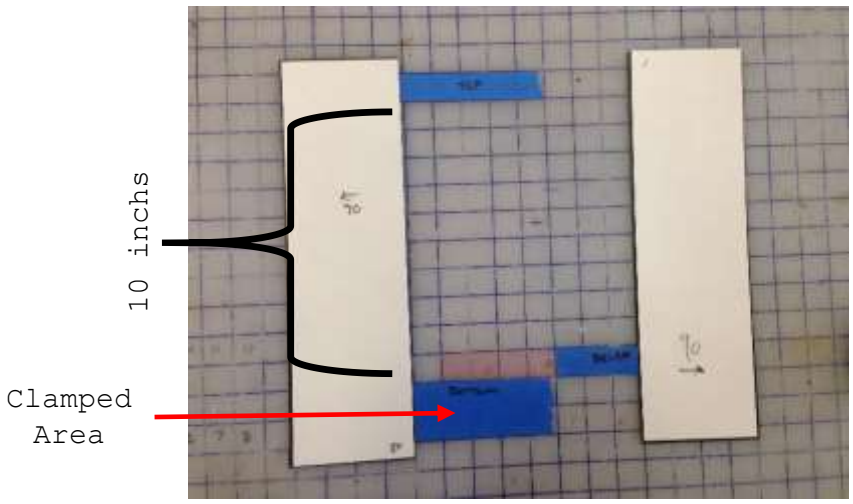

Figure 2-12 Delamination increment jig. Each square on the table is 1 square inch, jigged with tape marking off a 10 inch plate length and the clamping area for the vibration fixture.(Pre-cooked samples.)

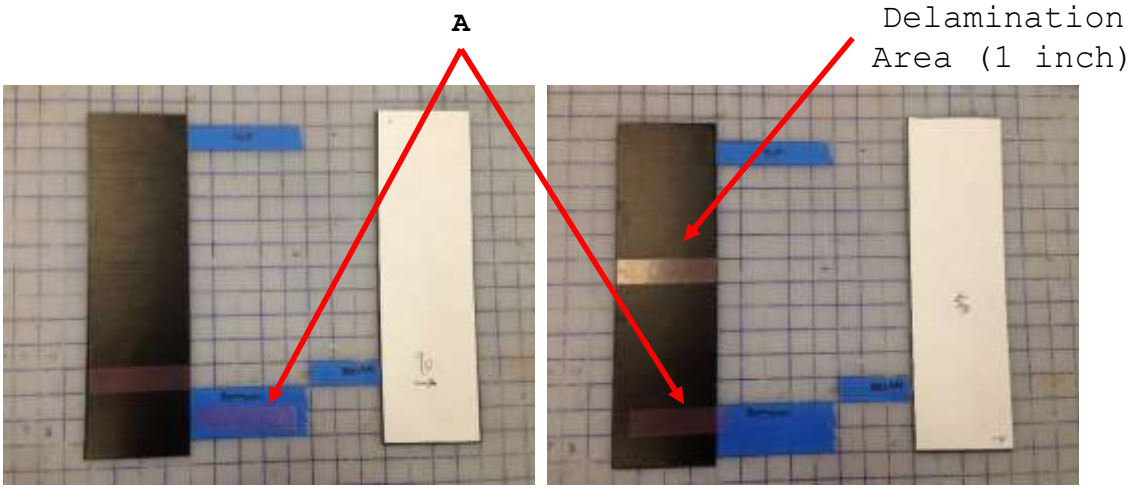

Figure 2-13 “A” area is bagging used to mark were to measure 10 inches from to ensure each test area is 10 inches long and cutting was consistent across each test article. Delamination area is shown. A tail was left out of each sample to pull the delamination material out of the plates.

Figure 2-14 All 11 plates marked as to show how they are laid up with delamination areas marked prior to curing in the autoclave.

2.3.2. Curing Process

Protective film was removed from the uncured composite laminates (Figure 2-14, white paper) and then placed on two caul plates to be prepped for the autoclave (Figure 2-15). Once bagged (Figure 2-16), the labs vacuum was used to debulk the material (Figure 2-17) and check for leaks. Once inspection was complete, the plates were then transferred to the autoclaves' vacuum to keep positive pressure on the test articles' and prepare for autoclave process.

Figure 2-15 Test article positioning on caul plates surface before vacuum bagged.

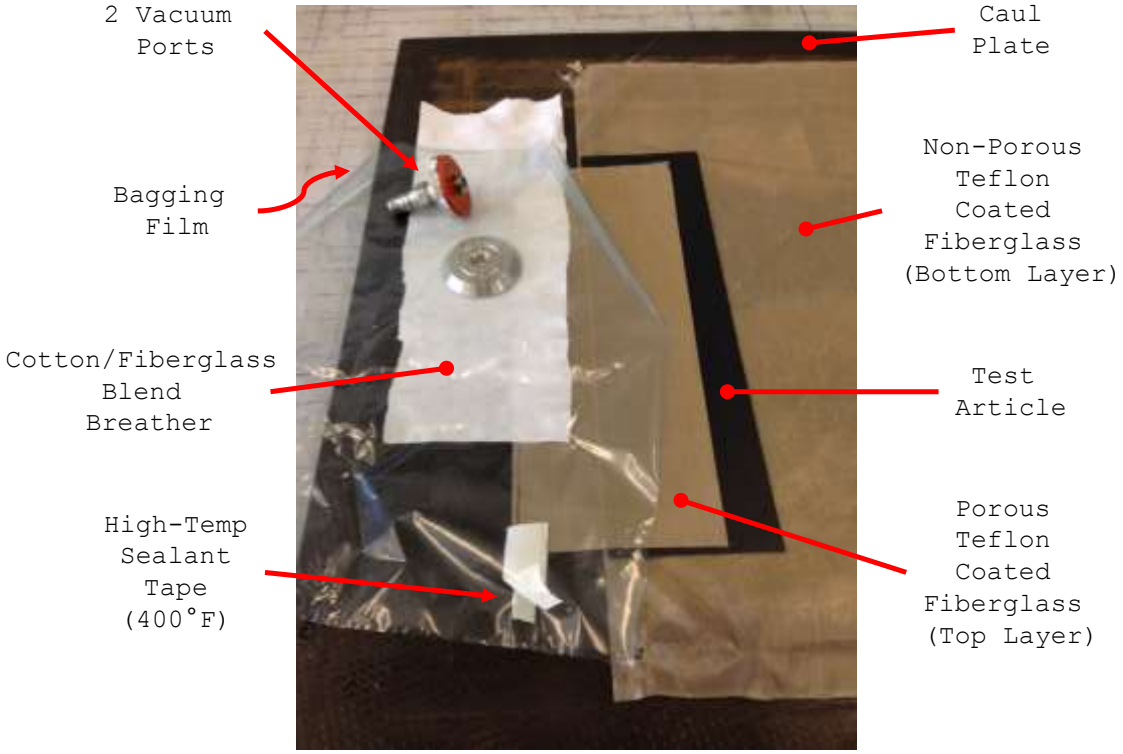

Figure 2-16 Bagging technique.

Figure 2-17 Vacuum sealed to 15 psi prior to being placed in the autoclave.

The autoclave curing cycle is shown in Figure 2-18. It is very similar to the MTP-8 press. The pressure was held at 30 pounds per square inch ramping up twice at 3°F per minute with two soak times (45 minutes at 190°F and 120 minutes at 250°F). The final temperature after ramping down is 140°F to end the cure cycle for roughly a total of 5 hours and 30 minutes.

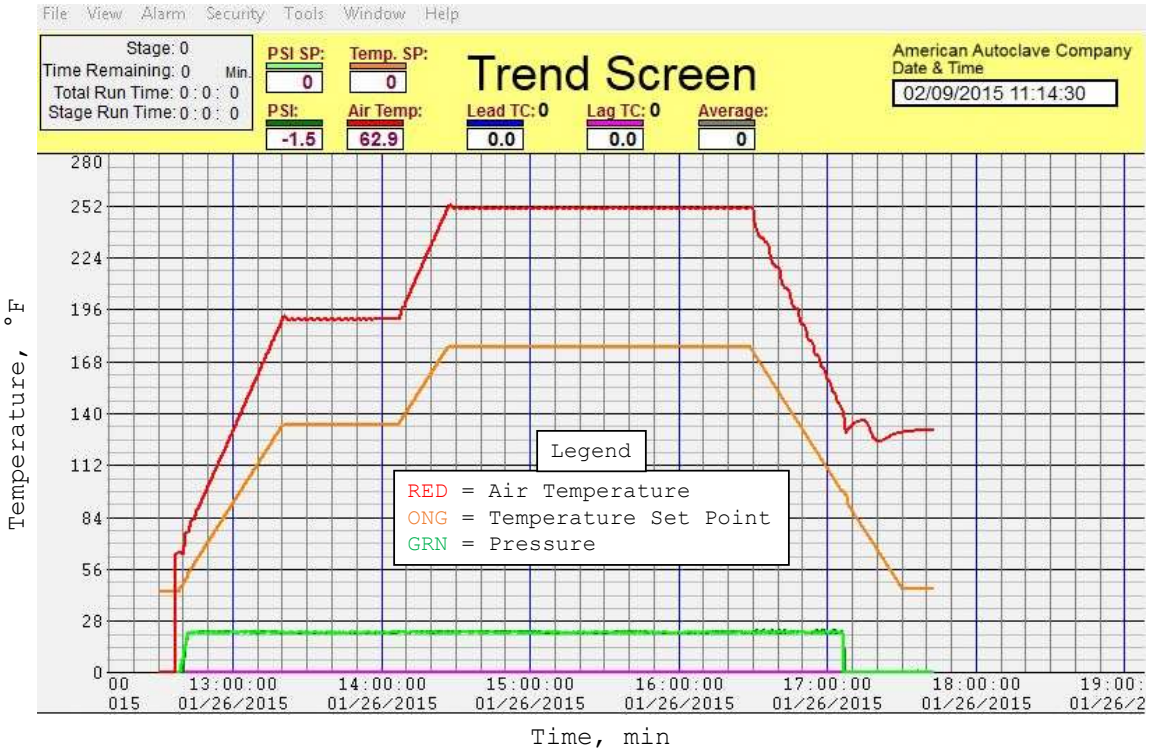

Figure 2-18 Cure cycle output from autoclave.

2.3.3. Preparing Specimens for Testing

After curing in the autoclave, the test articles were removed from the vacuum bagging material. The high-temperature non-porous poly-vac bag was pulled out of each delaminated region. As seen in Figure 2-19, the specimens were then cut to 3 X 12 inch plates using a high-speed, diamond coated table saw. The 10 inch test area was marked off, as well as the vibration fixture clamped location—requiring a 2 inch clamping area. Cutting was done with a slow feed rate to ensure smooth edges and accurate cuts so each test articles are of the same dimensions. Care was also taken to eliminate any edge delamination and small cracks caused by the ripping action of the saw. The edges were then sanded

with a fine grit sanding block to “de-bur” the edges as seen in Figure 2-20. De-burring helps remove any fine, cracked fibers that can cause propagating cracks through the layers of the test article.

Figure 2-19 Preparing specimens for testing.

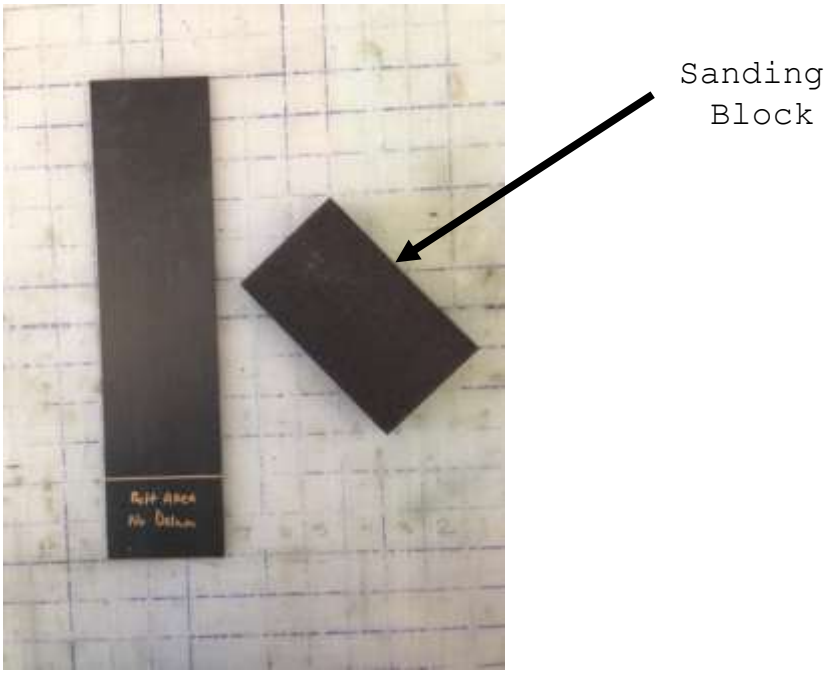

Figure 2-20 Test article edge to be sanded.

Each test articles final measurements and weight (found in Table 2-2 and Figure 2-21) were measured to ensure consistency across each plate. This supports the tests consistency and guaranteeing each plate nearly the same. Though it would be more accurate to weigh the test articles with units of kilograms, the test articles were weighed in pounds. This decision was made because the units used in analysis uses SI units and would be converted anyway.

Table 2-2 Test article final dimensions and weights.

Test Article	Length (in)	Width (in)	Thickness (in)	Weight (lb)
1	12.00±.05	3.00±.05	0.068±.001	0.1320±.0005
2	12.00±.05	3.00±.05	0.068±.001	0.1320±.0005
3	12.00±.05	3.00±.05	0.068±.001	0.1320±.0005
4	12.00±.05	3.00±.05	0.068±.001	0.1320±.0005
5	12.00±.05	3.00±.05	0.068±.001	0.1320±.0005
6	12.00±.05	3.00±.05	0.068±.001	0.1320±.0005
7	12.00±.05	3.00±.05	0.068±.001	0.1320±.0005
8	12.00±.05	3.00±.05	0.068±.001	0.1320±.0005
9	12.00±.05	3.00±.05	0.068±.001	0.1320±.0005
10	12.00±.05	3.00±.05	0.068±.001	0.1320±.0005
11	12.00±.05	3.00±.05	0.068±.001	0.1320±.0005

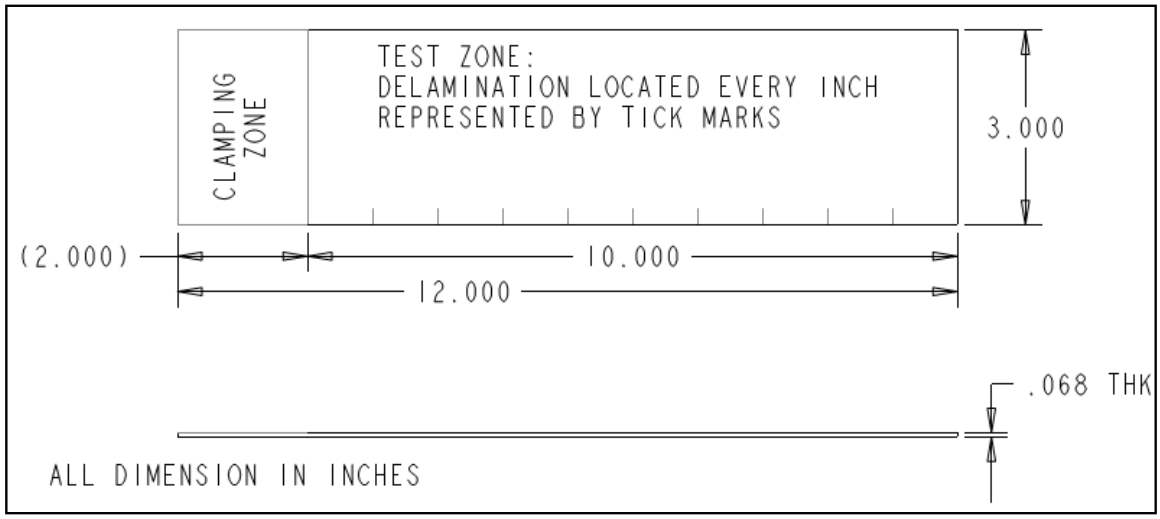

Figure 2-21 Test article dimensions. Delamination zone represented by tick marks.

CHAPTER 3

3. EXPERIMENTAL TESTING

Test methods are discussed formulating how the results will be obtained. Cantilever plate and vibration testing will be discussed.

3.1. Cantilever Plate Setup

The test specimens were clamped in a 6061-T6 aluminum clamp style vibration fixture. Each specimen had a 2 inch flange clamped in place in the fixture. Eight (8) #10-24 socket head cap screws, equally torqued to 10 foot-pound-force to fasten the top 2 inch wide, 15 inch long, ¾ inch thick top plate to the main vibration fixture body. The vibration body was fastened to a Unholtz-Dickie shaker head with five 3/8-16 socket head cap screws, torqued to 25 foot-pound-force. The vibration fixture drawing is shown in Figure 3-1 and located in the appendix.

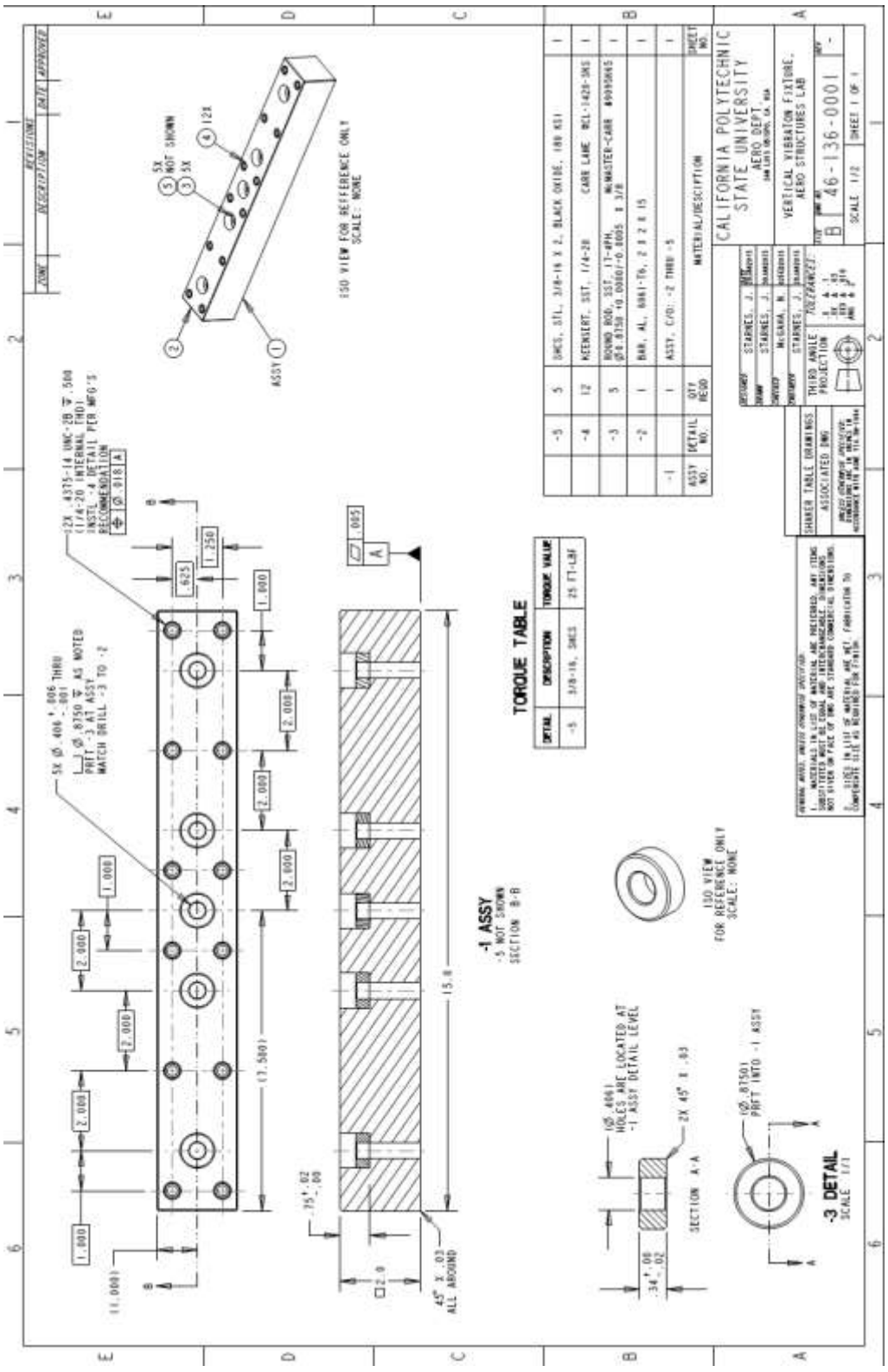

Figure 3-1 Vibration Fixture Drawing.

3.2. Vibration Test Procedures

The vibration fixture was fastened to an Unholtz-Dickie shaker head (Model S202-ST/SN 355) capable of producing 2,200 pound-force[37] and excited in the vertical axis. It should be noted that before fastening the vibration fixture to the shaker table, the shaker table should be level and the airbags are lifted as shown in Figure 3-2. Once the fixture is bolted to the shaker table, verify the bolts are torqued properly and the first natural frequency is as expected with accelerometers and a sinusoidal sweep ramping to 5,000 Hertz for a few seconds shown in Figure 3-3. Verifying the bolts are torqued properly is important because the shaker table and vibration fixture work in concert, which will give erroneous data if the clamping force is not properly achieved and equally balanced along the fixture.

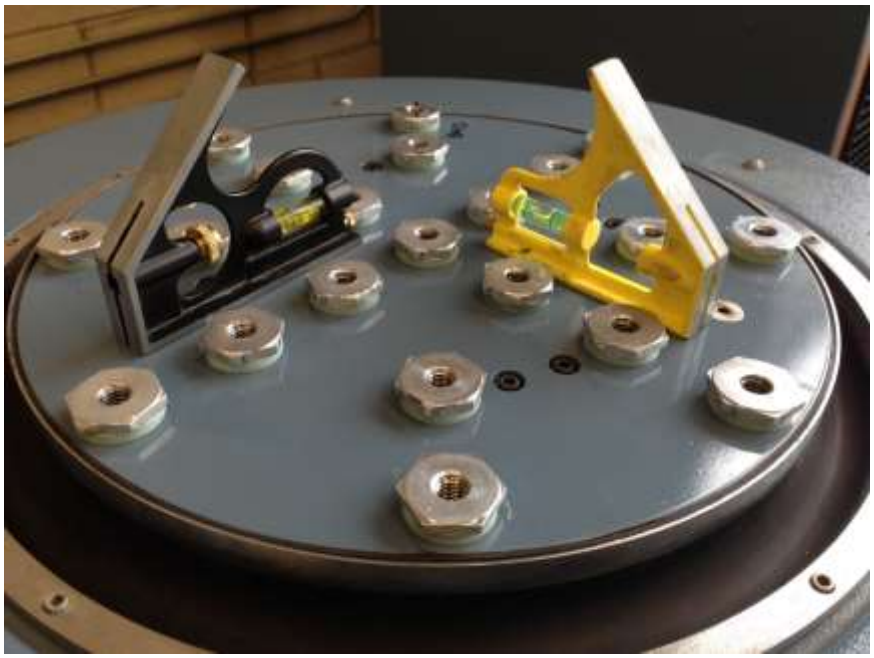

Figure 3-2 Check shaker head is balanced.

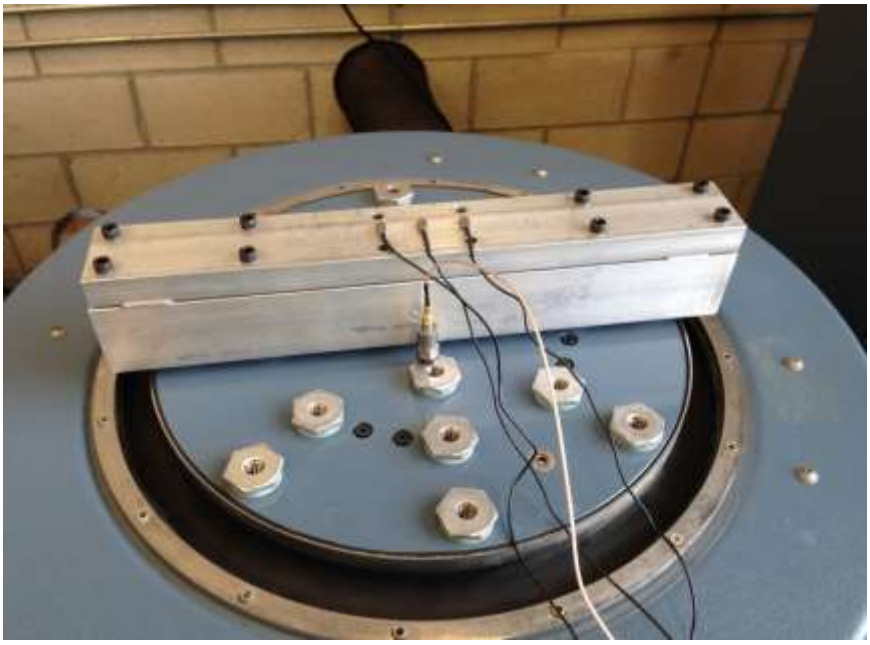

Figure 3-3 Check MODE 1 of vibration fixture and when peak slope begins to rise, ensuring no frequency coupling effect.

Each test specimens had an identical grid drawn on one face, spaced 1 inch axially and ¾ of an inch transversely accounting for 30 test locations (see Figure 3-4). The test specimens and the shaker table were instrumented with a PCB Piezotronics[39], general purpose accelerometer (Model 353B02) as the general “signal” or “control,” bonded with petro-wax to the shaker head oriented in the axial direction of the test. Additionally, a one-axis, 1.2 gram tear drop style VIP Sensors[38], piezoelectric accelerometer (Model 1011A) was used to measure the “response” across the face of each specimen. Figure 3-4 on the next page shows the test specimens instrumentation setup.

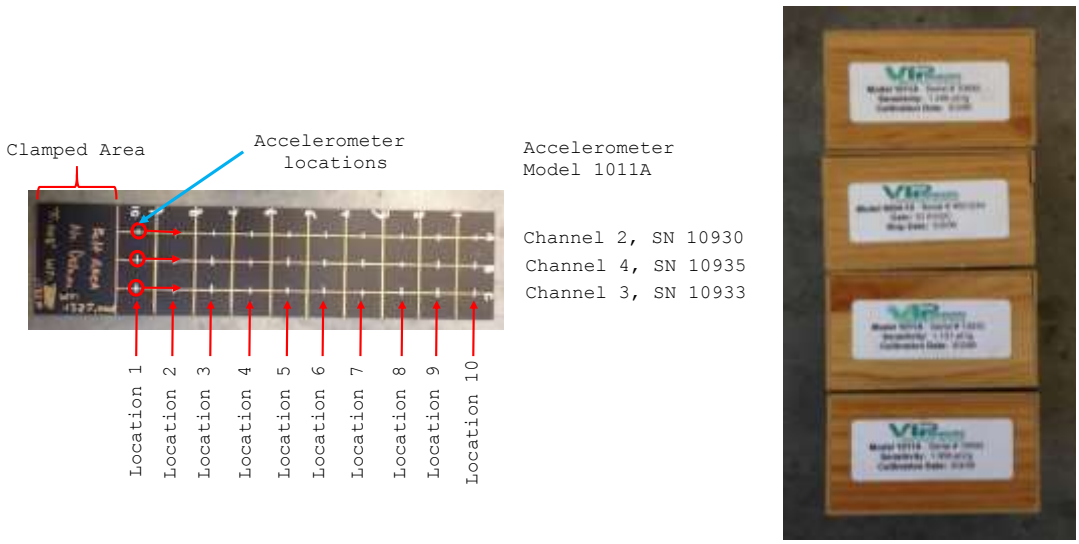

Figure 3-4 Clamped area, grid, accelerometers locations, and accelerometers serial numbers used.

Each test ran (110 total) had general scotch tape adhered to the surface of each plates' test zone, then the three accelerometers were bonded to scotch tape using petro-wax. Scotch tape was used to ensure no petro-wax was left behind after each test run, which could potentially added mass to each prescribed test. A VIP Sensors, charge converter (Model 5004-10) was used to amplify the accelerometer signal. The test set up described above is shown in Figure 3-5. Piezoelectric accelerometer data was collected 10 time at 3 locations as shown in Figure 3-6.

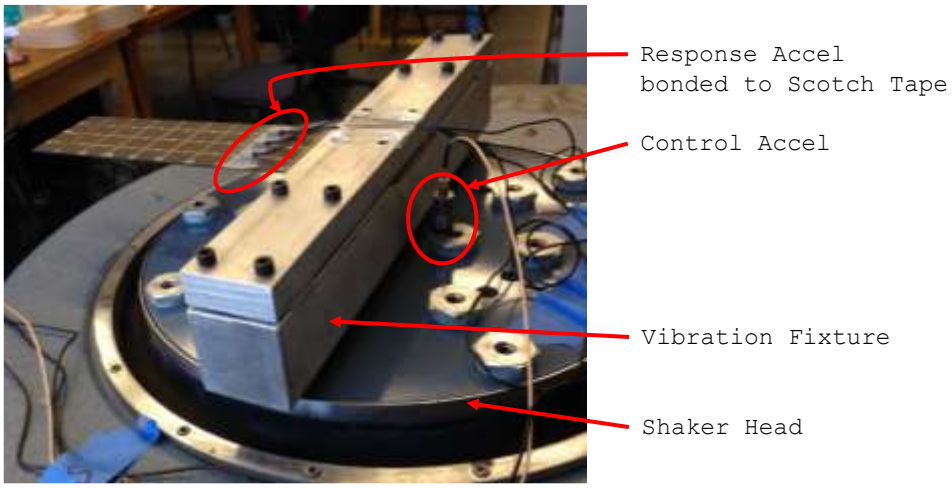

Figure 3-5 Control accelerometer location with respect to the system.

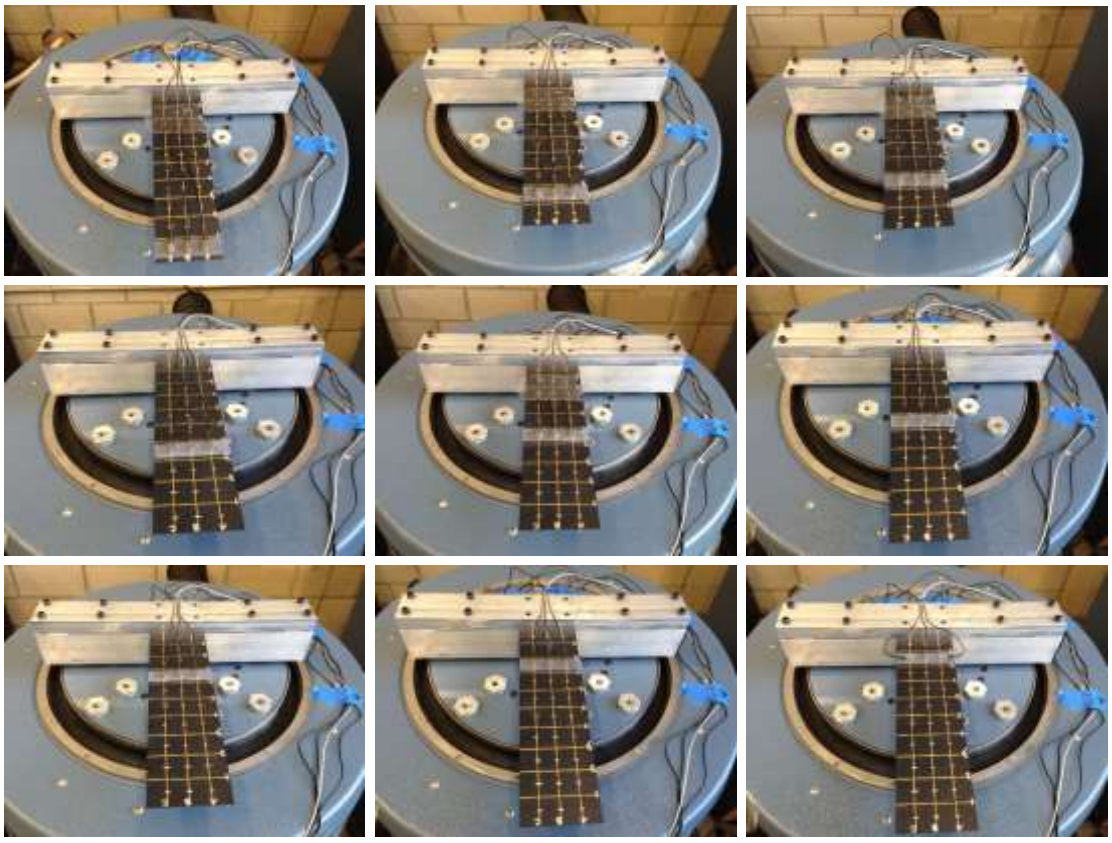

Figure 3-6 Accelerometer data points for each plate (9 shown, though there are 10 locations).

CHAPTER 4

4. NUMERICAL ANALYSIS

Post-processing usage is described as to how it is utilized. Analytical and finite element analysis methodology concludes this section.

4.1. Analytical Analysis Methodology

Post-process analysis methodology will use a quality test utilizing six-sigma technics that is statistical in nature to better understand amplitude difference between zones in each specimen. For this particular study and sample size, I am proposing to use control charts due to their simplicity and ease of quickly understanding variability. Control charts have two general purposes to improve projects. The most common is to track and monitor process stability and control. The less common and arguably more powerful use of control charts is to be used as an analysis tool and design optimization predictor.

Control charts can aid in visually telling a story. The purpose of any control chart is to see if the variation is due to chance or to changes in the process.[41] Controlled variation is characterized by a stable and consistent pattern of variation over time, and is associated with common causes. A process operating with controlled variation has an outcome that is predictable within the bounds of the control limits.

Uncontrolled variation is characterized by variation that changes over time and is associated with special causes resulting in a process with an unpredictable outcome. Depending on the expected outcomes, unpredictability

may satisfied or unsatisfied a particular test. In this study, unpredictability satisfies the end result by assuming each plate does not have delamination.

To review, any control chart has a set of common elements. The x-axis generally shows the time, date, period, or numbered location and the y-axis traditionally shows the observed value. There is an upper/lower control limit (UCL/LCL respectively) region, which is where 95 to 99 percent of the data should fall within. Values outside or creeping near the control limits mark statistically significant changes and may indicate a change in the underlying process. Creeping near the control limit is based on the users discretion and may need further independent investigation. Figure 4-1 shows an example of a control chart and how it is related to normal distribution curve.

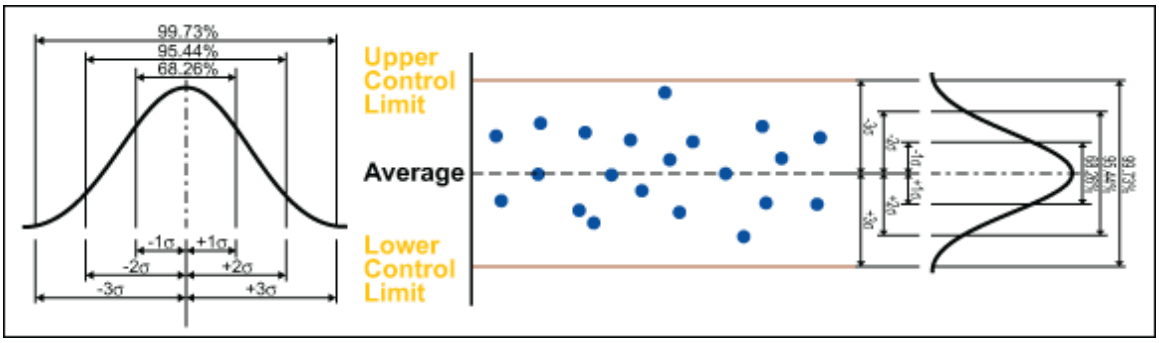

Figure 4-1 This is an example of the relationship of a control chart to a normal distributive curve.[41]

From the experimental data, a damping ratio can be calculated to later enter into the FEM to better understand the time response. MatLAB software script was written to read in the experimental data FRF, run through the half-power

bandwidth calculation to find damping ratios, then write out the found damping ratio. The MatLAB script can be found in the appendix.

4.1.1. Analytical Analysis Procedures

From the abundant amount of control charts available, a control chart selection guide in Figure 4-2 helps determine which chart could work for the type of data being collected. For this study, an X-mR (Shewhart's) chart was chosen, which is applicable when one data point is collected at each point in time.[41] X stands for an observation and mR is referring to a moving range.

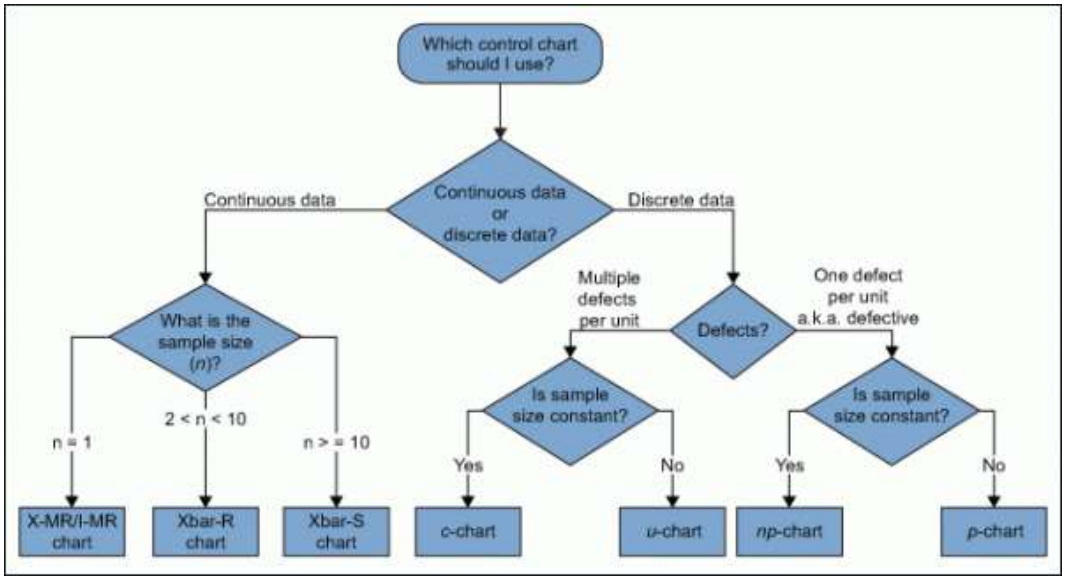

Figure 4-2 Control chart selection guide.[41]

A Shewhart's chart is actually two charts (X_bar-chart and R-chart) used in tandem that monitors the process average, as well as process variation. The X_bar-chart is used to evaluate consistency of process averages by plotting the average of each subgroup. The X_bar-chart is used when subgroups of two

(n+1) or more observations can be collected or measured. Each subgroup is a snapshot of the process at a given point in time.

The R-chart shows short-term variability in the process and evaluates the consistency and stability of the process variation. The moving range (R-chart) is the difference between consecutive observations and is expected to be predictable.[41] One crucial point is to look at the R-chart first; if the R-chart is out of control, then the control limits on the X_bar chart are meaningless.[41]

Moving forward with the analysis method, a Microsoft Excel macro was constructed to systematically read in the central accelerometer's experimental data. The centerline accelerometers' acceleration across each zone of each delaminated specimens was observed in time. For instance, comparing zone 1 locations of all 10 delaminated specimens to each other, then zone 2 locations of all 10 specimens to each other, and so on. Figure 4-3 helps visually explain how each zone for all specimens are analyzed.

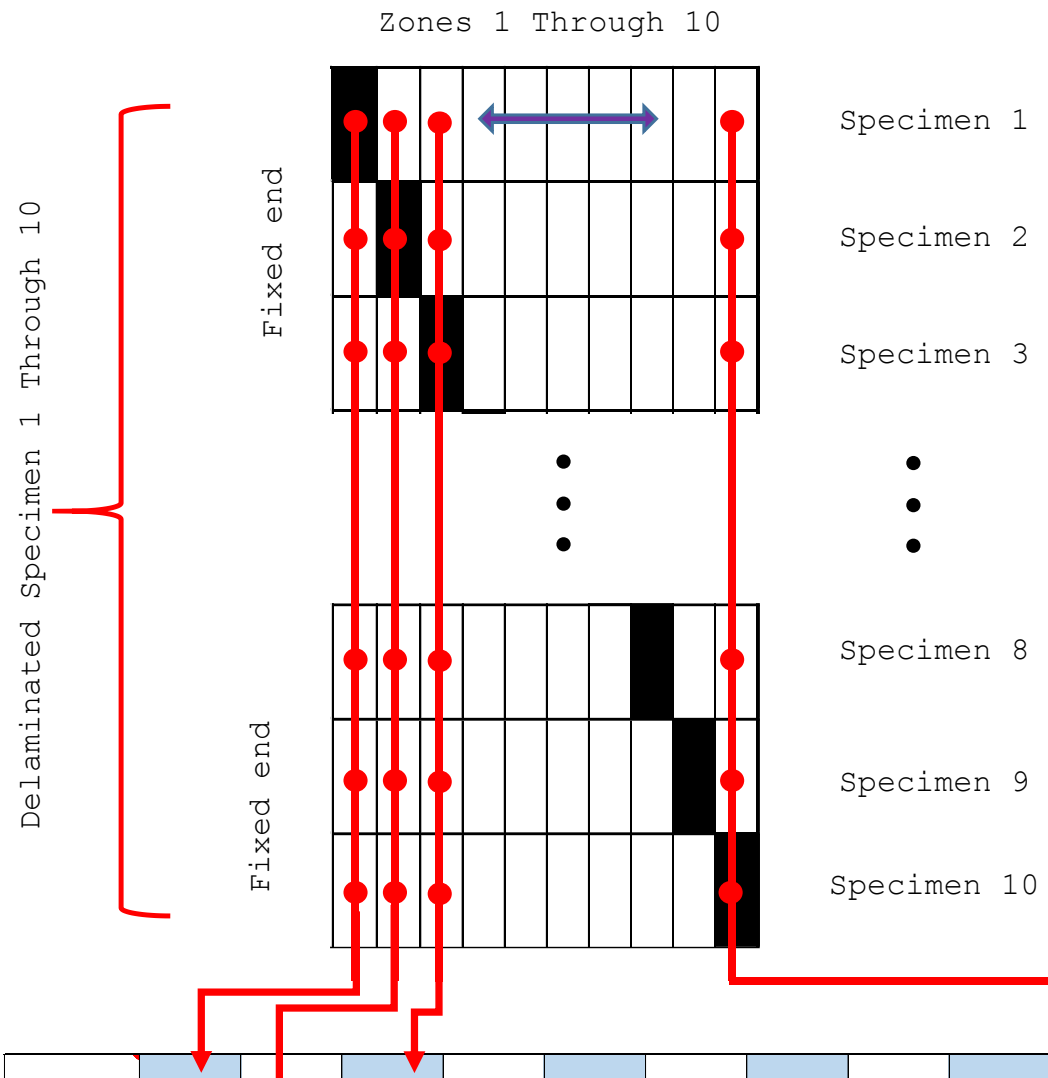

Delaminated Specimen	X-Chart; Zone 1	X-Chart; Zone 2	X-Chart; Zone 3	X-Chart; Zone 4	X-Chart; Zone 5	X-Chart; Zone 6	X-Chart; Zone 7	X-Chart; Zone 8	X-Chart; Zone 9	X-Chart; Zone 10
1	30.868	31.879	28.071	22.492	17.994	14.310	8.511	4.002	1.728	4.529
2	38.168	28.454	28.653	23.477	18.487	12.153	8.301	1.919	1.373	2.858
3	33.595	34.007	24.820	24.367	19.246	14.414	7.983	5.824	1.985	5.284
4	36.132	34.501	30.575	19.564	20.319	20.690	8.658	3.794	1.677	0.864
5	35.492	32.130	30.488	26.259	15.649	16.616	10.599	5.504	1.917	0.847
6	37.994	34.436	31.958	24.755	19.322	11.603	10.248	4.066	1.745	4.462
7	37.968	34.077	30.192	23.908	18.202	15.749	6.143	5.190	1.819	2.998
8	35.823	33.295	29.502	23.227	18.291	12.964	9.834	2.116	2.121	0.878
9	38.388	33.640	30.491	24.737	19.685	14.443	8.100	3.682	0.880	2.067
10	37.283	34.449	30.124	25.322	20.028	13.262	9.097	3.498	1.486	2.366

Figure 4-3 Macro data input is tabulated. Macro computes each column creating 10 graphs at once. Red area is the expected delamination zone. All values in table above are G_{rms}.

4.2. Finite Element Analysis Methodology

ANSYS was used to help determine Mode Shapes (MS) through modal analysis and dampening related to each zone through transient responses. Modal Analysis is a tool used to determine natural frequencies of a mechanical structure and can be used for finding MS and transient responses. Transient or natural response is any event that changes the equilibrium state, generally associated with some sort of dampening.[40] Data will be conditioned using MatLAB to find the dampening factors for all flexural bending modes for each specimen. ANSYS software will be used to determine the amount of time it takes for each specimen to stop through free vibrating. This should show that specimens with delaminated regions require less time to come to rest than those of non-delaminated specimens through structural dampening.

In ANSYS, a macromechanical behavior of composites approach is used and assumes each specimen is a solid body. The found material properties from material testing in chapter 2 (Table 2-1) were manually entered into ANSYSs' engineering materials library to be set as a global parameter. SOLID186 elements are a common element type in ANSYS used for modal and transient response and will most likely encompass the majority of the total element count.

It should be noted that cohesive zone techniques will not be used for these delaminated specimens, since cohesive zones are typically used for crack propagation, fracture mechanics, etcetera. Furthermore, ANSYSs' PrePost/ACP module was not used. It is thought that PrePost/ACP is at a higher level of

analysis containing a higher fidelity than what is needed for this study. For modal and transient response, the PrePost/ACP module is not ideal unless this investigation was related to vibrational failure or flutter response in the composite laminates causing damage to the specimens.

4.2.1. Finite Element Model and Analysis Procedures

Each specimen was modeled using Pro/E-Wildfire 4.0, assembled, and saved as a STEP file to be imported into ANSYS Workbench. Once the STEP files is imported in to ANSYS, the ANSYS project schematic can be optimized to suit the analysis strategy and maximize computer usage.

Once ANSYS project schematic is optimized, material properties can be globally assigned. The geometry was opened in ANSYS Design Modeler to add an additional 10 points along the surface to simulate central axis grid for each specimen. This is beneficial because the points do not change the geometry or add mass, though only specify locations to interrogate during post-processing of the FEM. A good example is probing the accelerometer node locations to analyze the response.

Each geometer is constrained in ANSYS allowing to connect solids to each other (see Figure 4-4). The geometry is modeled to be symmetric about the planner centerline (top/bottom are same) aiding in building the constraints for the delaminated zone in each specimen. Then, all surface are bonded around the delaminated area, shown in Figure 4-4. The boundary conditions set in ANSYS are “BONDED” using CONTA174 and TARGE170 elements.

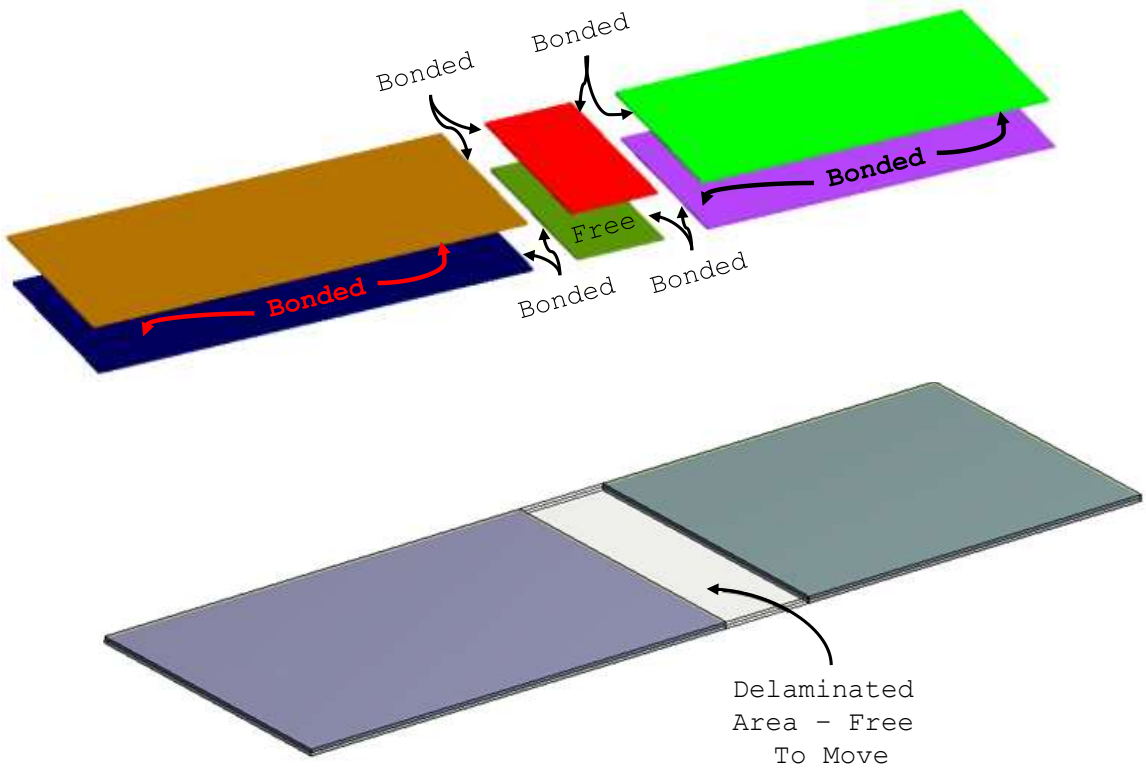

Figure 4-4 Example of connected constraints, similar for each specimen. Example is specimen 5.

CONTA174 are used to represent contact and sliding between 3-D "target" surfaces, such as TARGE170 and a deformable surface. This element has three degrees of freedom at each node allowing translation in the nodal x, y, and z directions. The elements are located on the surfaces of 3-D solid or shell elements (SOLID186), which matches the geometric surface element faces with which it is connected. Contact occurs when the element surface penetrates one of the target segment elements on a specified target surface. If there is no penetration, ANSYS builds an imaginary boundary between mating surfaces. Figure 4-5 shows the ANSYS CONTA174 element type.

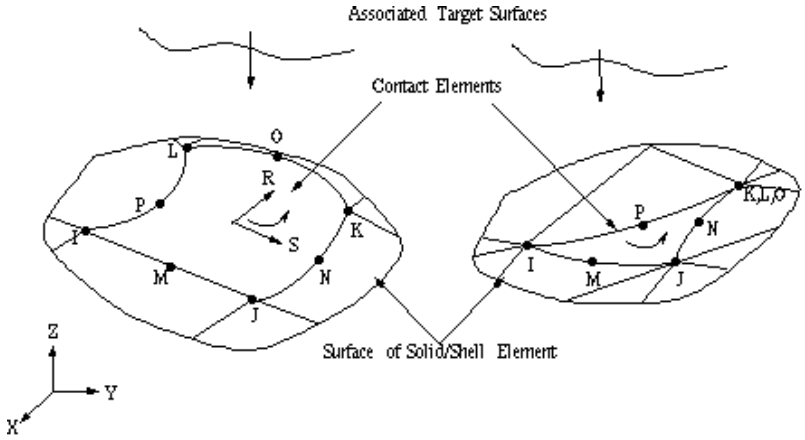

Figure 4-5 ANSYS CONTA174 element type.

TARGE170 elements are used to represent various 3-D "target" surfaces for the associated “contact” elements, such as CONTA174. The contact elements themselves overlay the solid elements bounding the deformable body and are theoretically in contact with the target surface, defined by TARGE170. The target surface is discretized by a set of target elements and paired with its associated contact surface via a shared real constant set. Any translational or rotational displacement on the target segment element are optional; as well as imposing forces and moments on target elements, as required. Figure 4-6 shows the ANSYS TARGE170 element type.

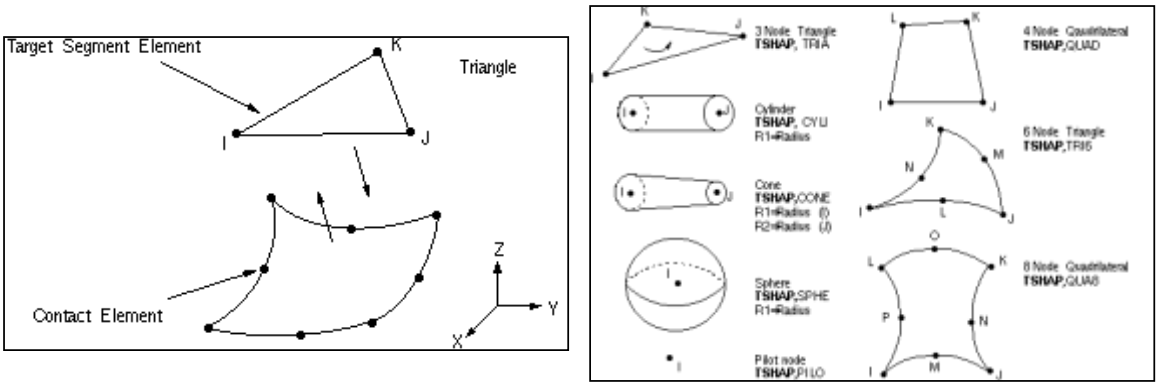

Figure 4-6 ANSYS TARGE170 element type. A shape can be specified based on the geometry of the object or if the “contact” and “target” are two different geometry’s.

SOLID186 elements (see Figure 4-7) were used for all 3D solid specimens, SOLID186 elements are defined by ANSYS as a higher order 3-D element containing 20 nodes and exhibits three degrees of freedom per node; translating in the x, y, and z nodal directions. The element supports plasticity, hyper-elasticity, creep, stress stiffening, large deflection, and large strain capabilities. The total elements used in the course, 0.200 inch tetrahedral mesh for all 3D solid specimens contained 27,053 nodes and 12,827 elements total. The mesh and node count includes the “contact” and “target” elements, respectively.

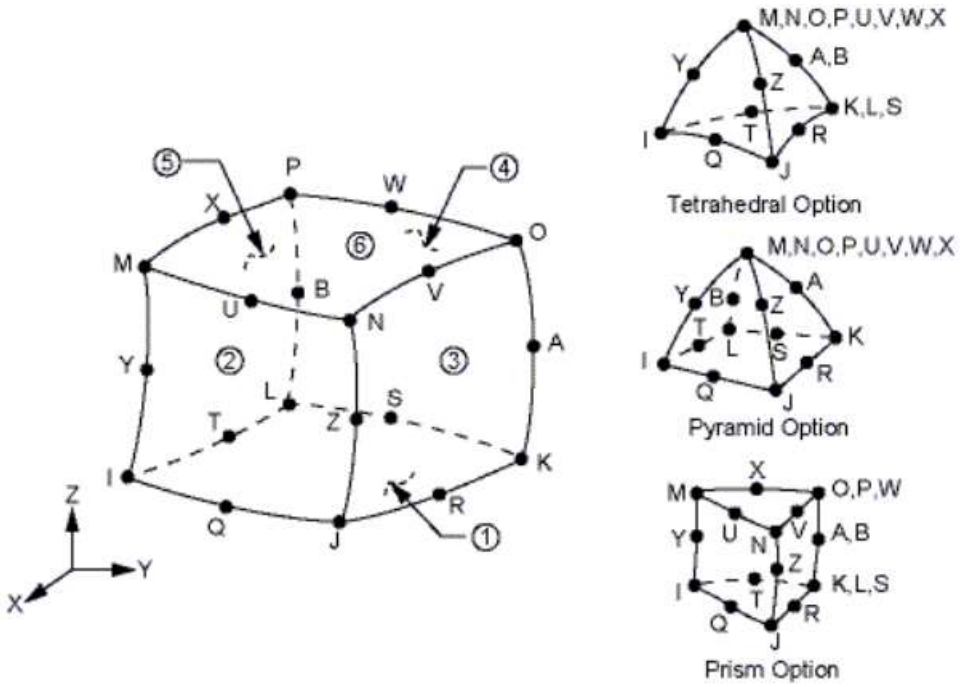

Figure 4-7 ANSYS SOLID186 element type.

Additional boundary conditions used are common to clamping one edge and the rest free, where the fixed support represents the clamped surface. A gravitational constant was included as a global parameter. At this time, modal analysis and mode shapes (MS) can be determined from the given FEM boundary conditions.

The transient response boundary conditions are the same for the modal response analysis, since the modal analysis results are a function of the transient solution. Additionally, a force of 50 pound-force in the y direction was given to the free end to excite the model. Each natural frequency is preselected investigate and the dampening ratios were entered into ANSYSs' solver to understand the local time response. Post-processing the results locally interrogated the known

delaminated zone and compared this to the same zone in an non-delaminated specimen. This allowed for a better understanding of how the damping effected each area, comparatively. The transient response control setup, solution method, and damping ratio inputs are shown in Figure 4-8 and the overall boundary conditions are shown in Figure 4-9.

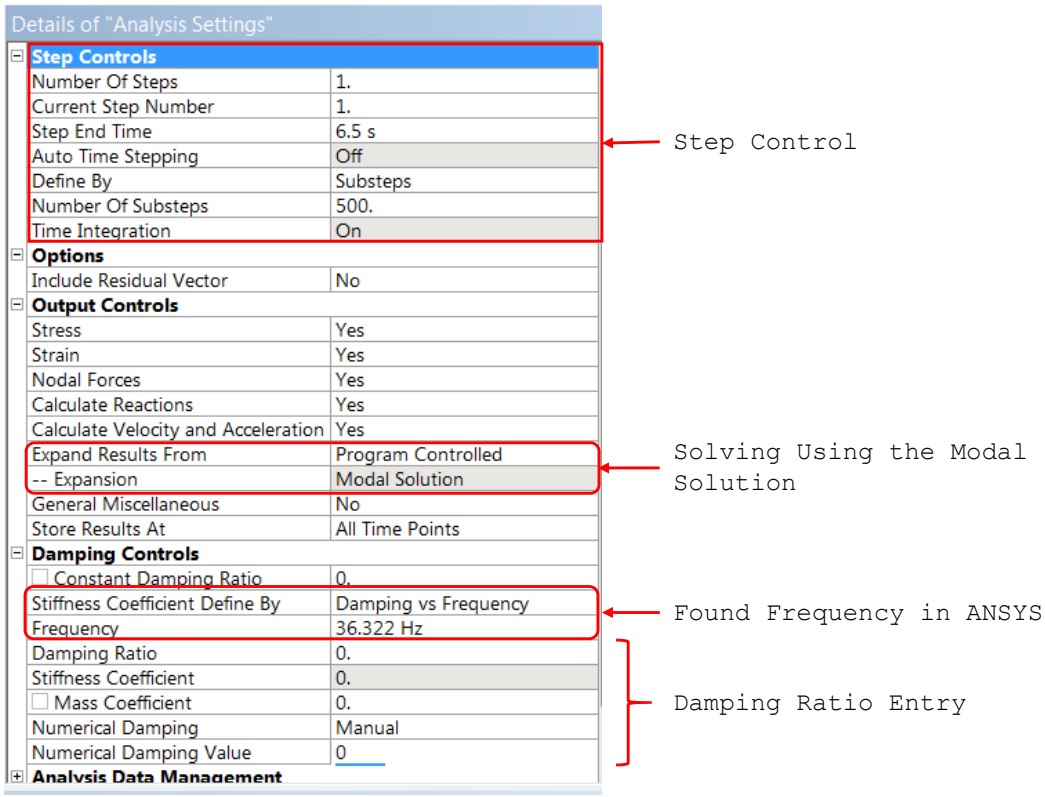

Figure 4-8 Example of transient response control setup.

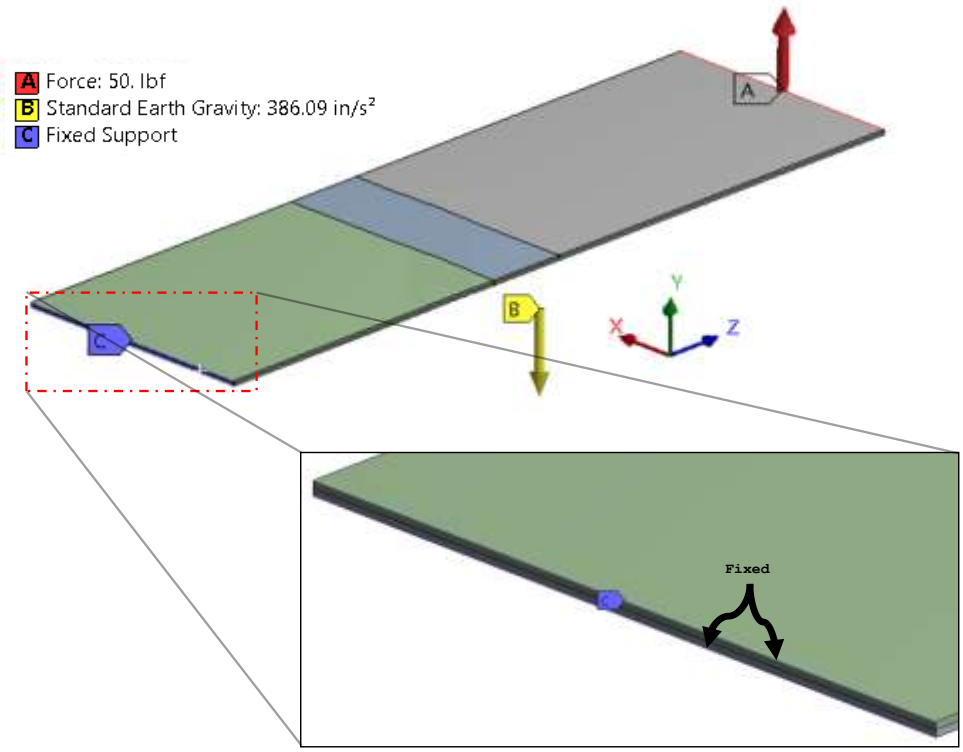

Figure 4-9 Boundary conditions for each test specimen in ANSYS. Fixed on top/bottom line to represent clamping line.

CHAPTER 5

5. NUMERICAL AND EXPERIMENTAL RESULTS DISCUSSION

The numerical and experimental test results of this study are explained, showing a change in amplitude between delaminated and non-delaminated specimens. Similarities and correlations between the experiment and numerical models are highlighted, exhibiting the amplitudes for the delaminated specimens are lower than those of the non-delaminated specimens. Software tools are displayed through their uses.

5.1. Experimental Results

Preliminary plate frequency calculations were conducted to have a foundation of what modes will be found during experimental testing (see appendix [14,40]). The calculated theoretical natural frequencies had a strong correlation between the experimental frequencies of the non-delaminated test specimen with a 4% difference.

It should be noted before discussing the collected experimental data that when looking at the Power Spectrum of a typical vibration signal (Figure 5-1), one thing that can be confusing is the units of the Y axis. For a Power Spectrum, the units are shown as g^2/Hz, or often G_{rms}^2/Hz. In this case, the “rms” is not referencing the rms calculation in the time domain. Rather, it is an indication of the measurement used for the sinusoidal components represented in the Fourier Transform.

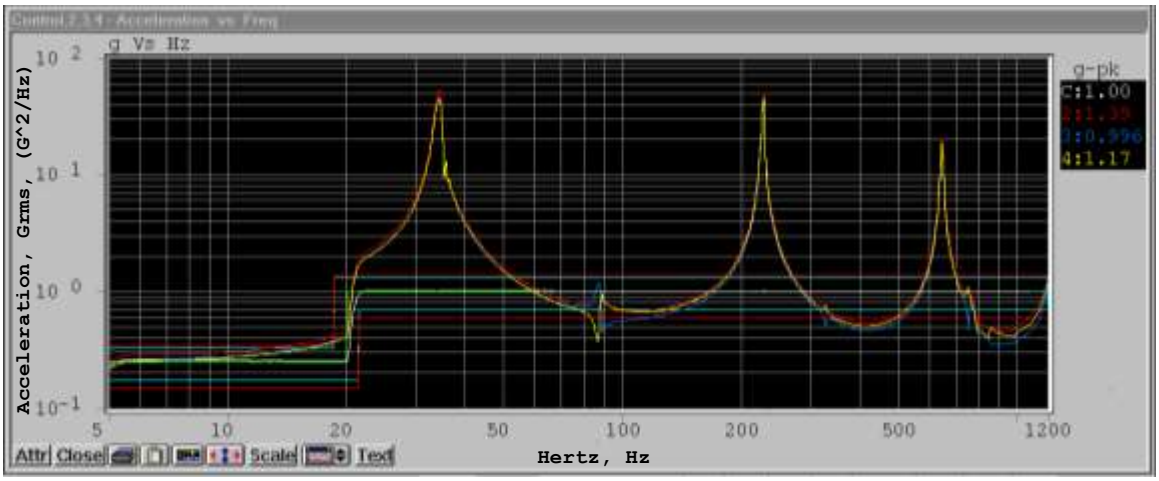

Figure 5-1 Test data example from Unholtz-Dickie shaker software on a log-log scale.

The Fourier Transform of a signal shows the frequency and amplitude of the sine waves that, when summed, would form the time domain signal. If the amplitude of these sine waves is measured as an rms value, then the resultant Y axis units for the Power Spectrum in the frequency domain is G_{rms}^2/Hz. Therefore, amplitude and accelerations are sometimes used synonymously.

Therefore, the data collected was in the form of Microsoft Excel spreadsheets generated by the Unholtz-Dickie shaker software and onboard data acquisition system. The data generates an accelerations (G_{rms}) vs frequency (HZ) graph for each designated test area for each plate, thus consisting of 10 graphs per plate. From the frequency response graphs, the natural frequencies or modes were easily found. The data was organized in Microsoft® Office Excel to generate graphs, calculations, etcetera due to the ease of use and built in calculation scrip's.

For each data point collected, a graph was generated. The absolute difference in peak-amplitudes at each mode in the flexural (axial) directions was analyzed. This aided in addressing two questions; (1) primarily whether delamination can be found across each zone transversely, and (2) whether the two out board accelerometers were needed in discovering the delaminated zones.

It was determined that there was no significant difference between the three accelerometers in each region with respect to natural frequencies and flexural bending modes. This insignificance is due to the two outboard accelerometers (SN10930 and SN10933 respectively, see Figure 3-4) being balanced masses at equal distance about the center line of torsional rotation in the plate during excitation, Therefore, it is safe to assume flexural bending modes are discoverable and that only one accelerometer is needed to find these modes, preferably the central accelerometer (SN10935).

Furthering discovery, it was found when graphing the amplitude data points on a general bar graph that each tested location or zone with respect to the central accelerometer along the grid of each test specimen showed a difference in local amplitude compared to the non-delaminated specimen. More importantly, the graphs showed a visible amplitude change in the delaminated zones for each plate for the first three mode shape, respectively. The amplitude change is due to the fact that damage changes local stiffness and affects the dynamic responses of a structure. In this case the amplitude appears to be a damping effects. The graphs described are shown in Figure 5-2, Figure 5-3, Figure 5-4, and Figure

5-5. The left side of graphs (at the zero x-axis) are the fixed/clamped end and the right side of the graph (10 on the x-axis) are the free end.

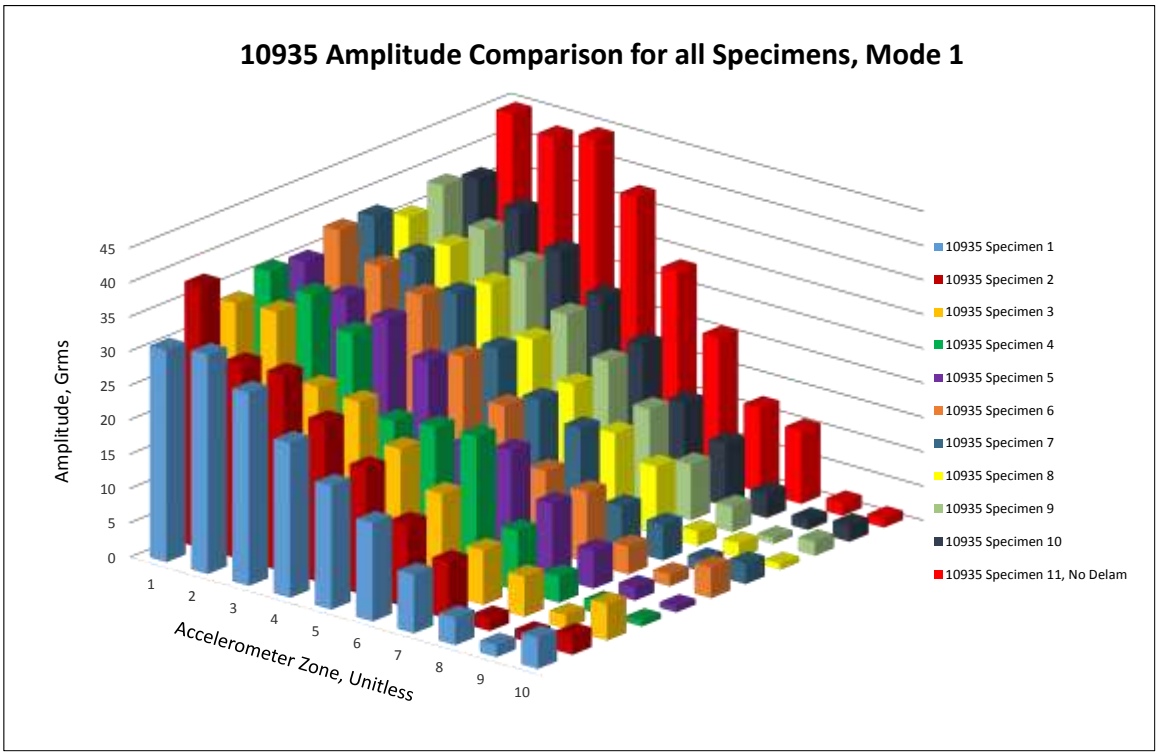

Figure 5-2 Bar graphs showing local amplitude comparison for all specimens for the first natural frequency. All specimens local amplitudes are lower than the non-delaminated specimen. Mode shape is not followed due to delaminated specimens. Amplitude is higher at fixed end due to G_{rms} units.

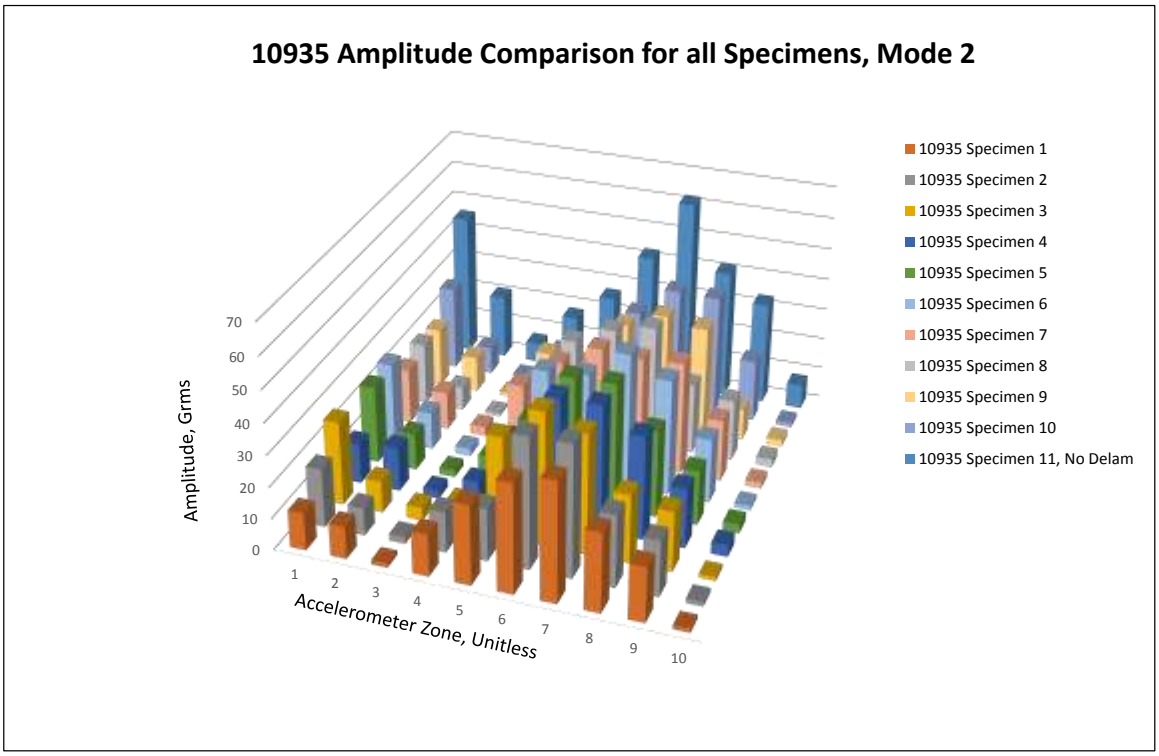

Figure 5-3 Bar graphs showing local amplitude comparison for all specimens for the second natural frequency. All specimens local amplitudes are lower than the non-delaminated specimen. Mode shape is not followed due to delaminated specimens.

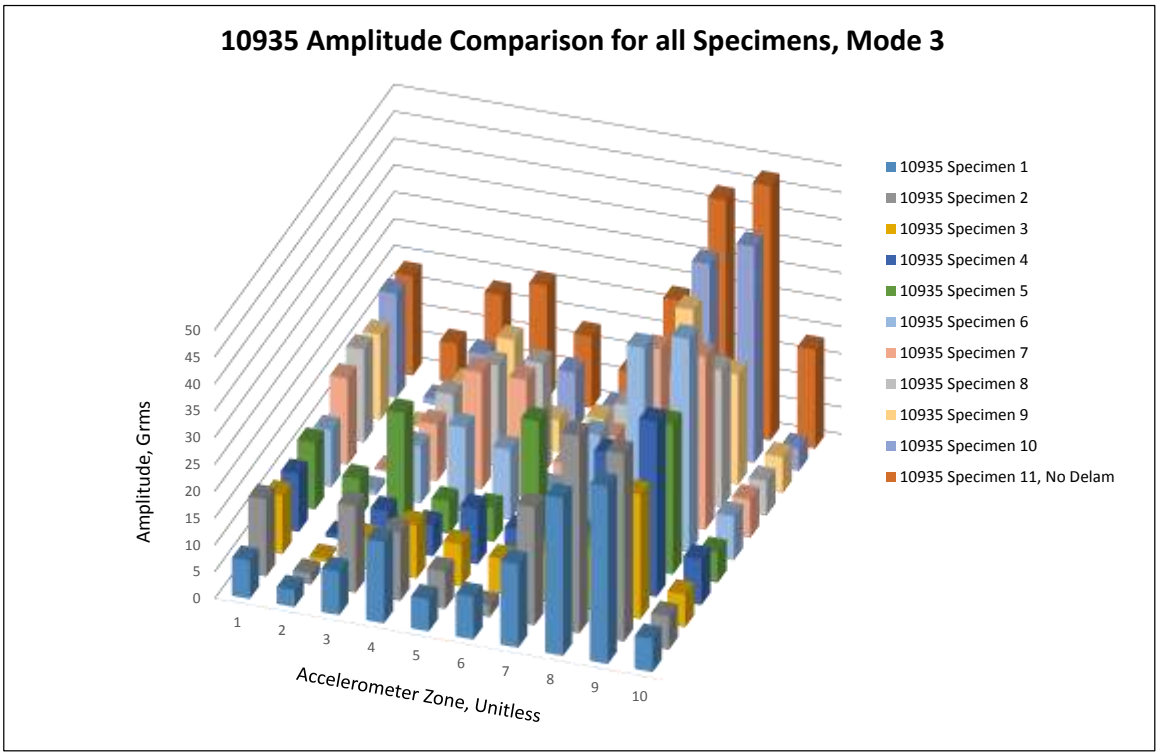

Figure 5-4 Bar graphs showing local amplitude comparison for all specimens for the third natural frequency. All specimens local amplitudes are lower than the non-delaminated specimen. Mode shape is not followed due to delaminated specimens.

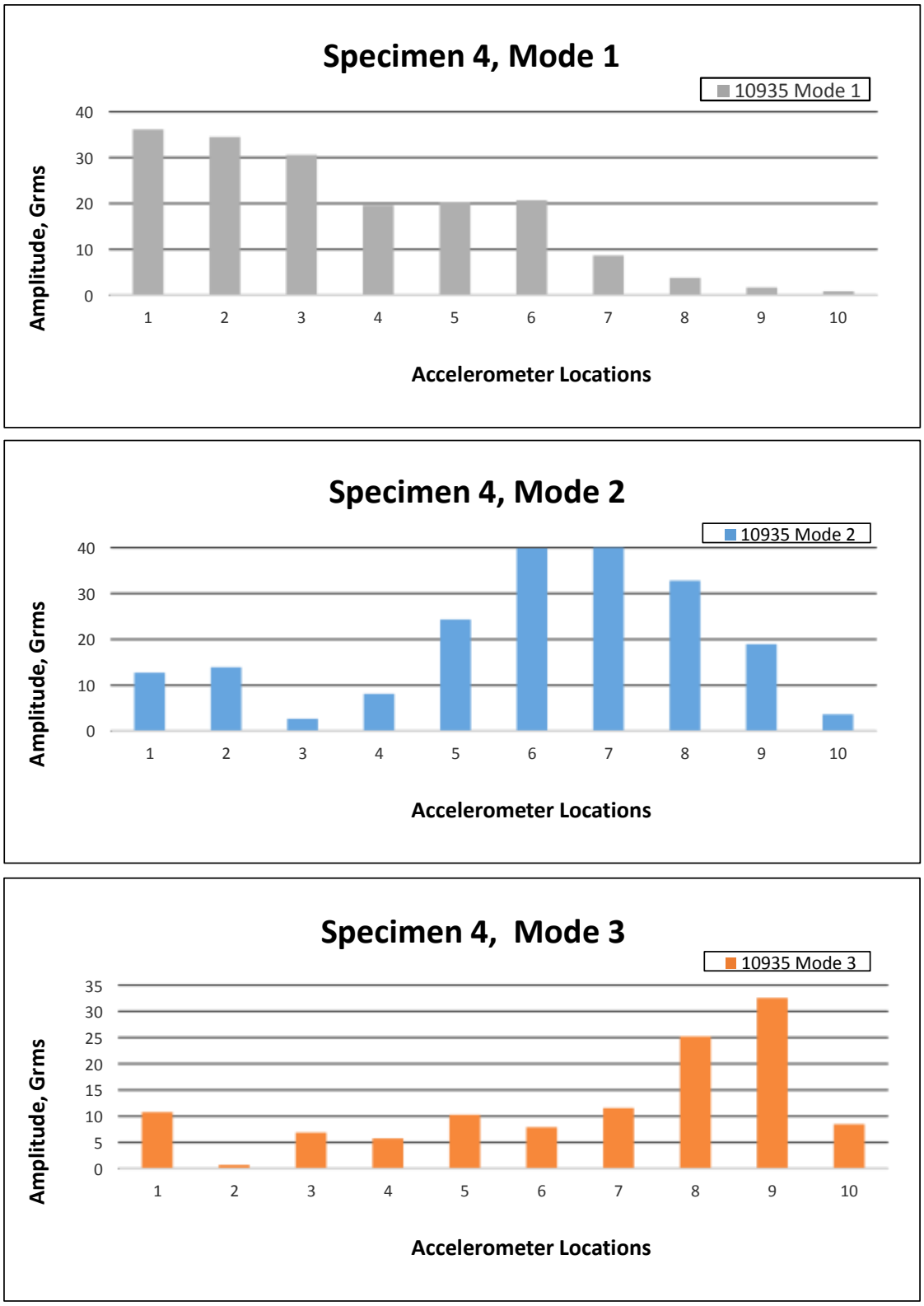

Figure 5-5 Specimen 4, delamination in location/zone 4.

These amplitudes changes in the delaminated zones are evident and meaningful. To be significant and not based on chance, the Shewhart's charts were generated to delineate these occurrences and show that the delaminated areas could be detected using this statistical method. In comparing the tested locations or zones to each other through the Shewhart's charts Excel Macro, the delamination zones become more significant. All the R-charts are in control and data points are within the upper and lower control limits for all mode cases, which defines the X-bar-charts to be a valid representation of the data.

From the Shewhart's charts, Mode 1 X_bar-chart results were most significant showing delaminated zones outside the lower control limit for all cases. Mode 2 and 3 gave scattered results, which may be due to the way the flexural bending modes shapes change the amplitude causing a higher variance. Figure 5-6s' R-chart is in control and X_bar-chart shows the delamination location where the data point is below the lower control limit. The other Shewhart's charts can be found in the appendix.

To further study the local amplitude zones, modal analysis will help show what each mode shape looks like for each specimen. The transient response will show the damping effect between non-delaminated and delaminated plates using the calculated damping ratio. Figure 5-6 compares zone 4 for all specimens relating to mode 1.

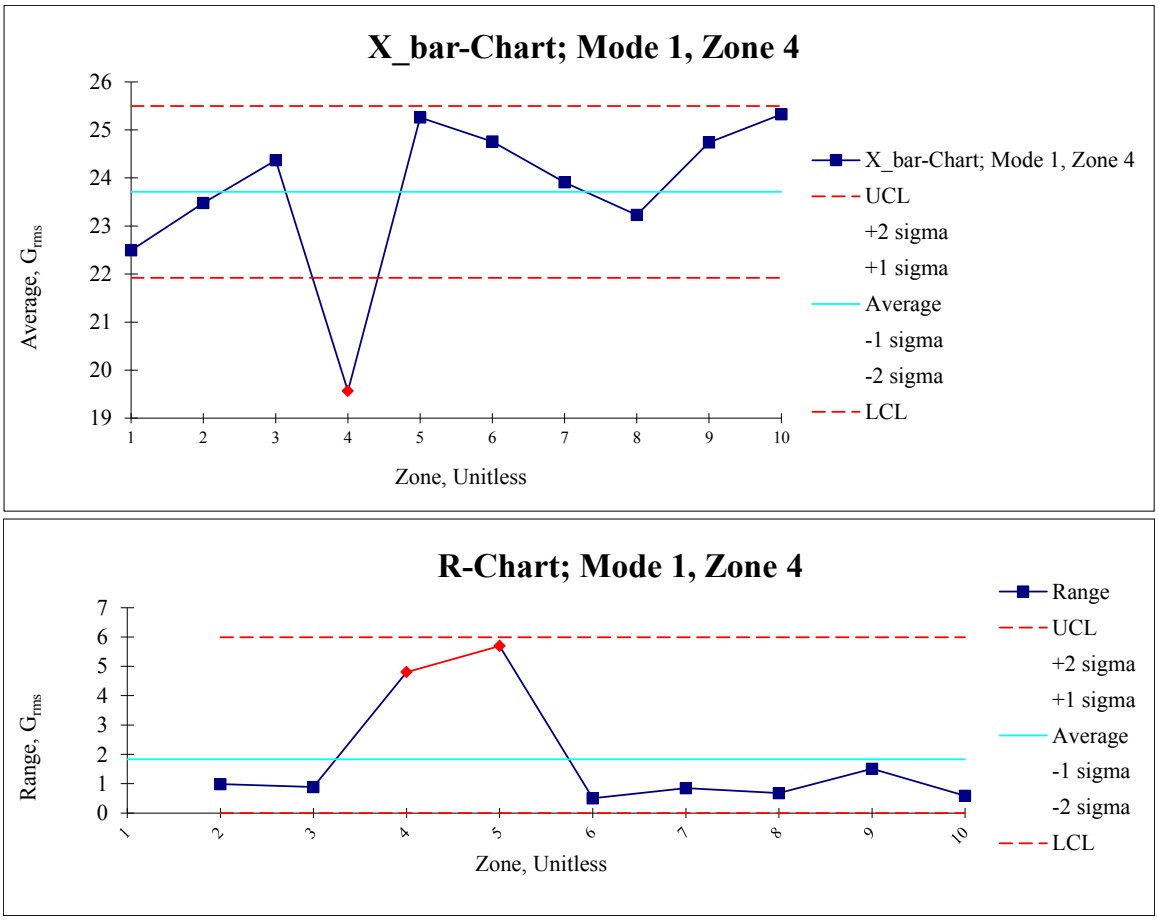

Figure 5-6 Mode 1, zone 4 investigation showing R-chart in control and the X-bar-chart has data point 4 below the lower control limit siting delamination.

5.2. Finite Element Analysis Results

The vibration response was explored further using ANSYS FEA software. The flexural bending mode shapes (MS) were found for each plate, showing that the non-delamination specimen conformed to the theoretical flexural bending MS of the system (see Figure 5-7).

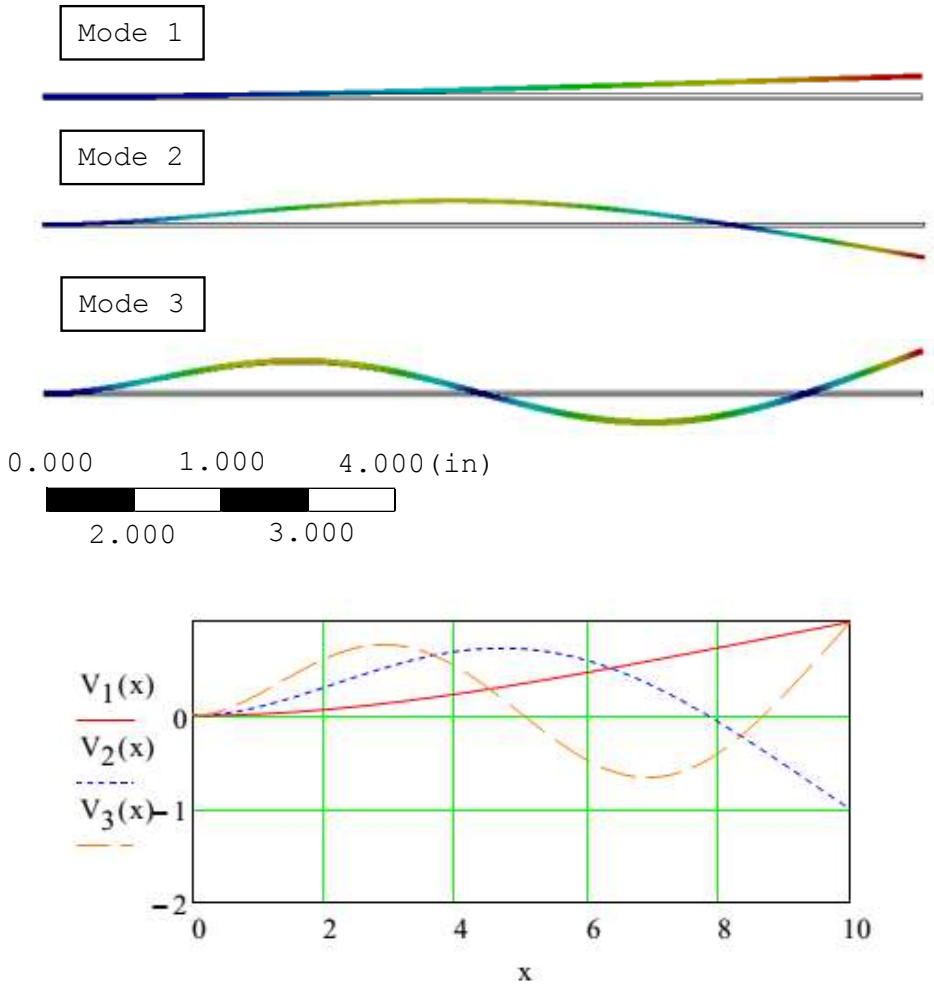

Figure 5-7 Comparison between first three theoretical flexural bending mode shapes (bottom graph) and FE flexural bending mode shapes (top three) of non-delaminated specimen.

The delaminated plates were as predicted, having similar flexural bending MS and natural frequencies seen in Figure 5-8 with characteristics of similar shapes—varying due to the delaminated zone. The percentage error among the samples between the experimental data and the finite element analysis shows an error of no greater than 6.31% shown in Table 5-1 and Figure 5-9. See appendix for additional specimen mode shapes. The 6.31% error could be due to

intersecting nodes in the mesh, mesh refinement, and/or possibly mode shape distortion in the experimental data.

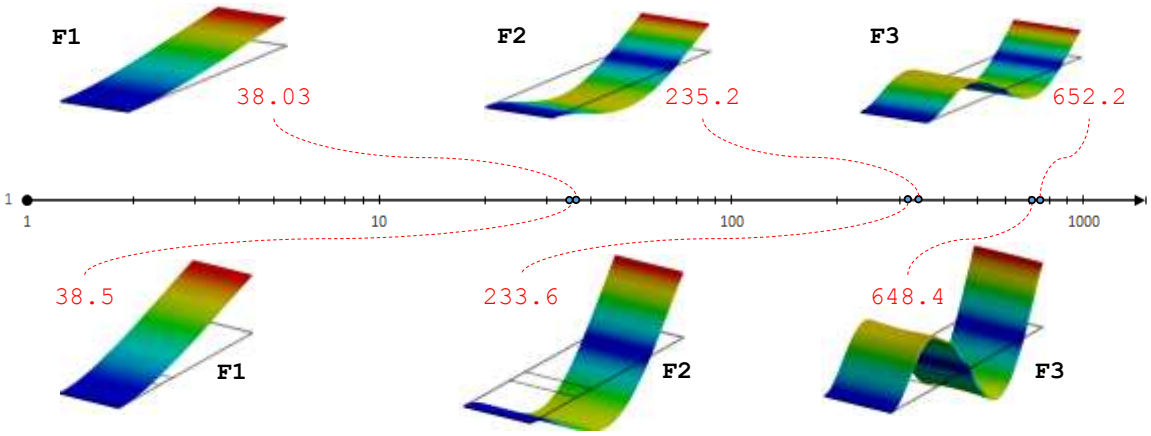

Figure 5-8 Vibrational flexural bending mode shapes for cantilever plates (top: non-delamination, bottom: specimen 6). The accelerometer resonance frequencies (in red) are indicated on the log axis and shown near the figure. The letter-number designation indicates the mode type (F = flexural) and order number. Top of axis is the non-delaminated plate; below is the 4 inch delaminated plate.

Table 5-1 Percentage error between experimental data and finite element analysis results.

		Specimen Number (SPEC)										
		No Delam	SPEC 1	SPEC 2	SPEC 3	SPEC 4	SPEC 5	SPEC 6	SPEC 7	SPEC 8	SPEC 9	SPEC 10
ANSYS FEA Results (Hertz)	Mode 1	37.51	35.89	38.07	39.11	38.58	30.19	37.48	37.45	37.41	37.45	37.21
	Mode 2	227.15	221.25	227.98	227.89	235.22	143.81	251.50	227.10	229.92	227.21	226.39
	Mode 3	628.47	619.82	631.35	656.50	669.59	587.67	633.05	628.44	658.31	638.80	623.94
Exper. Accel Data (Hertz)	Mode 1	38.03	36.56	38.85	38.71	38.51	28.90	38.76	38.30	37.40	38.80	38.62
	Mode 2	235.18	222.91	234.51	236.24	233.65	135.70	236.13	235.90	230.15	237.77	237.21
	Mode 3	652.24	617.99	651.02	654.07	648.36	575.16	652.52	657.34	641.30	661.84	660.94
% Error	Mode 1	1.36%	1.85%	2.02%	1.04%	0.19%	4.38%	3.37%	2.24%	0.02%	3.53%	3.72%
	Mode 2	3.47%	0.75%	2.82%	3.60%	0.67%	5.80%	6.31%	3.80%	0.10%	4.54%	4.67%
	Mode 3	3.71%	0.30%	3.07%	0.37%	3.22%	2.15%	3.03%	4.50%	2.62%	3.54%	5.76%

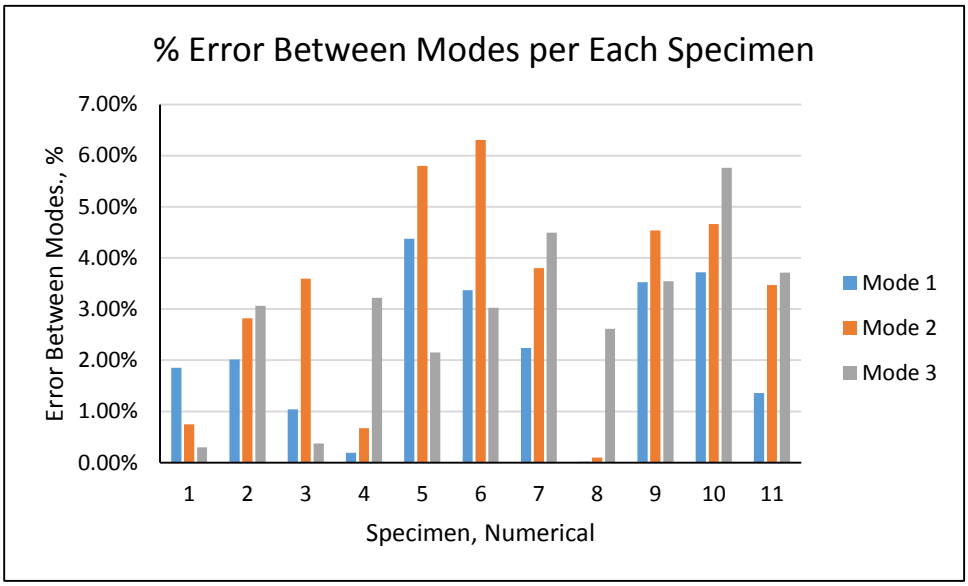

Figure 5-9 % Error for all three modes for each specimen. Specimen 11 is the non-delaminated specimen.

The FE analysis suggests that in each delaminated region for all delaminated specimens there are tension/compression effects in the region due to delaminated ply separation. All specimens show this relationship of tension/compression, which is a common discovery from previous research found in the reference section. This tension/compression would create a damping effect through the plate, which will cause the transient response to slow the plate specimens vibrational response. Figure 5-10 explicitly shows specimen 8 with zone 8 containing a delaminated region.

The transient response was considered for each local delaminated zone of each specimen and compared to the non-delaminated specimen, showing damping effects for each region (see Figure 5-11 and Figure 5-12).

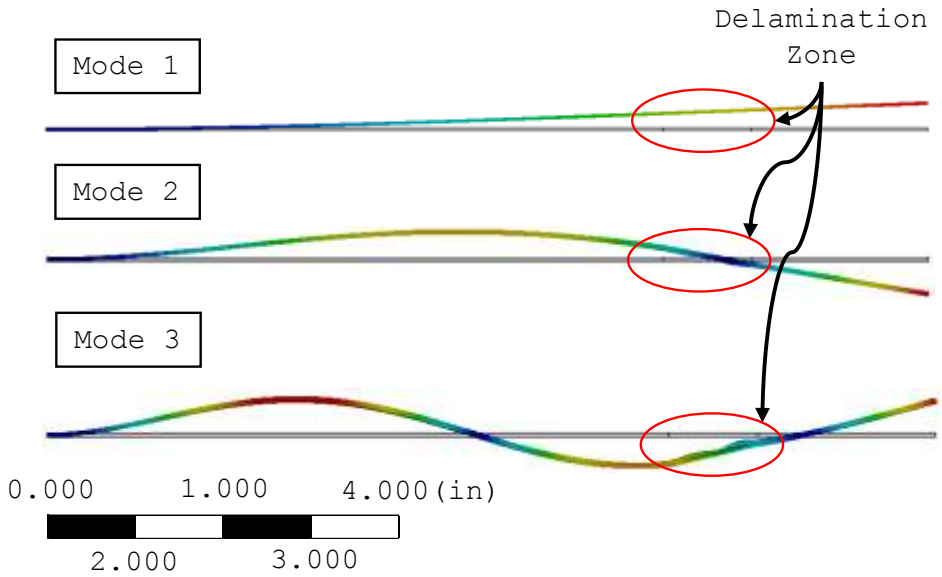

Figure 5-10 First three flexural bending mode shapes for specimen 8, delamination in zone 8.

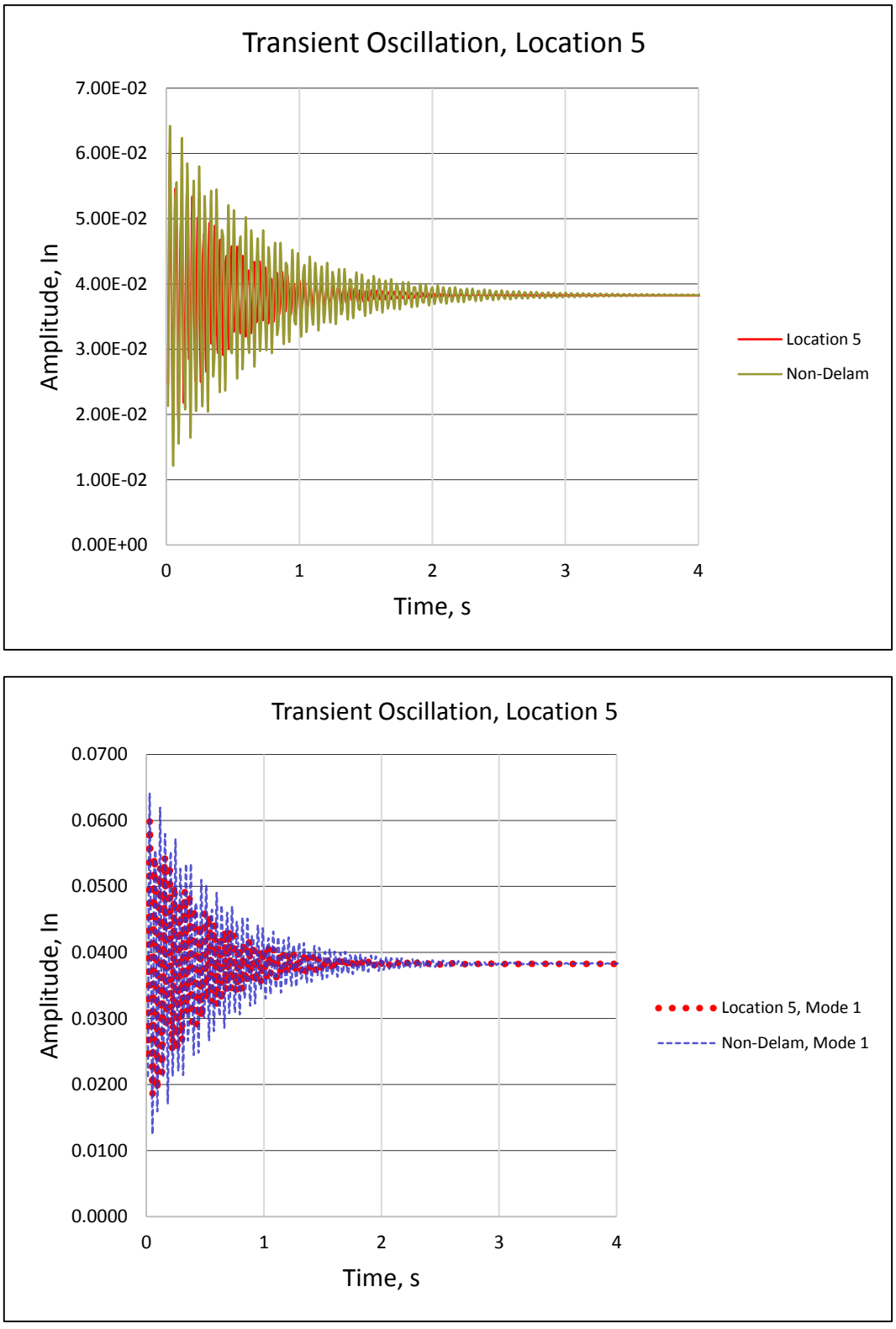

Figure 5-11 Transient response for specimen 5, mode 1.

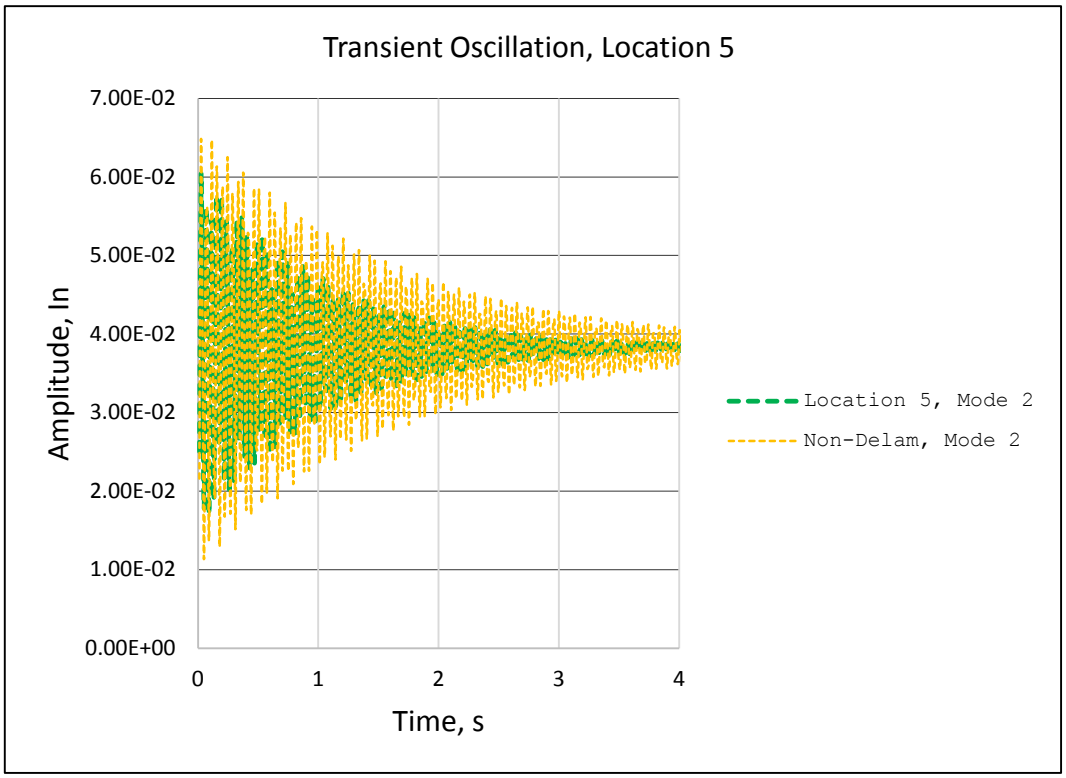

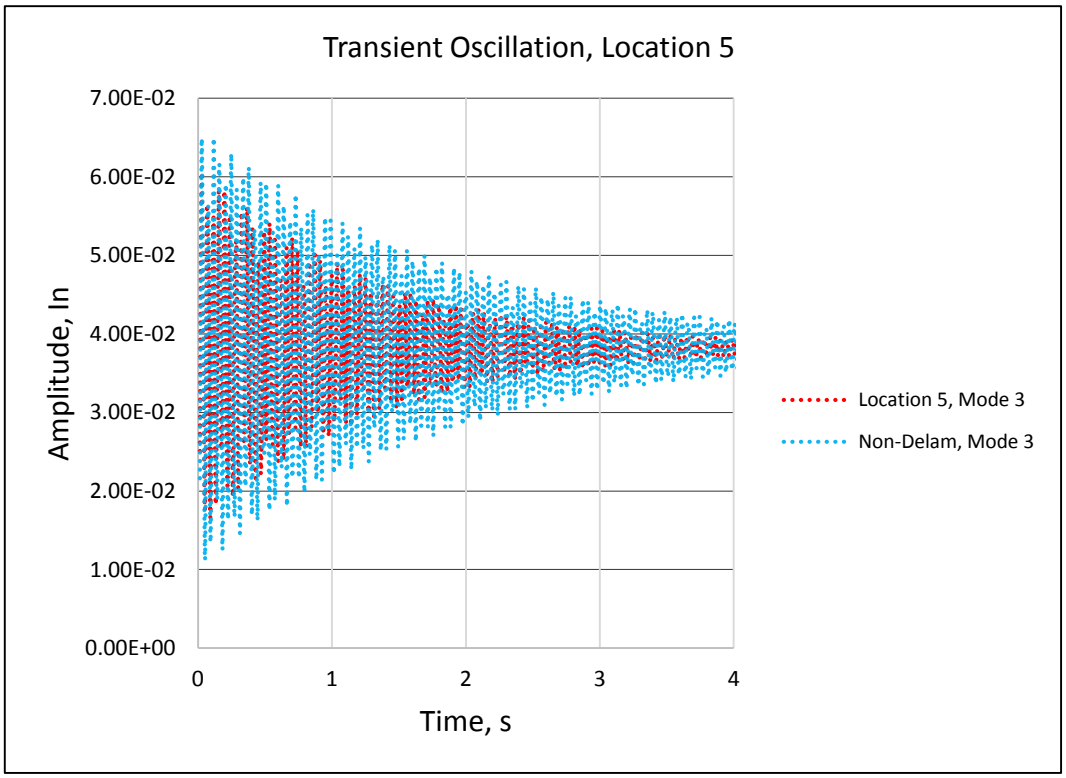

Figure 5-12 Transient response for specimen 5, mode 2-3

CHAPTER 6

6. CONCLUSION AND FUTURE RECOMMENDATIONS

This section concludes the thesis with elaborating on the results, emphasizing major results, and commenting on possible future recommendations.

6.1. Conclusion

The primary purpose of this thesis is to investigate the ability to locate delamination in composite laminate plates under dynamic loading and show a possible use of accelerometers as an alternative method of structural health monitoring in composite structures. An Unholtz-Dickie shaker system excited the specimens to develop a frequency response function. Dynamic response measurements using teardrop style piezoelectric accelerometers were taken along the surface face of each specimen, analyzing the frequency response functions and flexural bending modes. Each response was compared collectively to examine any acceleration differences and damping between specimens through the use of a Shewhart's control chart. Finite element analysis ensured correlation of the flexural bending mode shapes between theoretical, analytical, and experimental. The transient response function and half-power bandwidth damping ratio were also used to address damping within the delaminated specimens utilizing ANSYS finite element analysis software.

Between the data collected and various avenues of post processing, it has been found that accelerometers can be used to detect delamination in dynamically excited composite laminate materials. Between the FEA and the

experimental data, each mode shape's natural frequency were in agreement within 6.31% error or less; concluding that the FEA boundary conditions and material properties where sound.

In this study, a Shewhart's control chart was used to interrogate the first three flexural bending modes, effectively aiding in locating local area delamination of each delaminated specimen for mode 1. The control charts expressed an outlier outside the upper and lower control limits, defining one data point is significantly out of control (larger than 3-sigmas) and concludes that a delaminated area is located 100% of the time for Mode 1. Mode 1 is an important mode to monitor, especially for performance in vehicles such as aircraft and sport cars. For example, during flight testing of a new aircraft, it is typical to induce a dynamic signal into a structure that has a range of 1-50 Hertz. The higher bending flexural modes (mode 2 or higher) typically effect life cycle and fatigue. A Shewhart's control chart is a good statistical tool to use, aiding in finding amplitude changes (G_{rms} in this case) between zone locations for mode 1 of bending flexural modes.

Damping in the plates were discovered in the delaminated regions through an acceleration amplitude investigation at each flexural bending mode. The delaminated area induced relaxed stiffness globally, resulting in a damping effect. Evidence of this was found in the finite element analysis with extreme tension/compression through the delaminated zones. It is conclusive that the methods used throughout this study successfully located and identified delamination in composite laminate specimens.

It would be suggested that this method be tested in a maintenance setting. Maintenance crews for aircraft or other composite structured bodies could use this analysis to monitor failing areas over time or investigate known areas that fail with control charts and data point. The benefits are that through varying the location of the accelerometers, the first mode can render a damping effect and an amplitude change is easily visible through excitation. The benefit of using control charts are that they are easy to understand, quickly generate significant results, and requires minimal training to learn.

6.2. Future Considerations

Though it is not believed that the accelerometers mass used in this experiment had any bearing on the results, it might be interesting to repeat the experiment using MEMS accelerometers in place of the existing accelerometers used. This would minimize weight and come closer to looking purely at the plate itself. Another study that may have higher fidelity would be to use a 3-D laser vibrometer. This area of research in terms of detecting delamination is currently being conducted with great success. Varying the size, location, clamping style, bolted panels, and depth in the composite laminate plies may alter what was currently found and would be a viable next step to this study. Conducting a blind test on a group of specimens would be beneficial, as well.

REFERENCES

[1] Reddy, J.N. *Mechanics of Laminate Composite Plates and Shells: Theory and Analysis, 2nd Ed*. Florida: CRC Press LLC, 2004. Print.

[2] Federal Aviation Administration. *Aviation Maintenance Technician Handbook – Airframe Volume 1*. United States Department of Transportation, 2012. Print.

[3] Mathews, Bob. *Applied Stress Analysis section XI – Composite Materials (Analysis)*. Web Structsource, 1999-2013. Web 13, Jan. 2015. <http://www.structsource.com>.

[4] Sterkenburg, Ronald. "AT 27200 Introduction to Composite Technology." Purdue University. Niswonger Aviattion Technology Building RM 157, Composites Labratory, West Lafayette, IN. 15 December 2011. Course Instructor.

[5] Carter, J. "Effects of Low Velocity Impact on the Strength of Composite Sandwich Structures." Digital Commons. 25 Nov 2014. Web. 20 Jan 2015

[6] D3410: Standard Test Method for Compressive Properties of Polymer Matrix Composite Materials with Unsupported Gage Section by Shear Loading. ASTM.

[7] D3039: Standard Test Method for Tensile Properties of Polymer Matrix Composite Materials. ASTM.

[8] D2584: Standard Test Method for Ignition Loss of Cured Reinforced Resins. ASTM.

[9] Floor Vibrations. (n.d.). In Encyclopedia for UK steel construction. Retrieved from <http://www.steelconstruction.info/>

[10] Clements, Richard. *Low-collateral Damage Bone: New Weapon in the B-1's Arsenal.* Web The Aviationist, 03 Feb. 2012. Web 04, Feb. 2015. <http://theaviationist.com/>.

[11] Adams, Donald F.. *Thickness-tapered unidirectional composite specimens.* Web Composites World, 01 Jul. 2013. Web 21 Jan. 2015. <http.//compositesworld.com/>

[12] Adams, Donald F.. *Unidirectional composite axial tensile specimens*. Web Composites World, 01 Jan. 2006. Web 21 Jan. 2-15. <http.//compositesworld.com/>

[13] MATLAB, MathWorks, R2011b

[14] Mathcad 15.0, Parametric Technologies Corporation., MC15 M030

[15] ANSYS® Workbench™ Framework, ANSYS Inc., 16.0.0.780908

[16] Ousset Y, Roudolff F. *Numerical analysis of delamination in multi-layered composite plates.* Comput Mech 2000;20(1/2):122–6.

[17] Zak A, Krawczuk M, Ostachowicz W. *Numerical and experimental investigation of free vibration of multi-layer delaminated composite beams and plates.* Comput Mech 2000;26:215–309

[18] Yoon M. K., Heider D., Gillespie Jr. J. W., Krauthauser C., "Damage Detection in Large-Scale Composite Structures via Vibration Technique Using MEMS Accelerometers," Journal of Sound and Vibration," SAMPE Conference, Vol. 49, pp. 1913-1927.

[19] Ramkumar RL, Kulkarni SV, Pipes RB., 1979, *Free Vibration Frequencies of a Delaminated Beam.* Society of Plastics Industry, 22-E1–5

[20] Wang JTS, Liu YY, Gibby JA, 1982, *Vibration of Split Beams*. Journal of Sound and Vibration, 4 (84) 491–502

[21] Mujumdar P.M. and Suryanarayan, 1988, *Flexural vibrations of beams with delamination*. Journal of Sound and Vibration, 125 (3) , 441-461

[22] Hu, Jian Shiun and Chyanbin, 1995, *Free Vibration of Delaminated Composite Sandwich Beams*. AIAA Journal, 10(33)

[23] Yin WL, Jane KC., 1988, *Vibration of a Delaminated Beam-plate Relative to Buckled States*. In Proceedings of AIAA/ASME/ASCE/AHS/ASC 29th SDM Conference, Williamsburg, VA, 860-870.

[24] Chen HP, Goggin P., 1992, *Free Vibration of a Compressed Delaminated Plate.* Proceedings of AIAA/ASME/ASCE/AHS/ASC 33rd SDM Conference, Dallas, TX, 1830-1840.

[25] M.H. Shen and J.E. Grady, 1992. *Free Vibrations of Delaminated Beams.* AIAA Journal 30(5), 1361-1370

[26] Singh, Amit Kumar, 2010, *Effect of Vibration on Delaminated Beams*. Thesis submitted to National Institute of Technology Rourkela,769008

[27] D.Shu and H.Fan, 1996, *Free Vibration of Biomaterial Split Beam*. Composites: Part B, 1(27B)79–84

[28] Della, C. N. and Shu, D., 2009, *Free Vibration Analysis of Multiple Delaminated Beams under Axial Compressive Load.* Journal of Reinforced Plastics and Composites,11(28) 1356-1381

[29] Krawczuk M, Ostachowicz W, Zuk A., 1996, *Analysis of Natural Frequencies of Delaminated Composite Beams Based on Finite Element Method.* Structural Engineering and Mechanics (4)243-55.

[30] Wahyu Lestari' and Sathya Hanagud, 1999, *Health Monitoring of Structures - Multiple Delamination Dynamics in Composite Beams.* American Institute of Aeronautics & Astronautics, A99-24831

[31] Della, C. N. and Shu, D. 2006, *Vibration of Delaminated Multilayer Beams*. Composites Part B: Engineering, 2-3 (37) 227–236

[32] D. Shu and H. Fan, 1996, *Free Vibration of Biomaterial Split Beam.* Composites: Part B, 1(27B)79–84

[33] D. Shu, 1995, *Vibration of Sandwich Beams with Double Delamination's.* Composites Service and Technology, (54) 101-109

[34] Christian Della and Dongwei Shu, 2005, *Vibration of Beams with Double Delamination's*. Journal of Sound and Vibration, 3(282) 919 - 935

[35] Christian N. Della, Dongwei Shu , Yapu Zhao, 2005, *Vibration of Composite Beams With Two Overlapping Delamination's.* Acta Mechanica Sinica, 1(21)47 – 55

[36] Y. Zou, L. Tong and G. P. Steven, 2000, *Vibration-based Model-dependent Damage (Delamination) Identification and Health Monitoring For Composite Structures--A Review*. Journal of Sound and Vibration, 2(230), 375-378

[37] Unholtz-Dickie Corporation. Cal Poly San Luis Obispo, CA. *Test Vibration System: SAB15-S202/ST SO#7091,S/N355*. March, 2006.

[38] VIP Sensors. Online Catalog, 2007. Web. 08 Mar. 2015. <http://www.vipsensors.com/>

[39] PCB Piezotronics, Vibration Division. Online Catalog, 2011. Web. 08 Mar. 2015. <http://www.pcb.com/>

[40] C. M. Harris and A. G. Piersol. *Harris' Shock and Vibration Handbook.* McGraw-Hill, 2002. Printed.

[41] Corum, Christine. "MET 45100 Manufacturing Quality COntrol." Purdue University. West Lafayette, IN. 11 May 2010. Course Instructor.

[42] S.S Russell and M.D. Lansing. "Endoscopic Shearography and Thermography Methods for Non-Destructive Evaluation of Lined Pressure Vessels." *NDT.net.* May, 1999 Vol. No. 5. Web. 05 May 2015. <www.ndt.net>

[43] GE Measurement and Control Business, General Electric Corporation, 2015. Web. 05 May 2015.

APPENDICES

A. PRELIMINARY PLATE FREQUENCY CALCULATION

$L := 10in$ Length of Plate

$b := 3in$ Breadth of Plate

$t := .068in$ Plate Thickness

$w := .134lbf$ Weight of plate

$E_{1,2} = 1.091 \times 10^{7} \cdot psi$ Macro-modulus of Elasticity (Simplified)

$\nu := .3$ Poisson's Ratio

$g = 386.089 \cdot \frac{in}{s^2}$ Gravitational Acceleration

Plate stiffness $k := \frac{E_{1,2} \cdot t^3}{12 \cdot (1 - \nu^2)}$ $k = 314.242 \cdot lbf \cdot in$

Mass per unit area $\rho := \frac{w}{g \cdot L \cdot b}$ $\rho = 1.157 \times 10^{-5} \cdot \frac{lbf \cdot s^2}{in^3}$

Solutions to the Characteristic Equations: $\lambda_k := \begin{pmatrix} 2.121 \\ 5.419 \\ 8.718 \\ 12.016 \\ 15.315 \end{pmatrix}$

Natural Frequency $F_n := \frac{(\lambda_k)^2}{2 \cdot \pi \cdot l^2} \sqrt{\frac{k}{\rho}} = \begin{pmatrix} 37.315 \\ 243.58 \\ 630.431 \\ 1.198 \times 10^3 \\ 1.946 \times 10^3 \end{pmatrix} \frac{1}{s}$

From the solutions to the characteristic equations:

$\lambda_1 := \frac{2.121}{L}$ $\lambda_2 := \frac{5.419}{L}$ $\lambda_3 := \frac{8.718}{L}$

$r := 1 .. 3$ Step size

Resultant equation from the general equation of motion:

$k_r := \frac{\cosh(\lambda_r \cdot L) + \cos(\lambda_r \cdot L)}{\sinh(\lambda_r \cdot L) + \sin(\lambda_r \cdot L)}$

$C := .5$ Amplification Factor

First mode shape using displacement calculation:

$r := 1 \qquad x := 0, 0.01 .. L$

$V_1(x) := C \cdot \left[\cosh(\lambda_r \cdot x) - \cos(\lambda_r \cdot x) - k_r \cdot (\sinh(\lambda_r \cdot x) - \sin(\lambda_r \cdot x)) \right]$

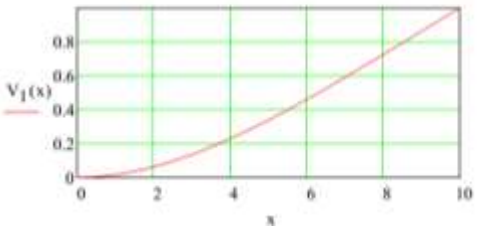

Second mode shape using displacement calculation:

$r := 2 \qquad x := 0, 0.01 .. L$

$V_2(x) := C \cdot \left[\cosh(\lambda_r \cdot x) - \cos(\lambda_r \cdot x) - k_r \cdot (\sinh(\lambda_r \cdot x) - \sin(\lambda_r \cdot x)) \right]$

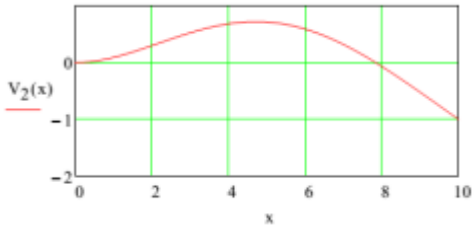

Third mode shape using displacement calculation:

$r := 3 \qquad x := 0, 0.01 .. L$

$V_3(x) := C \cdot \left[\cosh(\lambda_r \cdot x) - \cos(\lambda_r \cdot x) - k_r \cdot (\sinh(\lambda_r \cdot x) - \sin(\lambda_r \cdot x)) \right]$

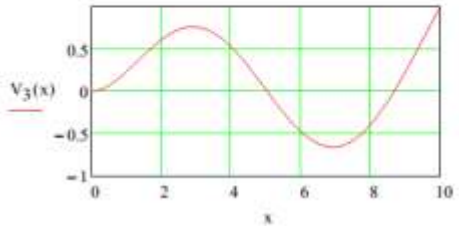

Combined mode shapes:

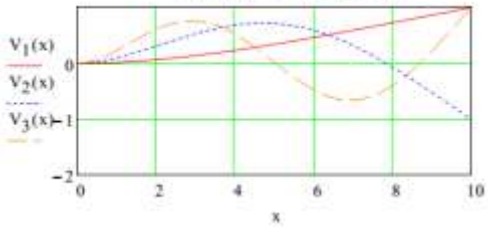

B. UNHOLTZ-DICKIE SHAKER SYSTEM SETUP WINDOWS

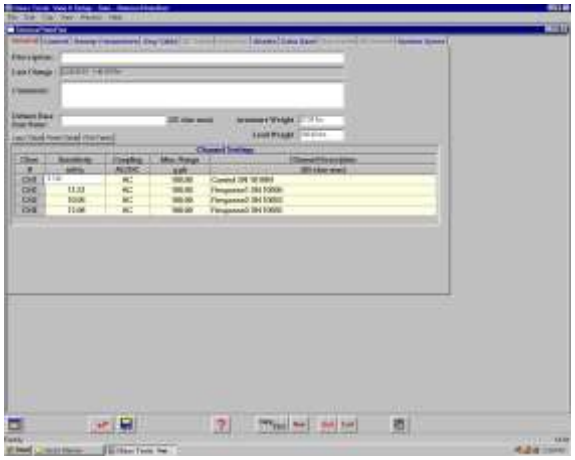

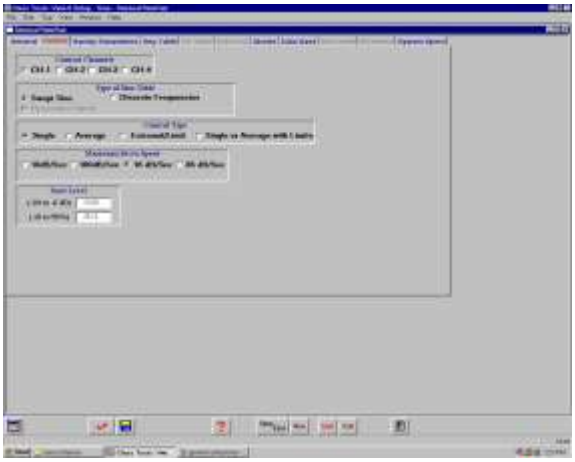

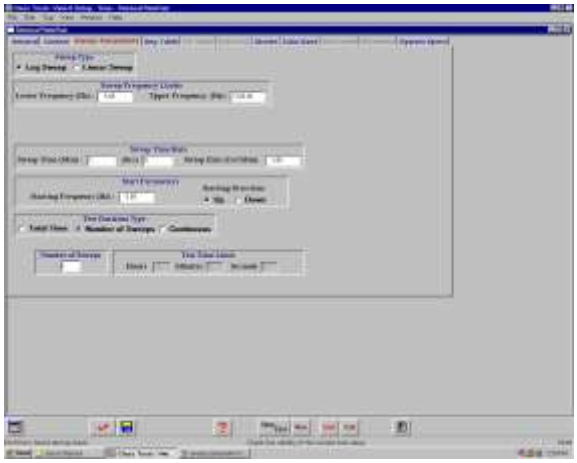

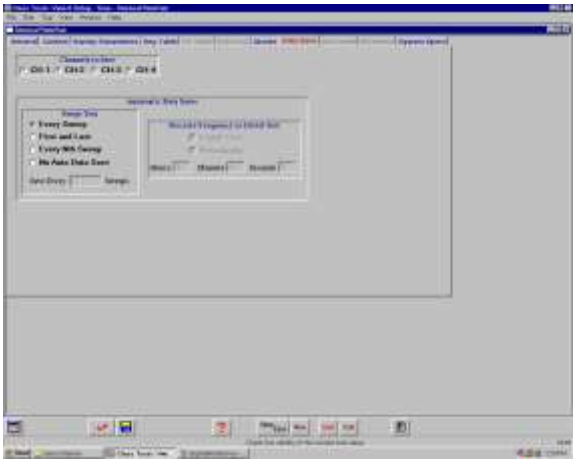

C. FINITE ELEMENT ANALYSIS PLOTS

All Modal Analysis Results.

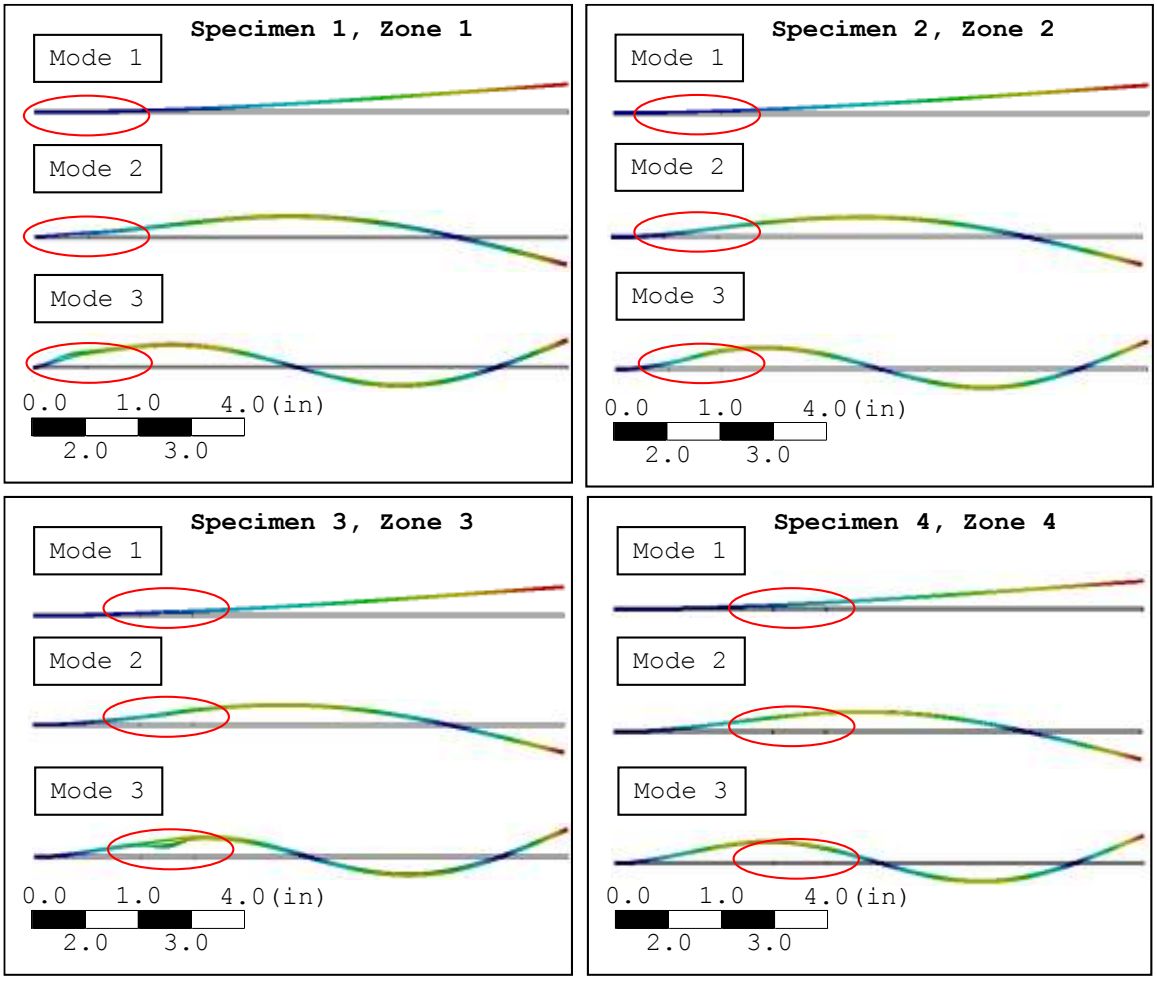

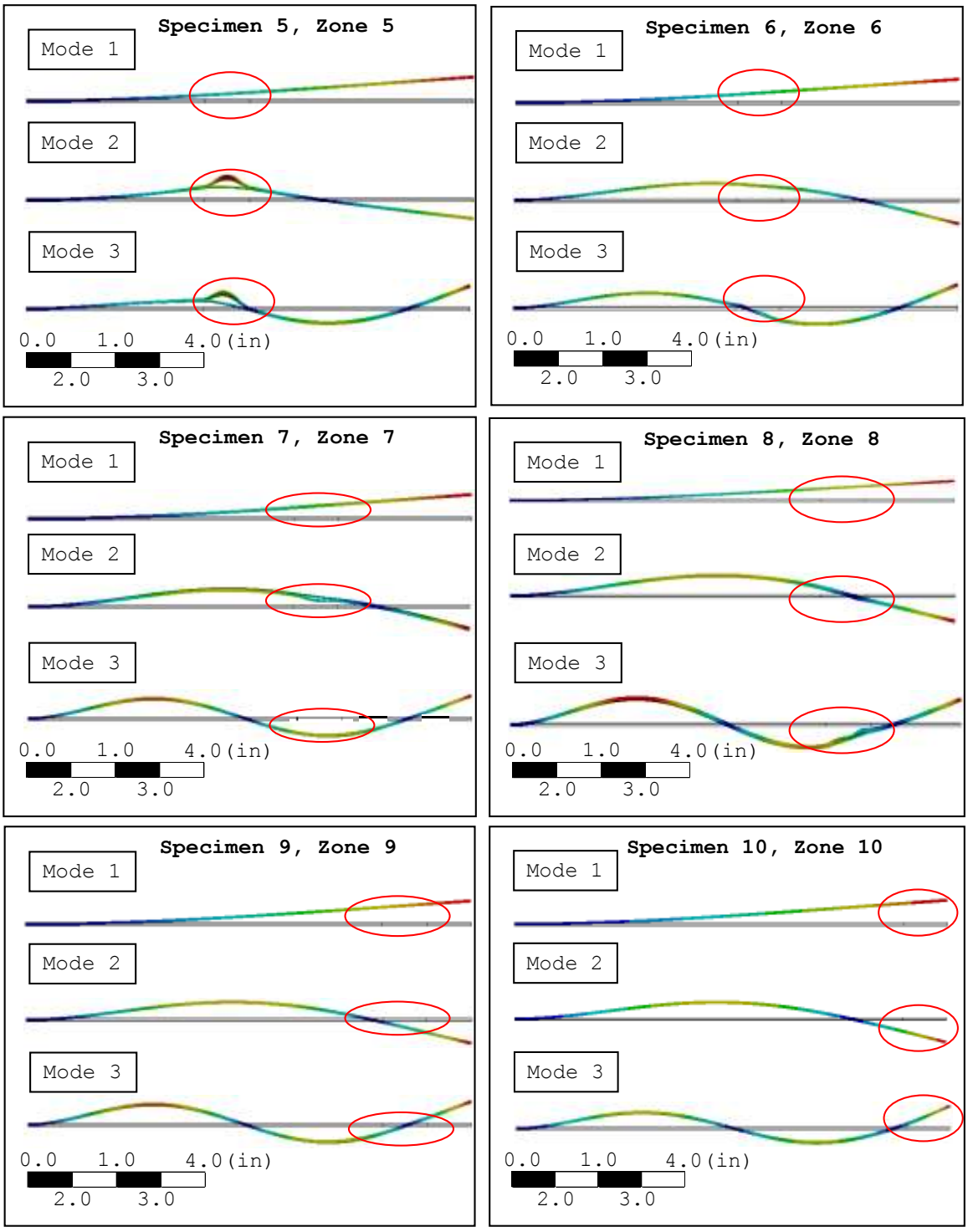
Specimen 5, Zone 5
Mode 1
Mode 2
Mode 3
0.0 1.0 4.0 (in)
2.0 3.0
Specimen 6, Zone 6
Mode 1
Mode 2
Mode 3
0.0 1.0 4.0 (in)
2.0 3.0
Specimen 7, Zone 7
Mode 1
Mode 2
Mode 3
0.0 1.0 4.0 (in)
2.0 3.0
Specimen 8, Zone 8
Mode 1
Mode 2
Mode 3
0.0 1.0 4.0 (in)
2.0 3.0
Specimen 9, Zone 9
Mode 1
Mode 2
Mode 3
0.0 1.0 4.0 (in)
2.0 3.0
Specimen 10, Zone 10
Mode 1
Mode 2
Mode 3
0.0 1.0 4.0 (in)
2.0 3.0

Sub-Sample of Transient Analysis Results: **Location 2**

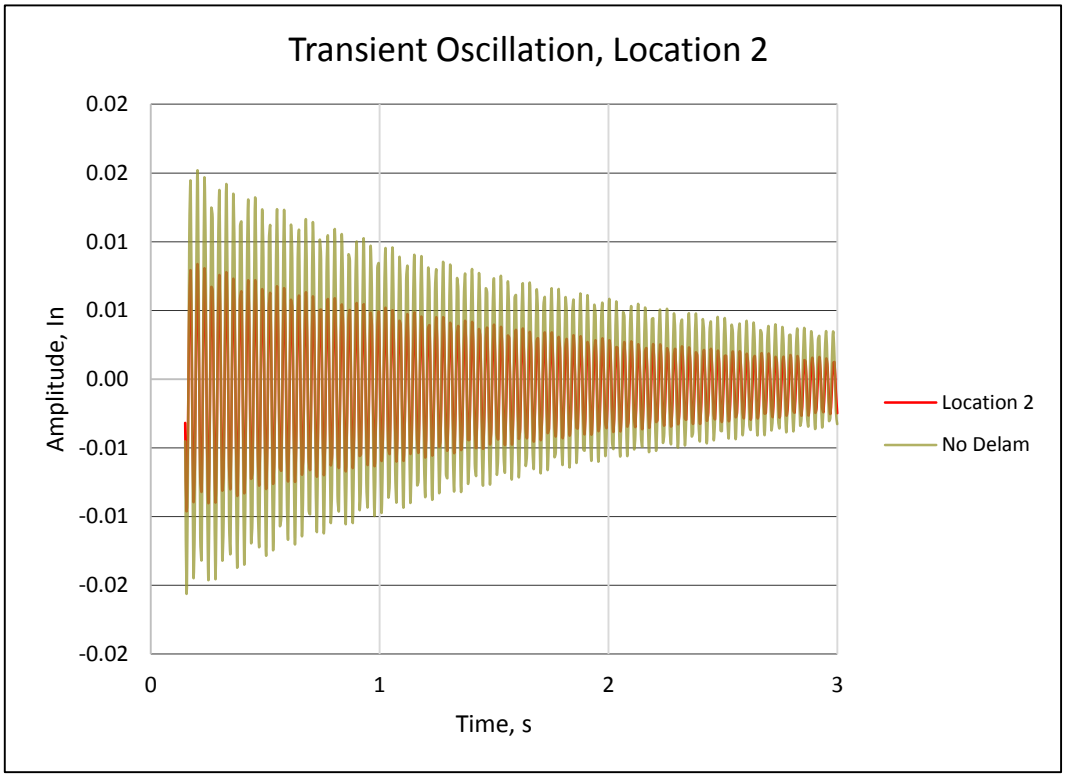

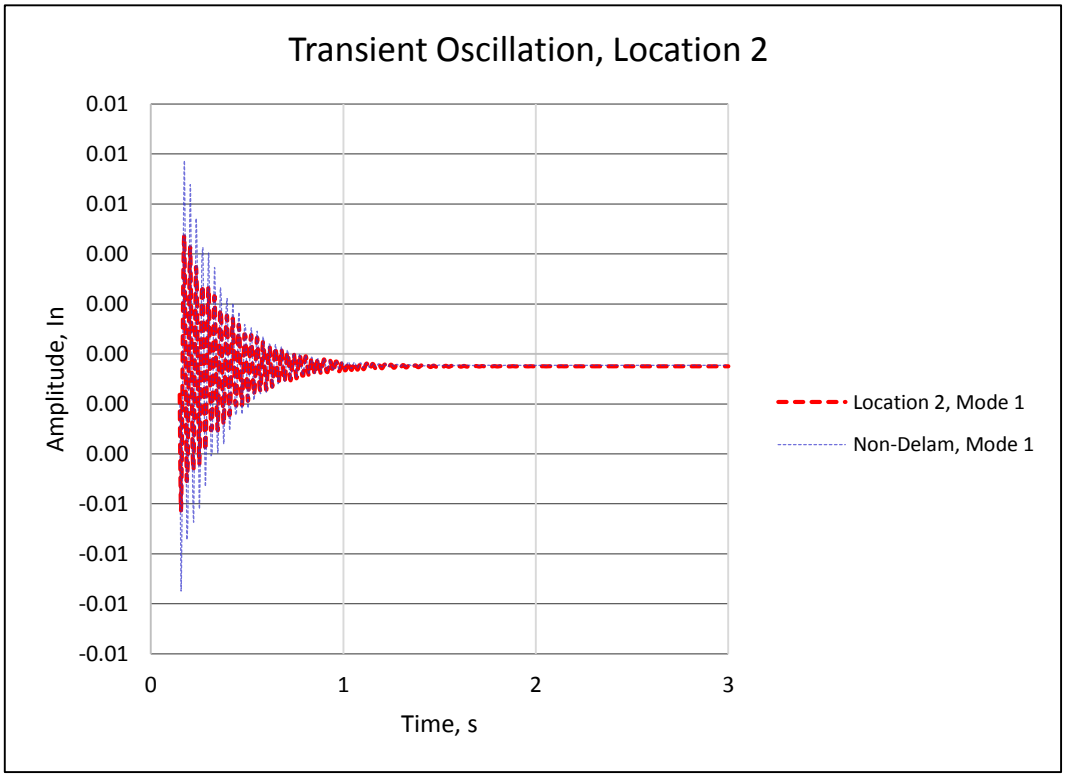

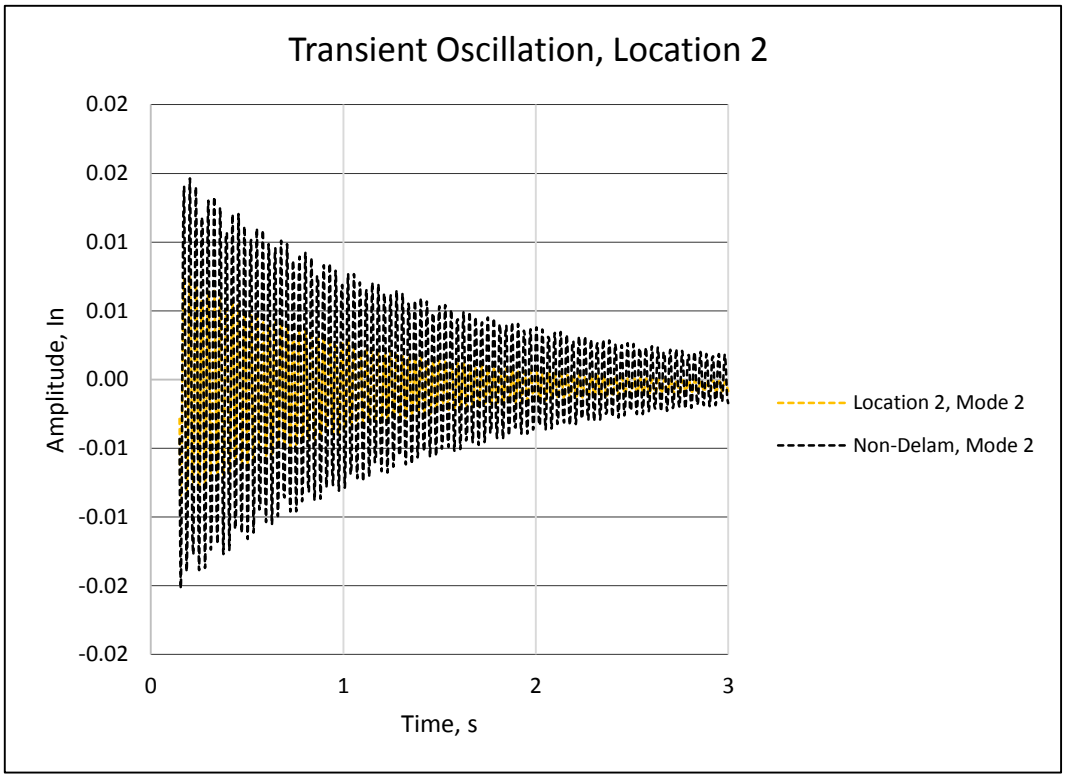
Transient Oscillation, Location 2
Amplitude, ln
0.02
0.02
0.01
0.01
0.00
-0.01
-0.01
-0.02
-0.02
0
1
2
3
Time, s
Location 2, Mode 2
Non-Delam, Mode 2

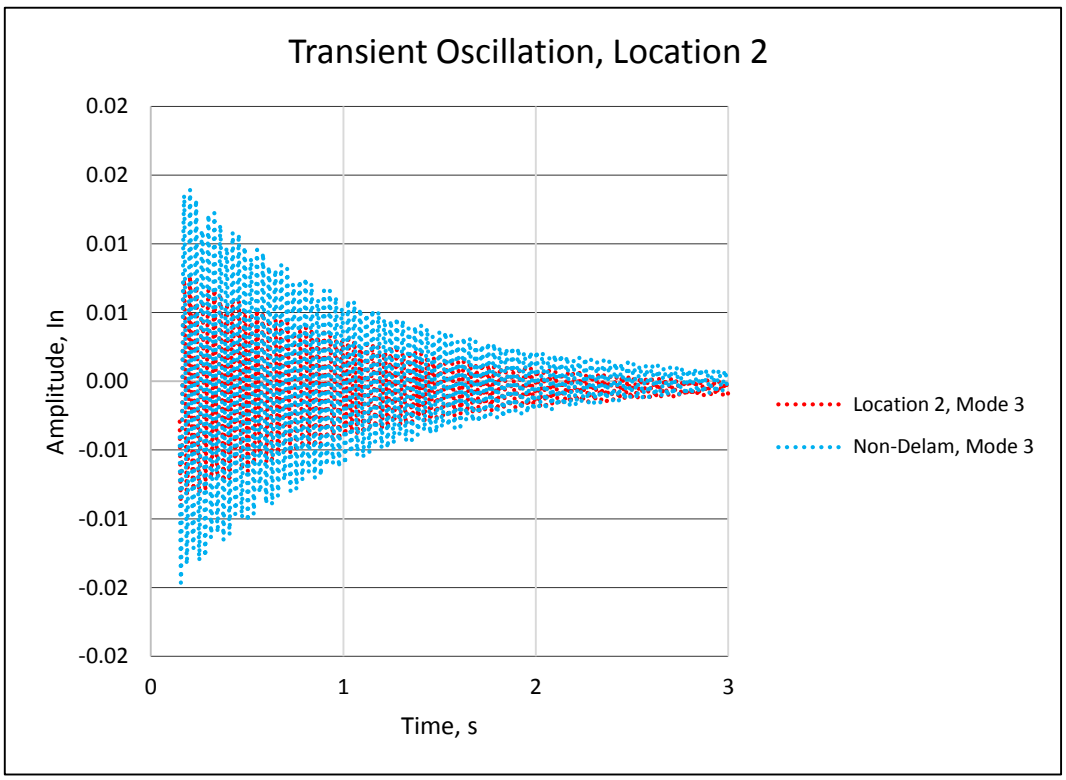
Transient Oscillation, Location 2
Amplitude, ln
0.02
0.02
0.01
0.01
0.00
-0.01
-0.01
-0.02
-0.02
0
1
2
3
Time, s
Location 2, Mode 3
Non-Delam, Mode 3

Location 8

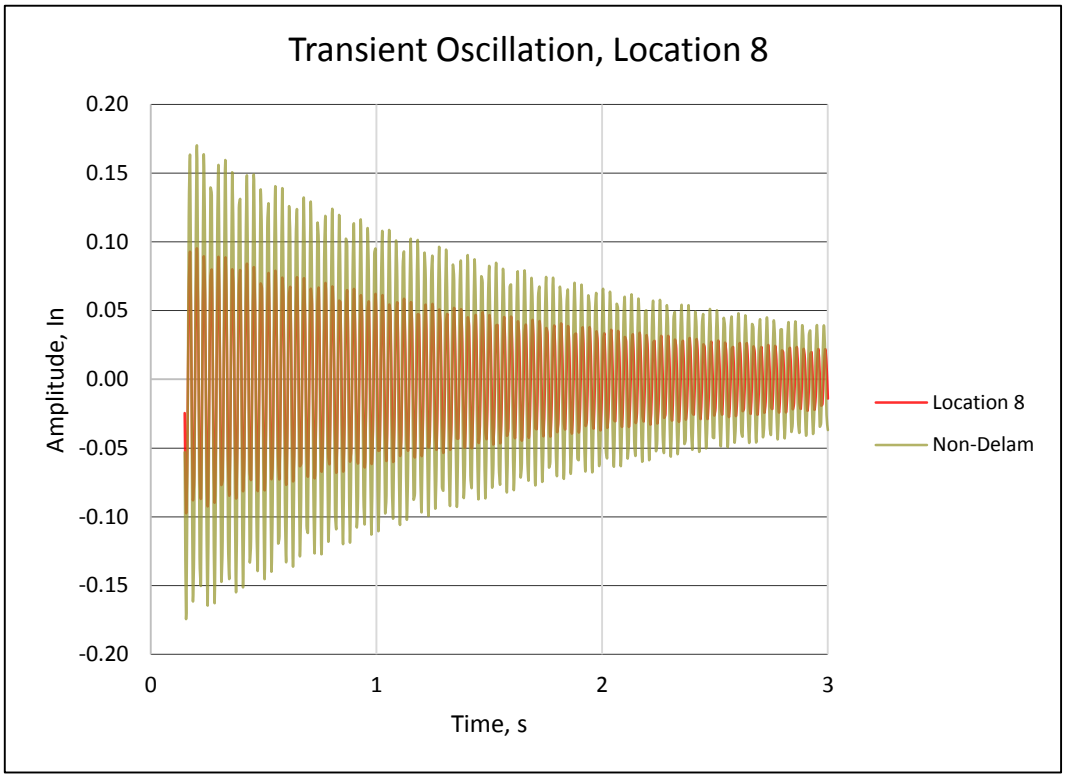
Transient Oscillation, Location 8
0.20
0.15
0.10
0.05
0.00
-0.05
-0.10
-0.15
-0.20
Amplitude, ln
0
1
2
3
Time, s
Location 8
Non-Delam

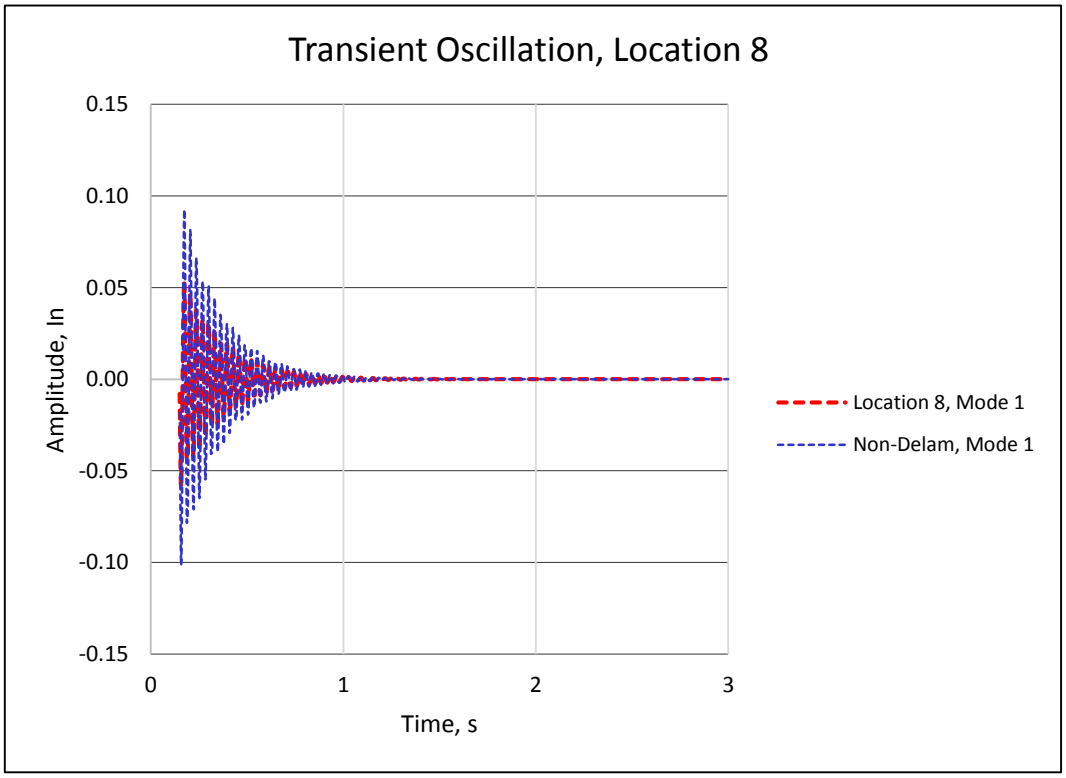
Transient Oscillation, Location 8
0.15
0.10
0.05
0.00
-0.05
-0.10
-0.15
Amplitude, ln
0
1
2
3
Time, s
Location 8, Mode 1
Non-Delam, Mode 1

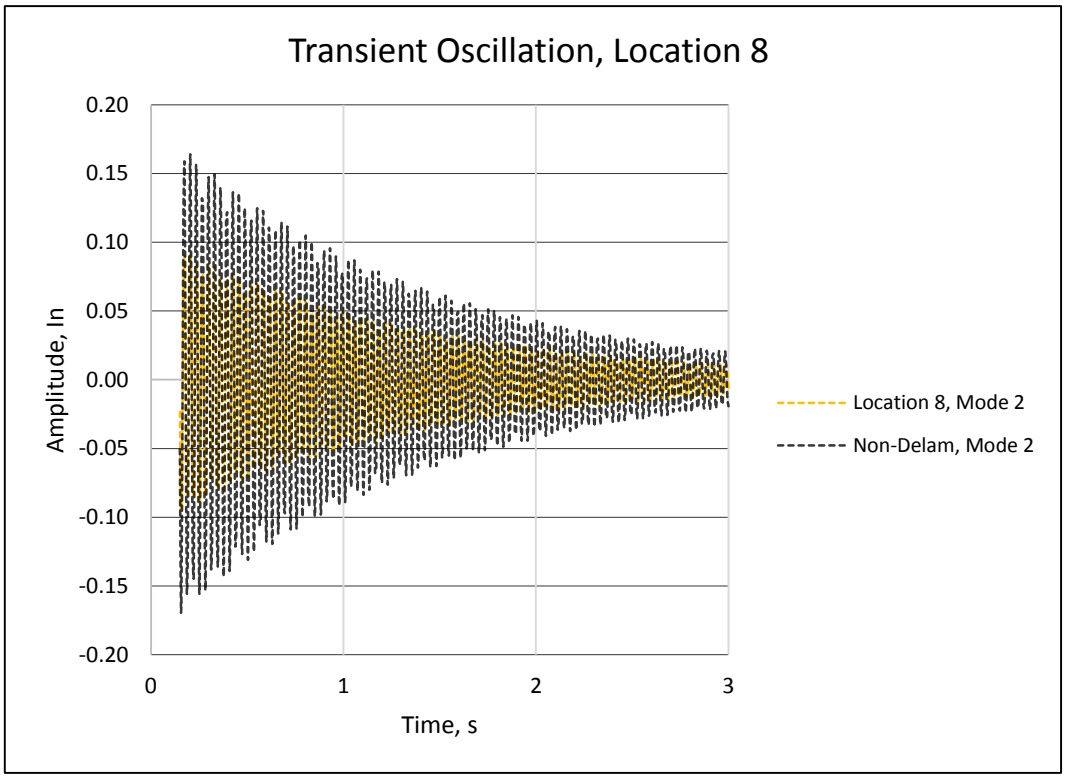
Transient Oscillation, Location 8
0.20
0.15
0.10
0.05
0.00
-0.05
-0.10
-0.15
-0.20
Amplitude, In
0
1
2
3
Time, s
Location 8, Mode 2
Non-Delam, Mode 2

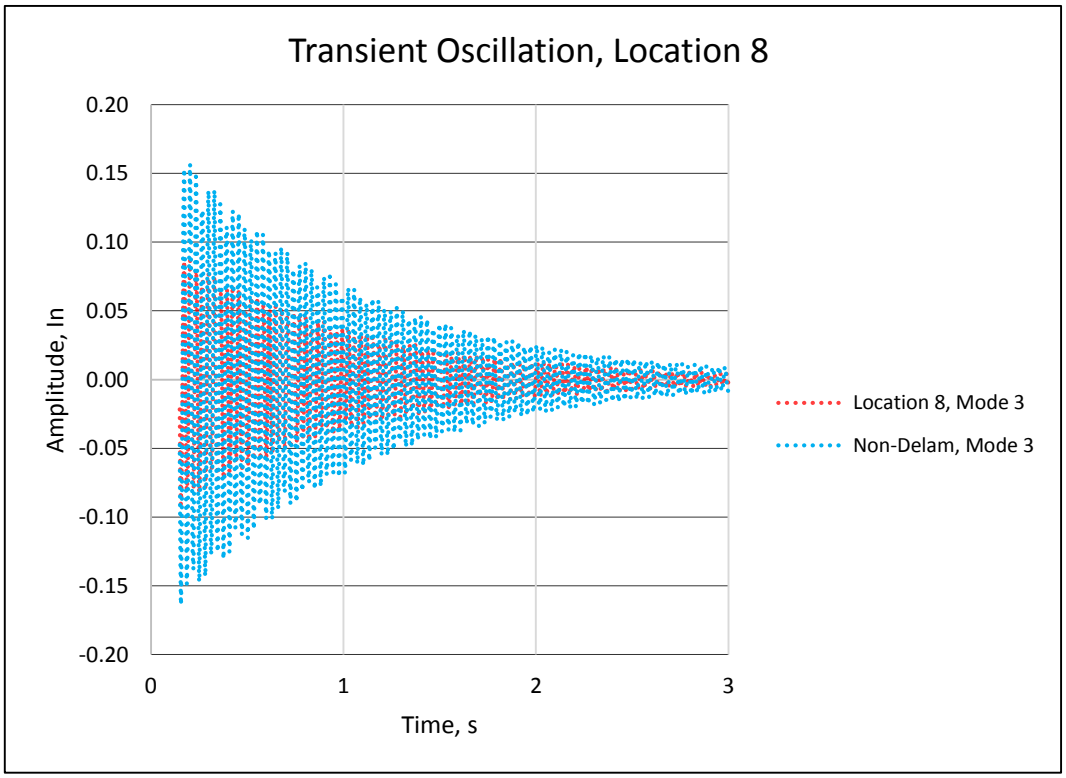
Transient Oscillation, Location 8
0.20
0.15
0.10
0.05
0.00
-0.05
-0.10
-0.15
-0.20
Amplitude, In
0
1
2
3
Time, s
Location 8, Mode 3
Non-Delam, Mode 3

D. SPECIMENS' EXPERIMENTAL FREQUENCIES AND AMPLITUDES

Experimental frequency for each zone for central Accelerometer. Mode columns are in Hertz.

	Specimen 1, Zone 1 Delam			Specimen 2, Zone 2 Delam			Specimen 3, Zone 3 Delam			Specimen 4, Zone 4 Delam			Specimen 5, Zone 5 Delam		
	Mode 1	Mode 2	Mode 3	Mode 1	Mode 2	Mode 3	Mode 1	Mode 2	Mode 3	Mode 1	Mode 2	Mode 3	Mode 1	Mode 2	Mode 3
Zone 1	33.150	214.822	614.435	35.340	226.929	649.065	35.179	227.969	652.037	35.019	224.865	643.161	26.500	131.151	581.653
Zone 2	34.542	225.895	634.405	36.656	237.539	667.105	36.322	239.719	670.160	36.322	237.539	664.064	27.362	137.282	573.735
Zone 3	35.664	229.013	608.846	37.847	238.626	643.161	37.674	243.028	637.310	37.503	238.626	634.405	28.122	139.177	565.924
Zone 4	36.656	220.793	603.307	38.722	234.305	634.405	38.545	232.173	634.405	38.369	231.115	634.405	28.772	134.796	589.681
Zone 5	37.162	215.806	625.768	39.436	225.895	655.023	39.256	227.969	667.105	39.077	224.865	658.023	29.303	131.751	563.344
Zone 6	37.674	215.806	637.310	39.980	224.865	667.105	39.798	227.969	673.229	39.616	226.929	667.105	29.572	131.751	568.515
Zone 7	38.020	218.784	603.307	40.347	231.115	637.310	40.163	232.173	637.310	39.980	230.061	634.405	29.707	133.570	592.381
Zone 8	38.020	225.895	595.094	40.532	237.539	628.634	40.163	238.626	628.634	39.798	237.539	625.768	29.707	137.282	568.515
Zone 9	37.503	232.173	620.076	39.798	243.028	652.037	39.798	244.141	658.023	39.436	243.028	652.037	29.437	139.814	558.219
Zone 10	38.369	235.378	640.229	40.904	244.141	676.312	40.532	248.644	679.409	40.532	244.141	673.229	29.036	140.454	589.681

	Specimen 6, Zone 6 Delam			Specimen 7, Zone 7 Delam			Specimen 8, Zone 8 Delam			Specimen 9, Zone 9 Delam			Specimen 10, Zone 10 Delam		
	Mode 1	Mode 2	Mode 3	Mode 1	Mode 2	Mode 3	Mode 1	Mode 2	Mode 3	Mode 1	Mode 2	Mode 3	Mode 1	Mode 2	Mode 3
Zone 1	35.179	227.969	646.106	34.700	226.929	649.065	34.072	221.804	640.229	35.179	227.969	658.023	35.019	227.969	658.023
Zone 2	36.322	239.719	667.105	36.157	238.626	673.229	35.179	232.173	661.036	36.489	240.817	676.312	36.489	239.719	679.409
Zone 3	37.674	243.028	640.229	37.332	241.920	643.161	36.322	234.305	631.513	37.674	241.920	646.106	37.674	240.817	646.106
Zone 4	38.545	232.173	637.310	38.194	234.305	640.229	37.332	227.969	625.768	38.545	236.456	646.106	38.545	238.626	646.106
Zone 5	39.256	227.969	664.064	38.722	230.061	673.229	38.020	224.865	655.023	39.436	227.969	670.160	39.256	227.969	670.160
Zone 6	39.798	227.969	670.160	39.436	227.969	676.312	38.545	221.804	658.023	39.798	230.061	682.521	39.616	229.013	679.409
Zone 7	40.163	232.173	640.229	39.616	231.115	646.106	38.899	225.895	628.634	40.163	233.237	649.065	39.980	233.237	646.106
Zone 8	40.163	238.626	628.634	39.798	238.626	631.513	38.899	233.237	614.435	39.980	240.817	637.310	39.980	240.817	634.405
Zone 9	39.616	245.259	655.023	39.256	244.141	658.023	38.545	238.626	637.310	41.468	247.510	664.064	40.904	246.382	664.064
Zone 10	40.532	244.141	676.312	40.163	245.259	682.521	39.798	239.719	664.064	40.717	247.510	685.646	40.347	249.782	685.646

	Specimen 11, Non-Delamination		
	Mode 1	Mode 2	Mode 3
Zone 1	34.384	227.969	643.161
Zone 2	35.502	240.817	670.160
Zone 3	36.824	241.920	637.310
Zone 4	37.674	236.456	637.310
Zone 5	38.545	224.865	664.064
Zone 6	38.899	223.840	667.105
Zone 7	39.256	230.061	640.229
Zone 8	39.436	237.539	628.634
Zone 9	38.899	243.028	655.023
Zone 10	39.980	245.259	679.409

Experimental amplitudes for each zone for central Accelerometer.

AMP columns are in G_{rms}.

	Specimen 1, Zone 1 Delam			Specimen 2, Zone 2 Delam			Specimen 3, Zone 3 Delam			Specimen 4, Zone 4 Delam			Specimen 5, Zone 5 Delam		
	AMP 1	AMP 2	AMP 3	AMP 1	AMP 2	AMP 3	AMP 1	AMP 2	AMP 3	AMP 1	AMP 2	AMP 3	AMP 1	AMP 2	AMP 3
Zone 1	30.868	11.913	7.070	38.168	18.722	14.348	33.595	26.684	10.976	36.132	12.729	10.769	35.492	24.630	12.409
Zone 2	31.879	10.237	3.106	28.454	8.813	2.023	34.007	10.232	0.627	34.501	13.908	0.691	32.130	11.588	7.140
Zone 3	28.071	1.356	8.075	28.653	2.235	16.120	24.820	4.280	5.990	30.575	2.675	6.882	30.488	2.250	20.906
Zone 4	22.492	13.378	15.062	23.477	12.927	12.744	24.367	8.560	9.911	19.564	8.119	5.764	26.259	9.052	6.042
Zone 5	17.994	25.376	5.946	18.487	16.723	6.969	19.246	32.015	7.853	20.319	24.320	10.275	15.649	23.423	6.309
Zone 6	14.310	34.795	7.882	12.153	41.674	2.171	14.414	42.368	6.547	20.690	39.852	7.898	16.616	39.524	23.955
Zone 7	8.511	38.049	15.499	8.301	41.958	21.901	7.983	38.156	9.180	8.658	39.999	11.554	10.599	39.957	4.917
Zone 8	4.002	25.121	29.306	1.919	23.010	36.758	5.824	21.753	11.691	3.794	32.799	25.218	5.504	27.646	10.138
Zone 9	1.728	17.455	32.988	1.373	17.861	34.925	1.985	19.183	23.239	1.677	18.940	32.552	1.917	17.460	27.900
Zone 10	4.529	1.217	6.165	2.858	1.556	6.225	5.284	1.318	6.102	0.864	3.654	8.473	0.847	2.892	5.706

	Specimen 6, Zone 6 Delam			Specimen 7, Zone 7 Delam			Specimen 8, Zone 8 Delam			Specimen 9, Zone 9 Delam			Specimen 10, Zone 10 Delam		
	AMP 1	AMP 2	AMP 3	AMP 1	AMP 2	AMP 3	AMP 1	AMP 2	AMP 3	AMP 1	AMP 2	AMP 3	AMP 1	AMP 2	AMP 3
Zone 1	37.9938	25.65597	10.58388	37.9679	17.56838	16.05894	35.823	19.87975	17.31402	38.3884	18.82399	15.92991	37.2827	26.96393	19.36969
Zone 2	34.4361	11.9647	0.882076	34.0771	12.24871	0.383743	33.2949	7.636674	0.361304	33.64	11.52394	0.274734	34.449	8.75495	1.109055
Zone 3	31.9585	2.484351	10.60696	30.1919	3.010655	10.51554	29.5023	1.073848	11.88447	30.4915	1.279823	9.931155	30.1244	1.076524	11.1114
Zone 4	24.755	6.625205	15.60817	23.908	19.32722	21.70433	23.2269	14.04212	18.84614	24.7374	17.44528	19.44226	25.322	12.00618	8.74355
Zone 5	19.322	32.89269	12.9938	18.2023	29.36813	21.84208	18.2911	30.00482	20.75749	19.6853	16.34306	5.99235	20.0284	13.80884	10.7061
Zone 6	11.6026	33.98371	7.399453	15.7492	35.92234	7.635553	12.9641	35.86484	6.704294	14.4426	31.45419	7.718973	13.2622	29.46896	5.788624
Zone 7	10.248	42.81322	18.78581	6.14304	35.0458	14.32222	9.83357	38.77281	15.85931	8.09991	36.6034	15.54191	9.09689	38.91241	14.95997
Zone 8	4.06649	36.81958	36.56296	5.19033	35.82198	32.04864	2.11628	22.46125	23.37662	3.68187	34.52412	31.05898	3.49797	38.64374	35.47169
Zone 9	1.74519	20.45218	39.69215	1.81916	19.81244	32.24054	2.12075	19.54686	25.5807	0.88049	10.06328	20.58634	1.48614	19.83281	40.25308
Zone 10	4.46153	1.484017	8.171369	2.99844	1.979207	7.145239	0.87755	2.643902	6.460428	2.06701	2.255822	6.716031	2.36557	1.368089	4.226685

	Specimen 11, Non-Delamination		
	AMP 1	AMP 2	AMP 3
Zone 1	44.731312	45.431178	18.48285
Zone 2	43.016001	20.491618	7.3921886
Zone 3	44.495457	6.2868832	17.922965
Zone 4	37.786594	17.604182	21.175372
Zone 5	28.688463	26.428	13.328638
Zone 6	20.756713	42.172984	8.0434013
Zone 7	12.207937	61.738398	22.961364
Zone 8	10.627572	41.170147	43.204565
Zone 9	1.8939353	32.816818	47.439496
Zone 10	1.3414289	7.7455055	18.37882

E. SUB-SAMPLE OF TEST DATA FREQUENCY RESPONSE PLOTS

The following FRF substantiates that there is no significant difference between the three accelerometers in each tested region with respect to natural frequencies and flexural bending modes.

Following plots are for the **non-delaminated case** (**specimen 11**). The graphs are Amplitude (G_{rms}) vs Frequency (Hz).

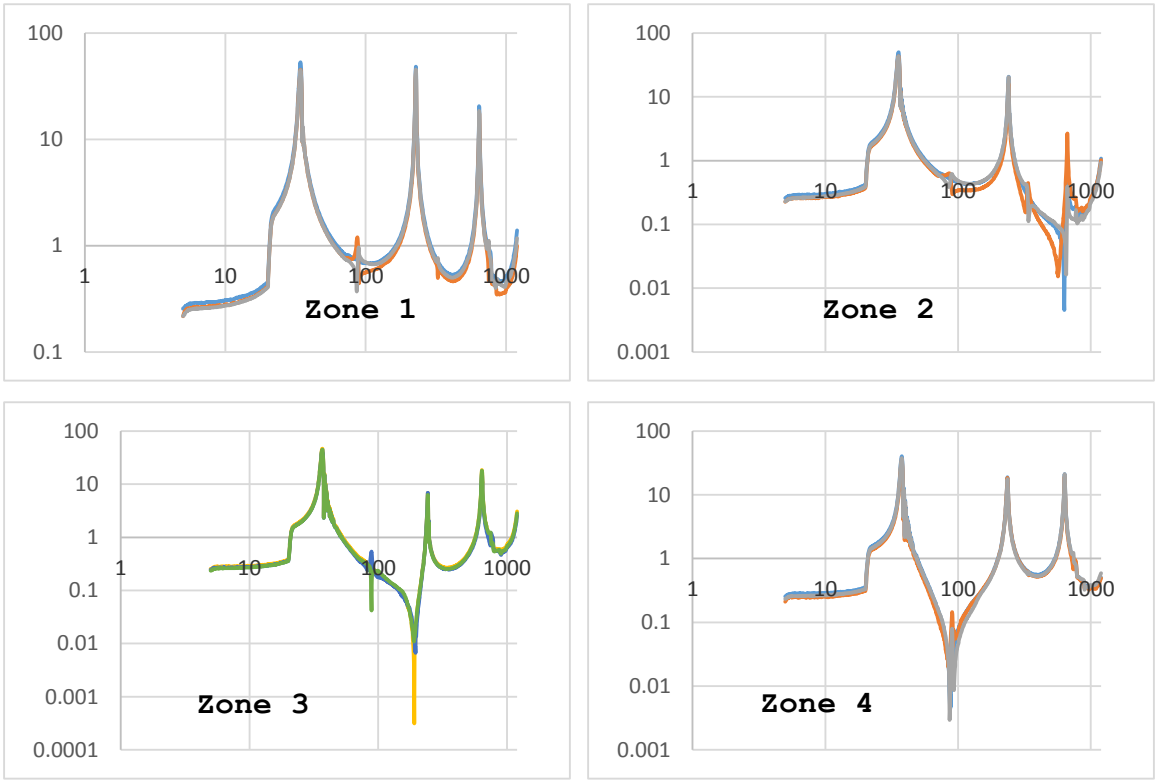

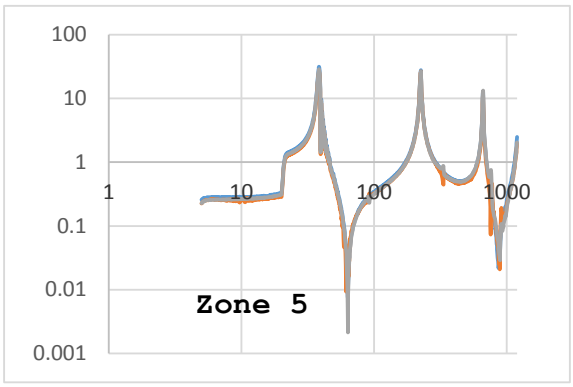
100
10
1
0.1
0.01
0.001
1
10
100
1000
Zone 5

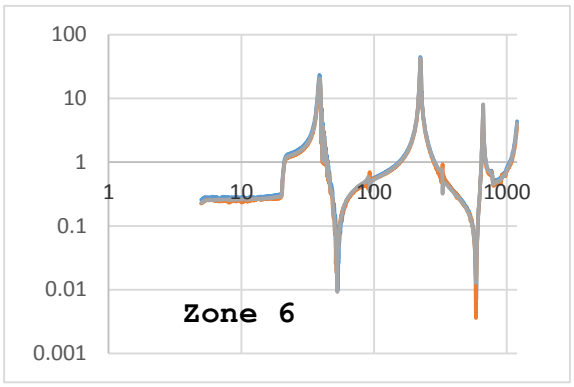
100
10
1
0.1
0.01
0.001
1
10
100
1000
Zone 6

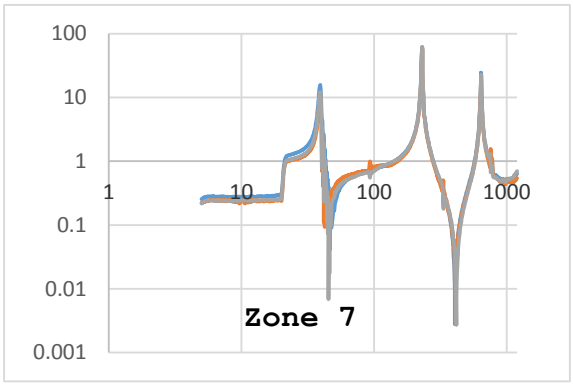
100
10
1
0.1
0.01
0.001
1
10
100
1000
Zone 7

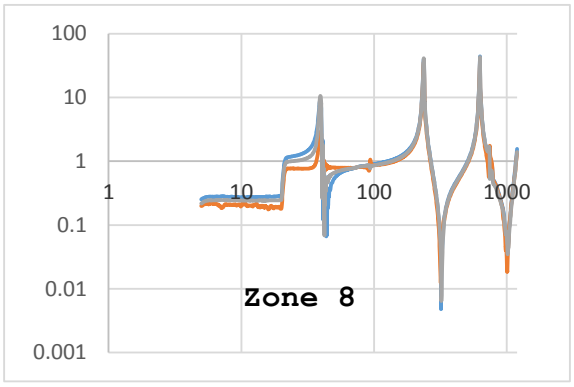
100
10
1
0.1
0.01
0.001
1
10
100
1000
Zone 8

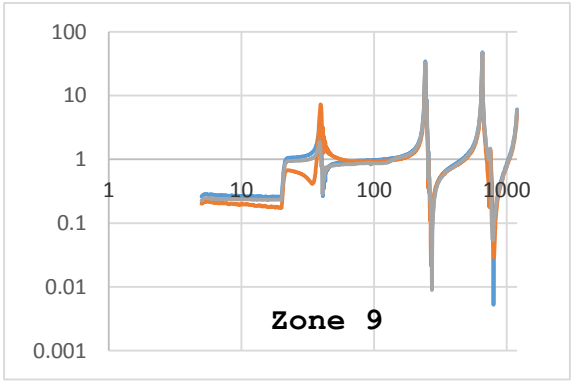
100
10
1
0.1
0.01
0.001
1
10
100
1000
Zone 9

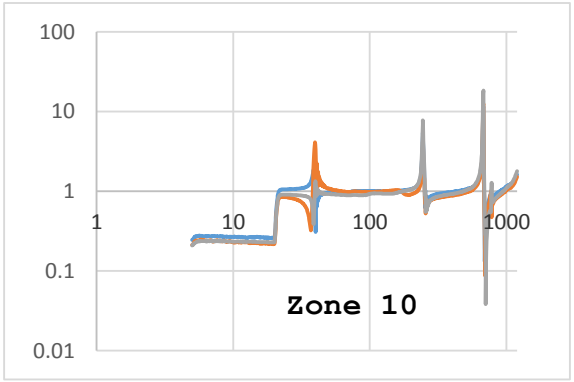
100
10
1
0.1
0.01
1
10
100
1000
Zone 10

Following plots are **specimen 2** with delamination in **zone**.

The graphs are Amplitude (G_{rms}) vs Frequency (Hz).

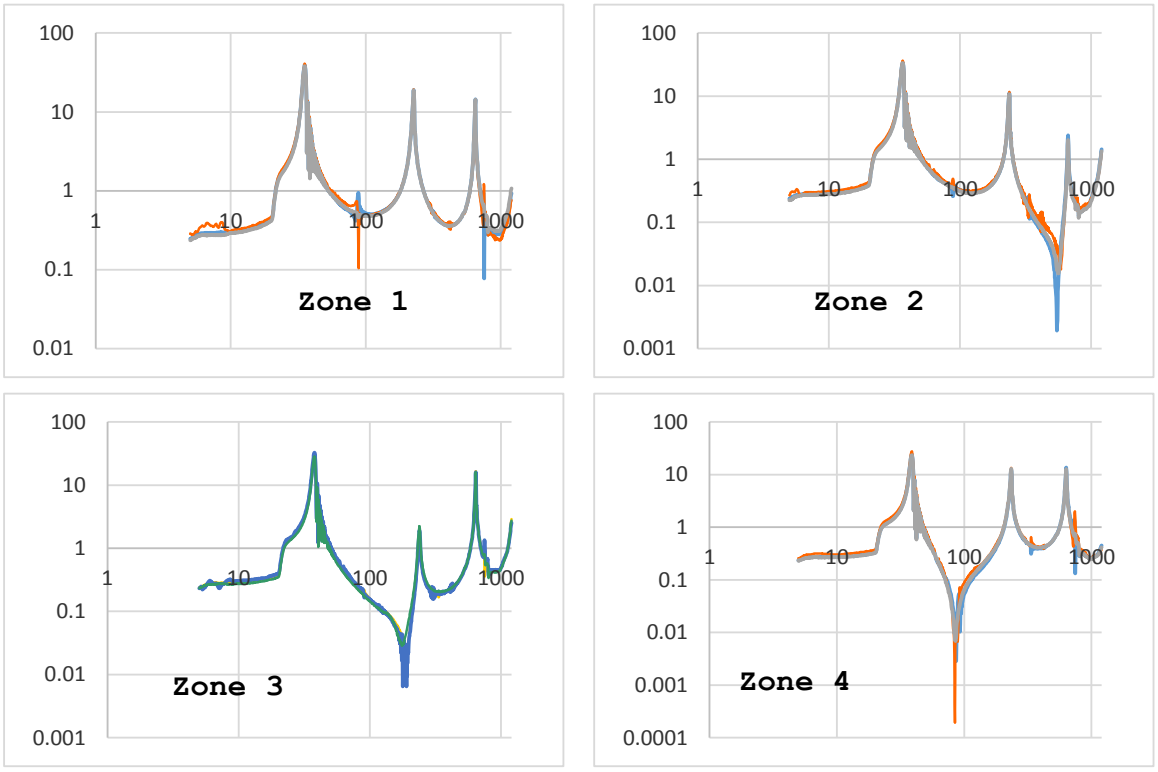

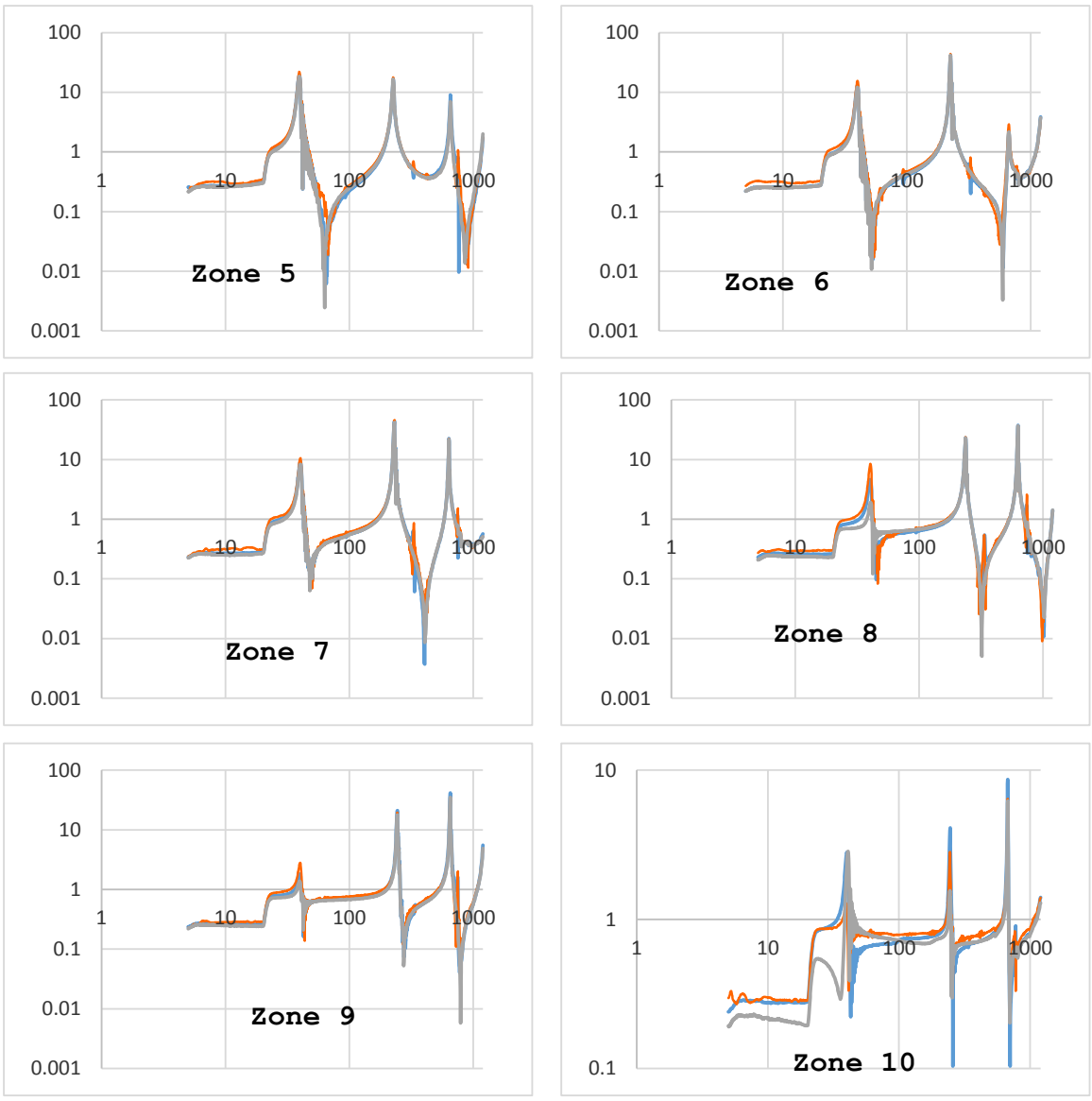
100
10
1
0.1
0.01
0.001
1
10
100
1000
Zone 5
Zone 6
Zone 7
Zone 8
Zone 9
Zone 10

Following plots are **specimen 5** with delamination in **zone**.

The graphs are Amplitude (G_{rms}) vs Frequency (Hz).

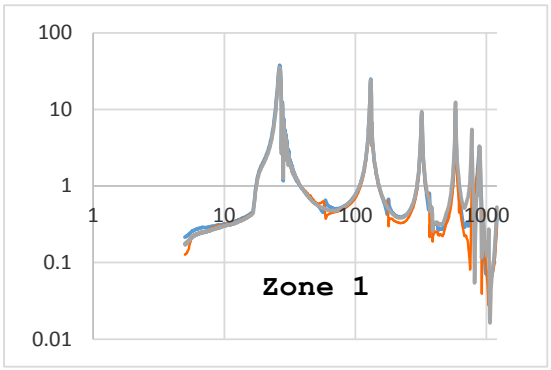

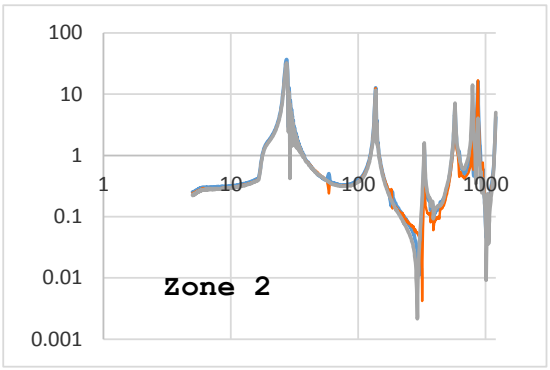

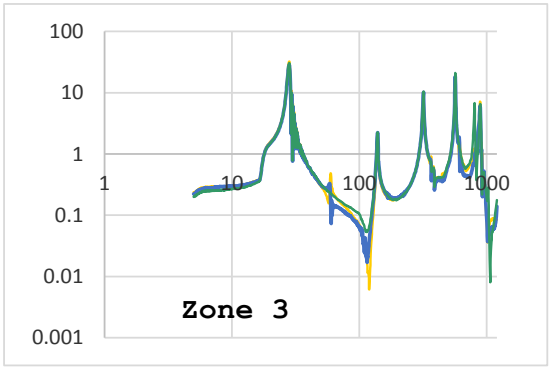

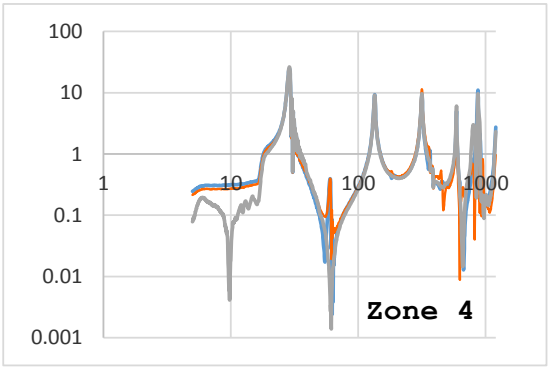

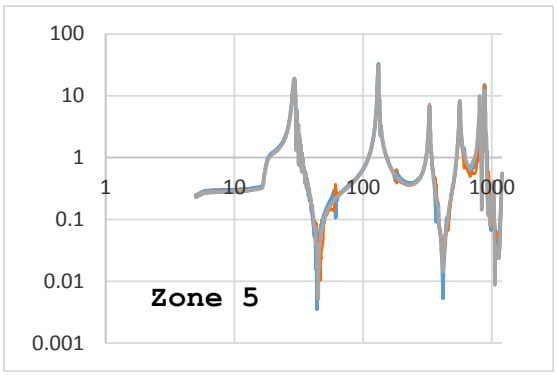
100
10
1
0.1
0.01
0.001
1
10
100
1000
Zone 5

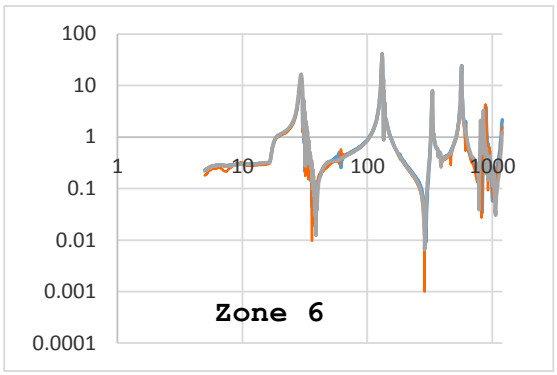
100
10
1
0.1
0.01
0.001
0.0001
1
10
100
1000
Zone 6

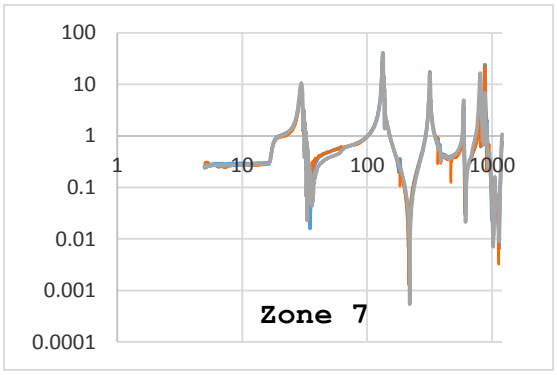
100
10
1
0.1
0.01
0.001
0.0001
1
10
100
1000
Zone 7

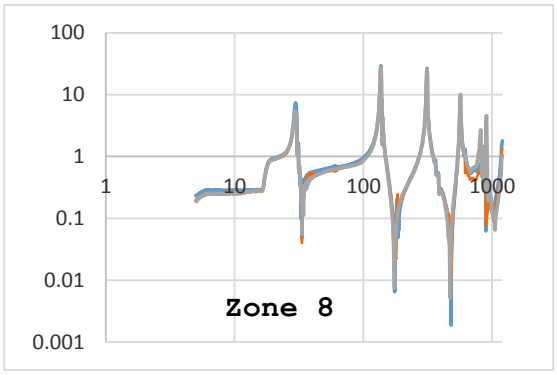
100
10
1
0.1
0.01
0.001
1
10
100
1000
Zone 8

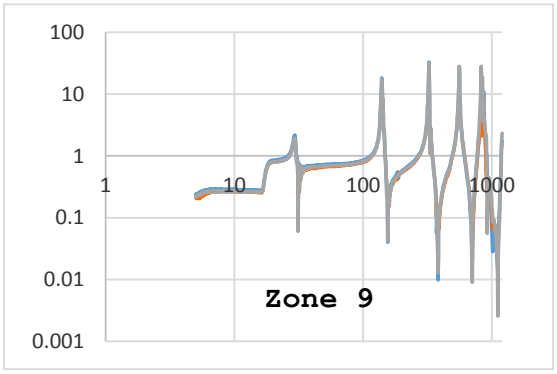
100
10
1
0.1
0.01
0.001
1
10
100
1000
Zone 9

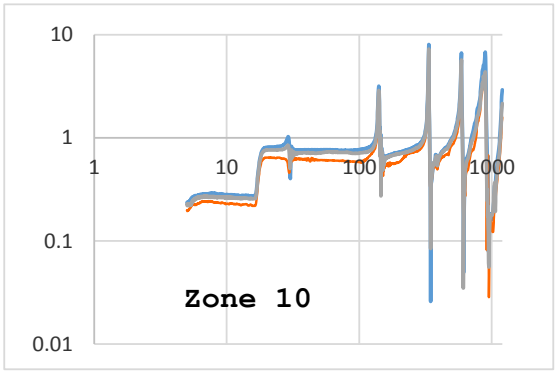
10
1
0.1
0.01
1
10
100
1000
Zone 10

Following plots are **specimen 8** with delamination in **zone**.

The graphs are Amplitude (G_{rms}) vs Frequency (Hz).

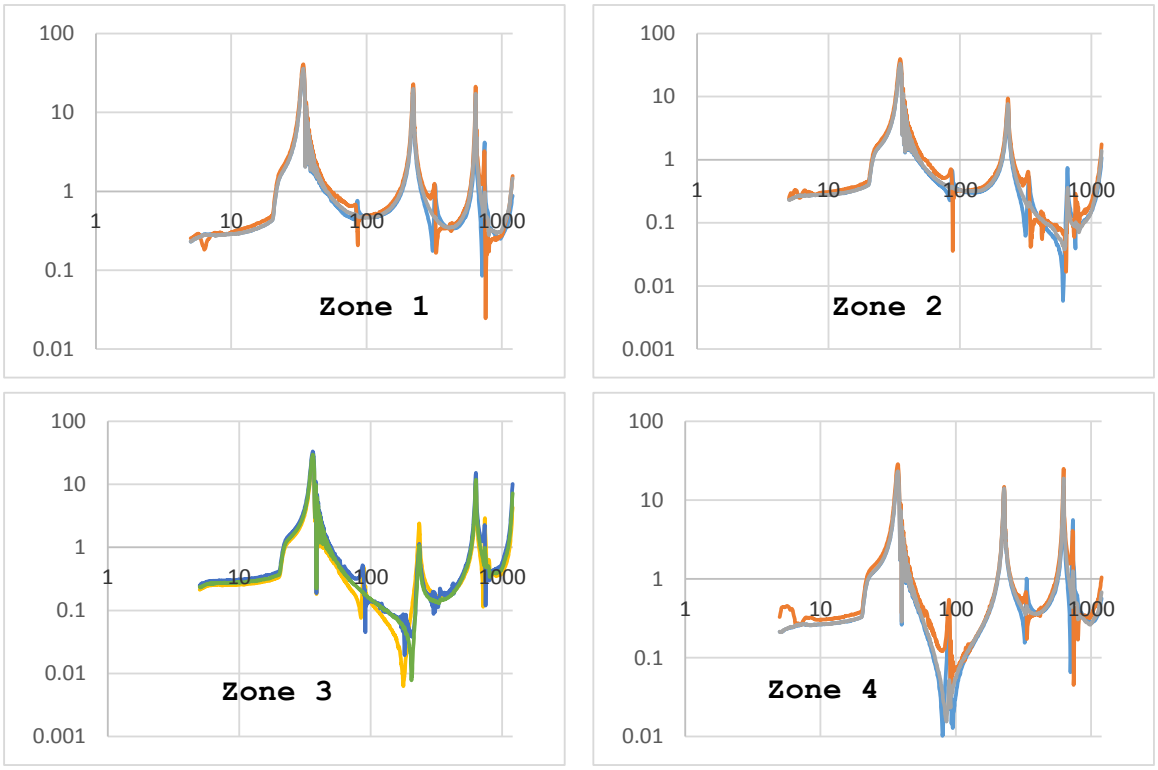

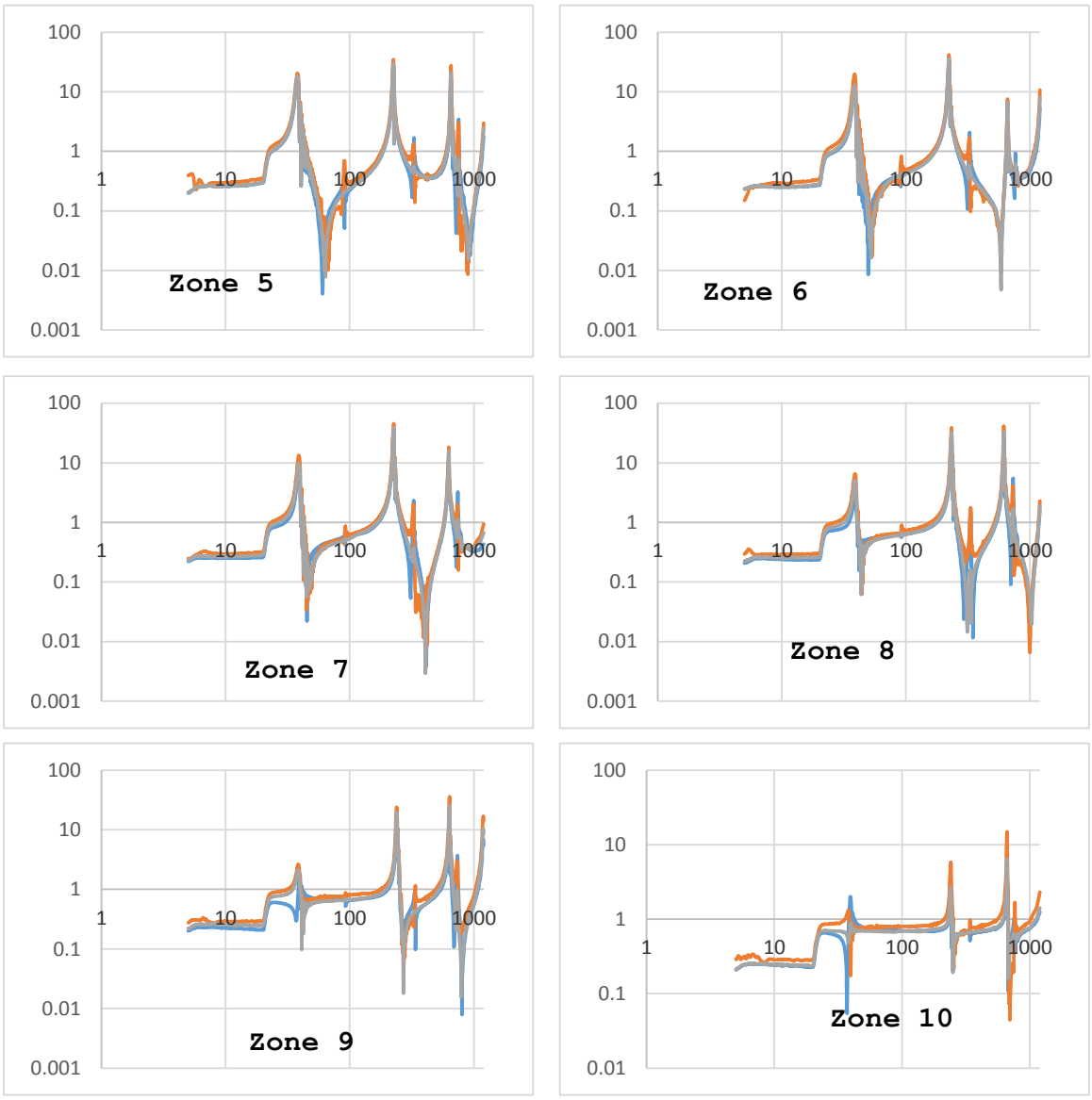
100
10
1
0.1
0.01
0.001
1
10
100
1000
Zone 5
Zone 6
Zone 7
Zone 8
Zone 9
Zone 10

F. MATLAB® SCRIPT FOR DAMPENING RATIO

Reads experimental data in and calculates the damping ratio using the half-power bandwidth method, then exports data to new excel worksheet.

```
sheets={'loc_1' 'Loc_2' 'Loc_3' 'Loc_4' 'Loc_6' 'Loc_7' 'Loc_8' 'Loc_9' 'Loc_10'
'No_Delam'};
for i=1:length(sheets)
    A=xlsread(file.xls',sheets{i},'A29:BP1228');
    dat(i).Hz=A(:,2);
    dat(i).Control=A(:,4);
    dat(i).Chan2=A(:,[9:6:end]);
    dat(i).Chan3=A(:,[11:6:end]);
    dat(i).Chan4=A(:,[13:6:end]);
end
close all
K=[1 2 3];
FN=[40 240 650];
tol=0.25;
for i=1:length(sheets)
    [m,n]=size(dat(i).Chan4);
    dat(i).fn=nan(length(FN),n);
    for j=1:n
        figure(j)
        plot(dat(i).Hz,dat(i).Chan4(:,j))
[a,b]=findpeaks(dat(i).Chan4(:,j),'minpeakheight',2.5,'minpeakdistance',50);
        hold all
        scatter(dat(i).Hz(b),a);
        for k=1:length(b)
            kk=find(dat(i).Hz(b(k))<(1+tol)*FN & dat(i).Hz(b(k))>(1-tol)*FN);
            dat(i).kk(K(kk),j)=k;
            dat(i).fn(kk,j)=dat(i).Hz(b(k));
        end
        for k=K
            if isnan(dat(i).fn(k,j))
                dat(i).zeta(k,j)=nan;
            else
                kk=dat(i).kk(k,j);
                ii=find(dat(i).Chan4(1:b(kk),j)<=a(kk)/sqrt(2),1,'last');
jj=find(dat(i).Chan4(b(kk):end,j)<=a(kk)/sqrt(2),1,'first')+b(kk);
                scatter(dat(i).Hz(ii),dat(i).Chan4(ii,j));
                scatter(dat(i).Hz(jj),dat(i).Chan4(jj,j));
```

```
            fn=dat(i).fn(k,j);
f1=interp1(dat(i).Chan4(ii:b(kk),j),dat(i).Hz(ii:b(kk)),a(kk)/sqrt(2));
f2=interp1(dat(i).Chan4(b(kk):jj,j),dat(i).Hz(b(kk):jj),a(kk)/sqrt(2));
            dat(i).zeta(k,j)=(abs(f2-fn)+abs(fn-f1))/(2*fn);
            scatter(f1,a(kk)/sqrt(2));
            scatter(f2,a(kk)/sqrt(2));
          end
        end
        clear a b
    end
end
for i=1:10
        headera{i}=['Location ' num2str(i)];
end

for j=1:length(FN)
    headerb{j,1}=['Mode ' num2str(j)];
end
for i=1:length(sheets)
    A=[dat(i).fn;dat(i).zeta];
    xlswrite('file_new.xls',A,sheets{i});
end
```

G. SHEWHART'S CHARTS

X_bar chart axis: Average, G_{rms} vs Zone, Unitless

R-Chart axis: Range, G_{rms} vs Zone, Unitless

Mode 1

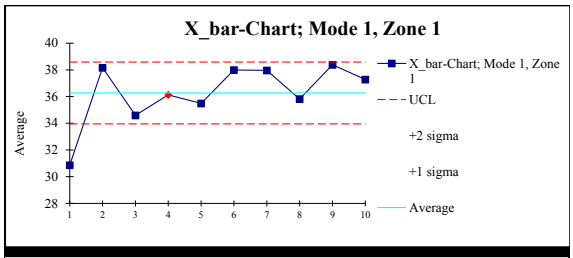

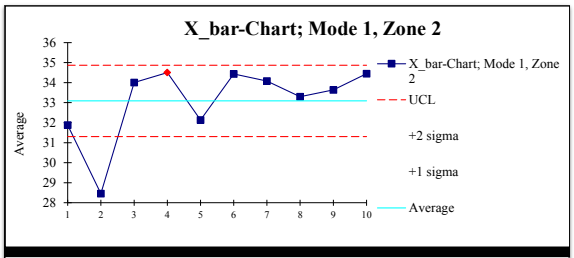

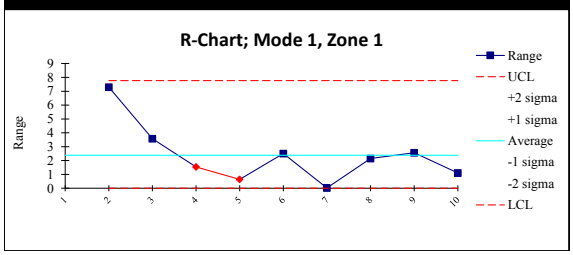

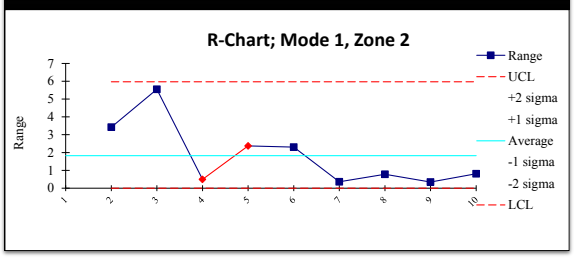

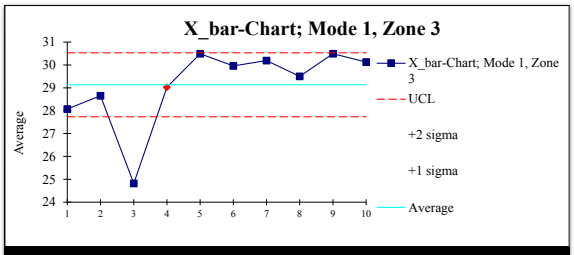

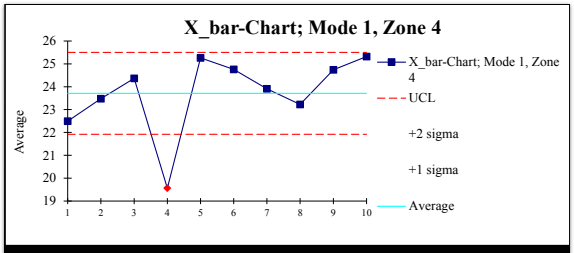

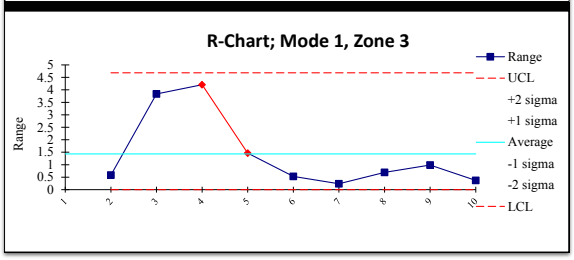

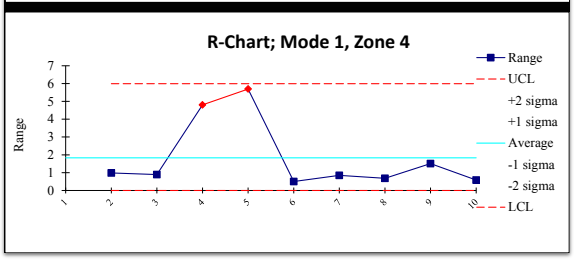

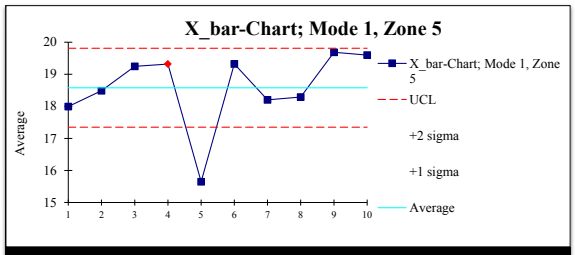
X_bar-Chart; Mode 1, Zone 5
Average
X_bar-Chart; Mode 1, Zone 5
UCL
+2 sigma
+1 sigma
Average

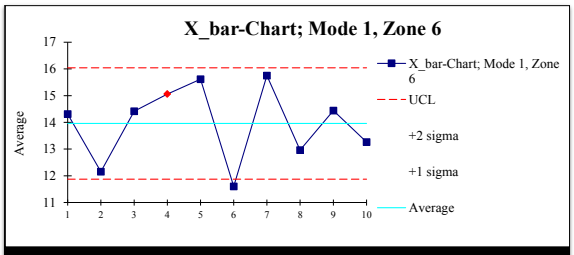
X_bar-Chart; Mode 1, Zone 6
Average
X_bar-Chart; Mode 1, Zone 6
UCL
+2 sigma
+1 sigma
Average

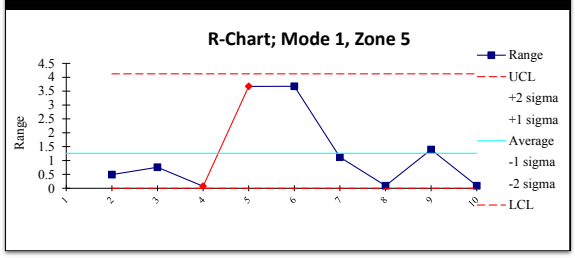
R-Chart; Mode 1, Zone 5
Range
Range
UCL
+2 sigma
+1 sigma
Average
-1 sigma
-2 sigma
LCL

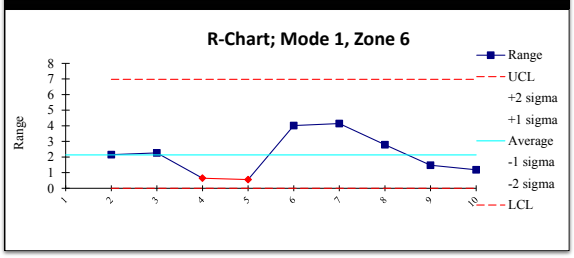
R-Chart; Mode 1, Zone 6
Range
Range
UCL
+2 sigma
+1 sigma
Average
-1 sigma
-2 sigma
LCL

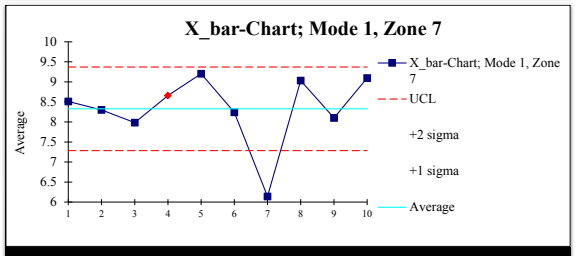
X_bar-Chart; Mode 1, Zone 7
Average
X_bar-Chart; Mode 1, Zone 7
UCL
+2 sigma
+1 sigma
Average

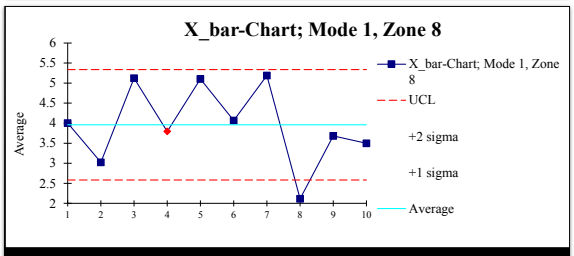
X_bar-Chart; Mode 1, Zone 8
Average
X_bar-Chart; Mode 1, Zone 8
UCL
+2 sigma
+1 sigma
Average

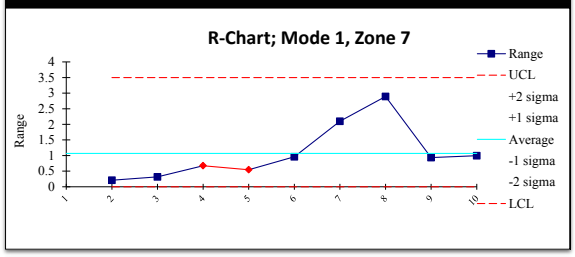
R-Chart; Mode 1, Zone 7
Range
Range
UCL
+2 sigma
+1 sigma
Average
-1 sigma
-2 sigma
LCL

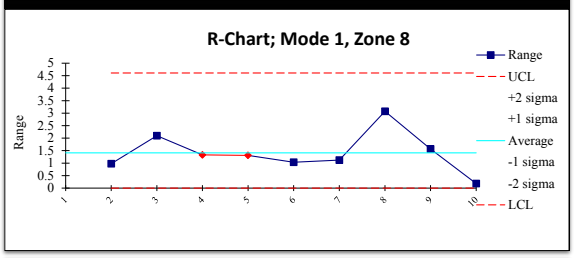
R-Chart; Mode 1, Zone 8
Range
Range
UCL
+2 sigma
+1 sigma
Average
-1 sigma
-2 sigma
LCL

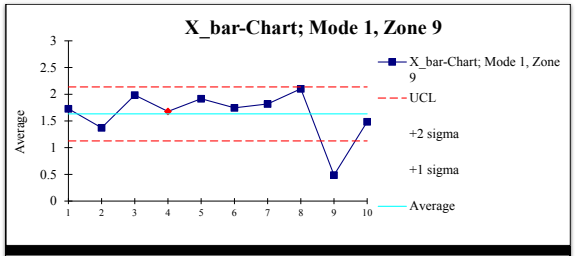
X_bar-Chart; Mode 1, Zone 9
Average
X_bar-Chart; Mode 1, Zone 9
UCL
+2 sigma
+1 sigma
Average

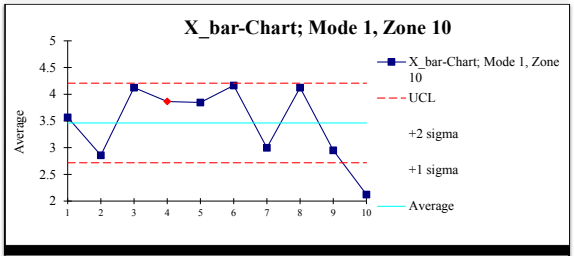
X_bar-Chart; Mode 1, Zone 10
Average
X_bar-Chart; Mode 1, Zone 10
UCL
+2 sigma
+1 sigma
Average

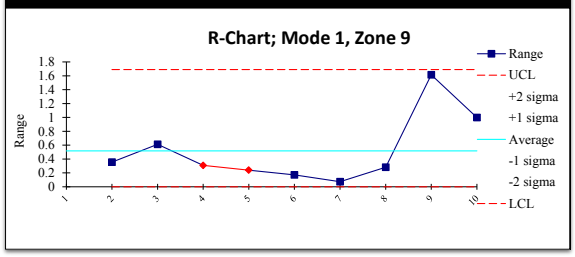
R-Chart; Mode 1, Zone 9
Range
Range
UCL
+2 sigma
+1 sigma
Average
-1 sigma
-2 sigma
LCL

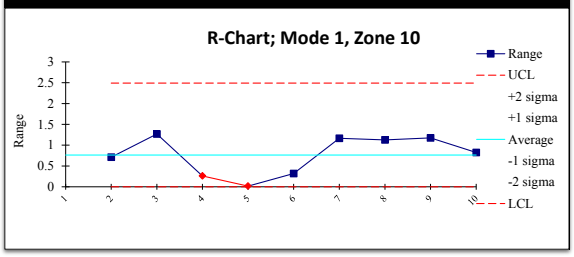
R-Chart; Mode 1, Zone 10
Range
Range
UCL
+2 sigma
+1 sigma
Average
-1 sigma
-2 sigma
LCL

Mode 2

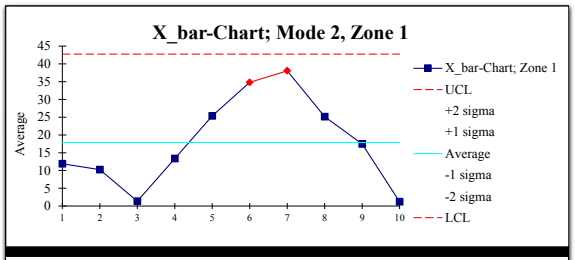
X_bar-Chart; Mode 2, Zone 1
Average
X_bar-Chart; Zone 1
UCL
+2 sigma
+1 sigma
Average
-1 sigma
-2 sigma
LCL

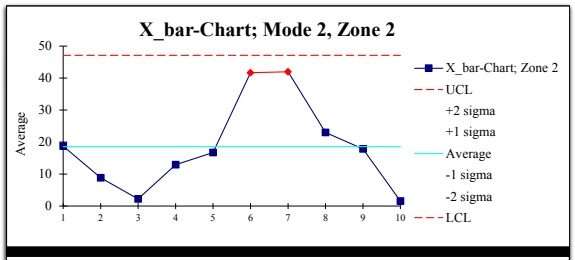
X_bar-Chart; Mode 2, Zone 2
Average
X_bar-Chart; Zone 2
UCL
+2 sigma
+1 sigma
Average
-1 sigma
-2 sigma
LCL

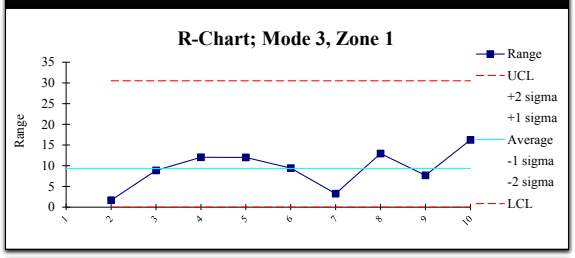
R-Chart; Mode 3, Zone 1
Range
Range
UCL
+2 sigma
+1 sigma
Average
-1 sigma
-2 sigma
LCL

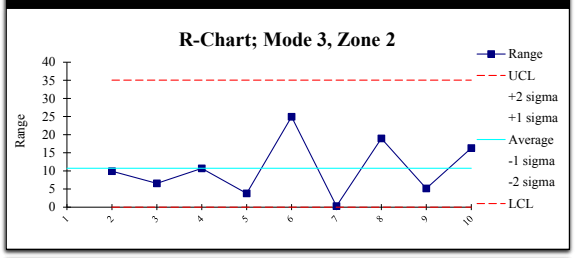
R-Chart; Mode 3, Zone 2
Range
Range
UCL
+2 sigma
+1 sigma
Average
-1 sigma
-2 sigma
LCL

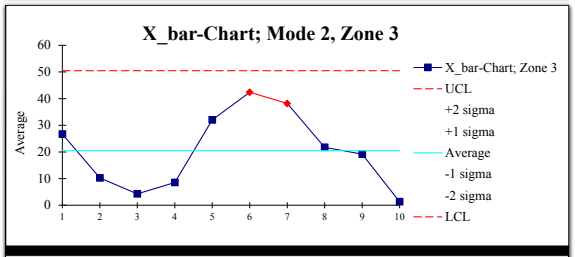
X_bar-Chart; Mode 2, Zone 3
Average
X_bar-Chart; Zone 3
UCL
+2 sigma
+1 sigma
Average
-1 sigma
-2 sigma
LCL

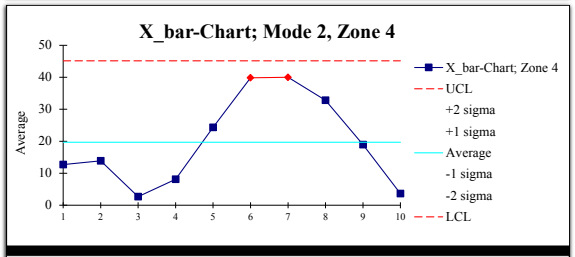
X_bar-Chart; Mode 2, Zone 4
Average
X_bar-Chart; Zone 4
UCL
+2 sigma
+1 sigma
Average
-1 sigma
-2 sigma
LCL

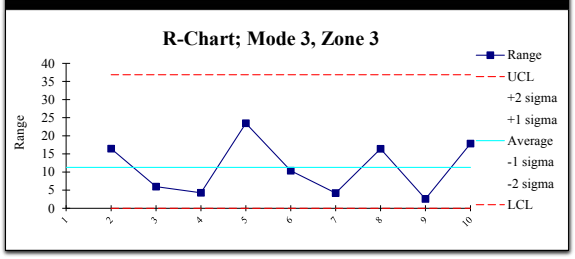
R-Chart; Mode 3, Zone 3
Range
Range
UCL
+2 sigma
+1 sigma
Average
-1 sigma
-2 sigma
LCL

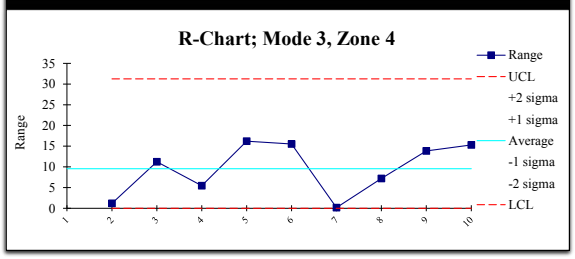
R-Chart; Mode 3, Zone 4
Range
Range
UCL
+2 sigma
+1 sigma
Average
-1 sigma
-2 sigma
LCL

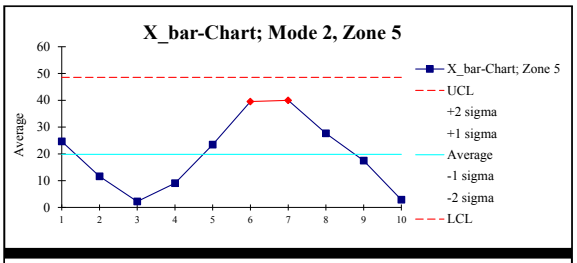
X_bar-Chart; Mode 2, Zone 5
Average
X_bar-Chart; Zone 5
UCL
+2 sigma
+1 sigma
Average
-1 sigma
-2 sigma
LCL

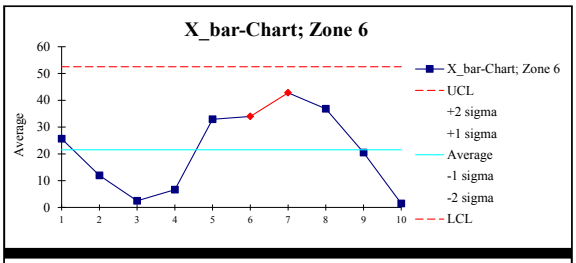
X_bar-Chart; Zone 6
Average
X_bar-Chart; Zone 6
UCL
+2 sigma
+1 sigma
Average
-1 sigma
-2 sigma
LCL

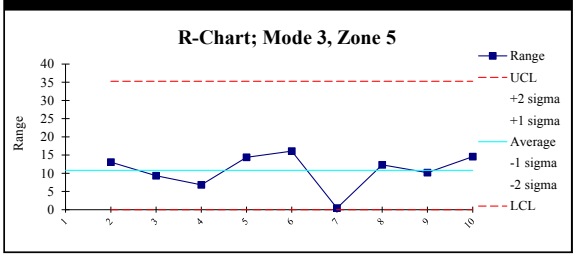
R-Chart; Mode 3, Zone 5
Range
Range
UCL
+2 sigma
+1 sigma
Average
-1 sigma
-2 sigma
LCL

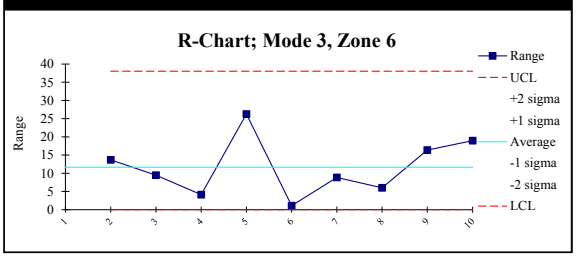
R-Chart; Mode 3, Zone 6
Range
Range
UCL
+2 sigma
+1 sigma
Average
-1 sigma
-2 sigma
LCL

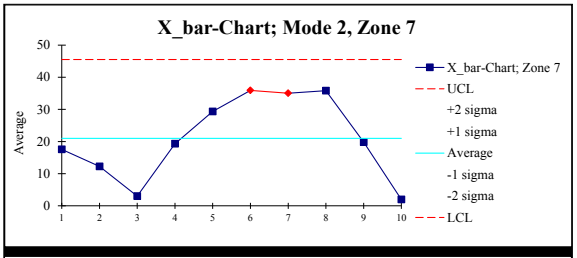
X_bar-Chart; Mode 2, Zone 7
Average
X_bar-Chart; Zone 7
UCL
+2 sigma
+1 sigma
Average
-1 sigma
-2 sigma
LCL

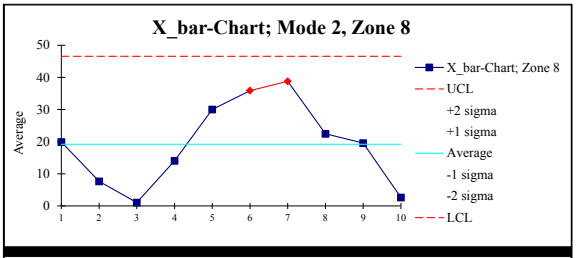
X_bar-Chart; Mode 2, Zone 8
Average
X_bar-Chart; Zone 8
UCL
+2 sigma
+1 sigma
Average
-1 sigma
-2 sigma
LCL

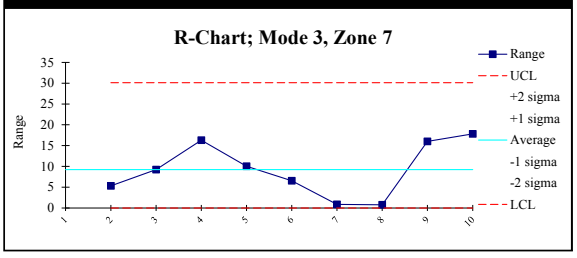
R-Chart; Mode 3, Zone 7
Range
Range
UCL
+2 sigma
+1 sigma
Average
-1 sigma
-2 sigma
LCL

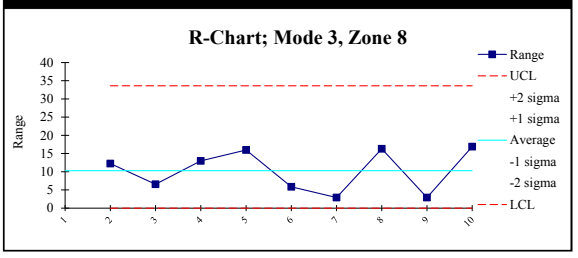
R-Chart; Mode 3, Zone 8
Range
Range
UCL
+2 sigma
+1 sigma
Average
-1 sigma
-2 sigma
LCL

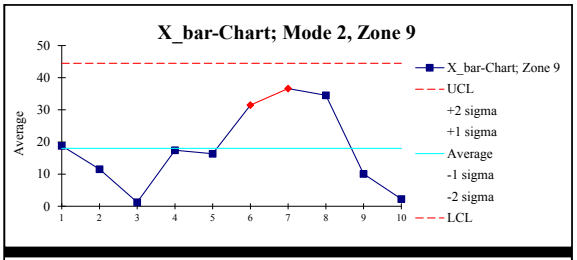
X_bar-Chart; Mode 2, Zone 9
Average
X_bar-Chart; Zone 9
UCL
+2 sigma
+1 sigma
Average
-1 sigma
-2 sigma
LCL

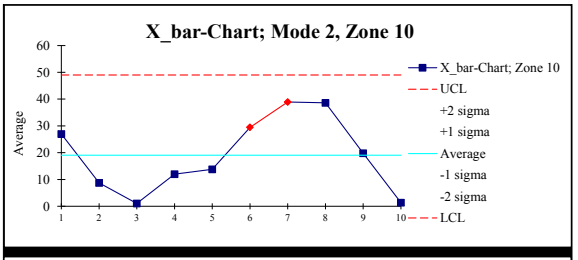
X_bar-Chart; Mode 2, Zone 10
Average
X_bar-Chart; Zone 10
UCL
+2 sigma
+1 sigma
Average
-1 sigma
-2 sigma
LCL

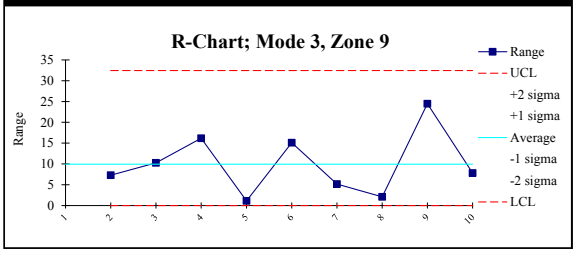
R-Chart; Mode 3, Zone 9
Range
Range
UCL
+2 sigma
+1 sigma
Average
-1 sigma
-2 sigma
LCL

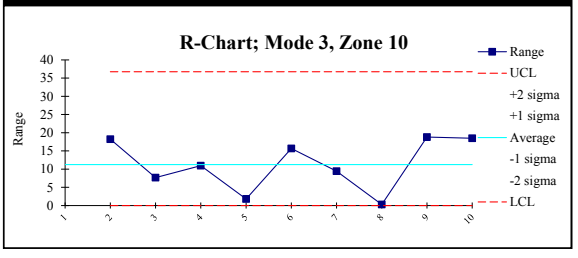
R-Chart; Mode 3, Zone 10
Range
Range
UCL
+2 sigma
+1 sigma
Average
-1 sigma
-2 sigma
LCL

Mode 3

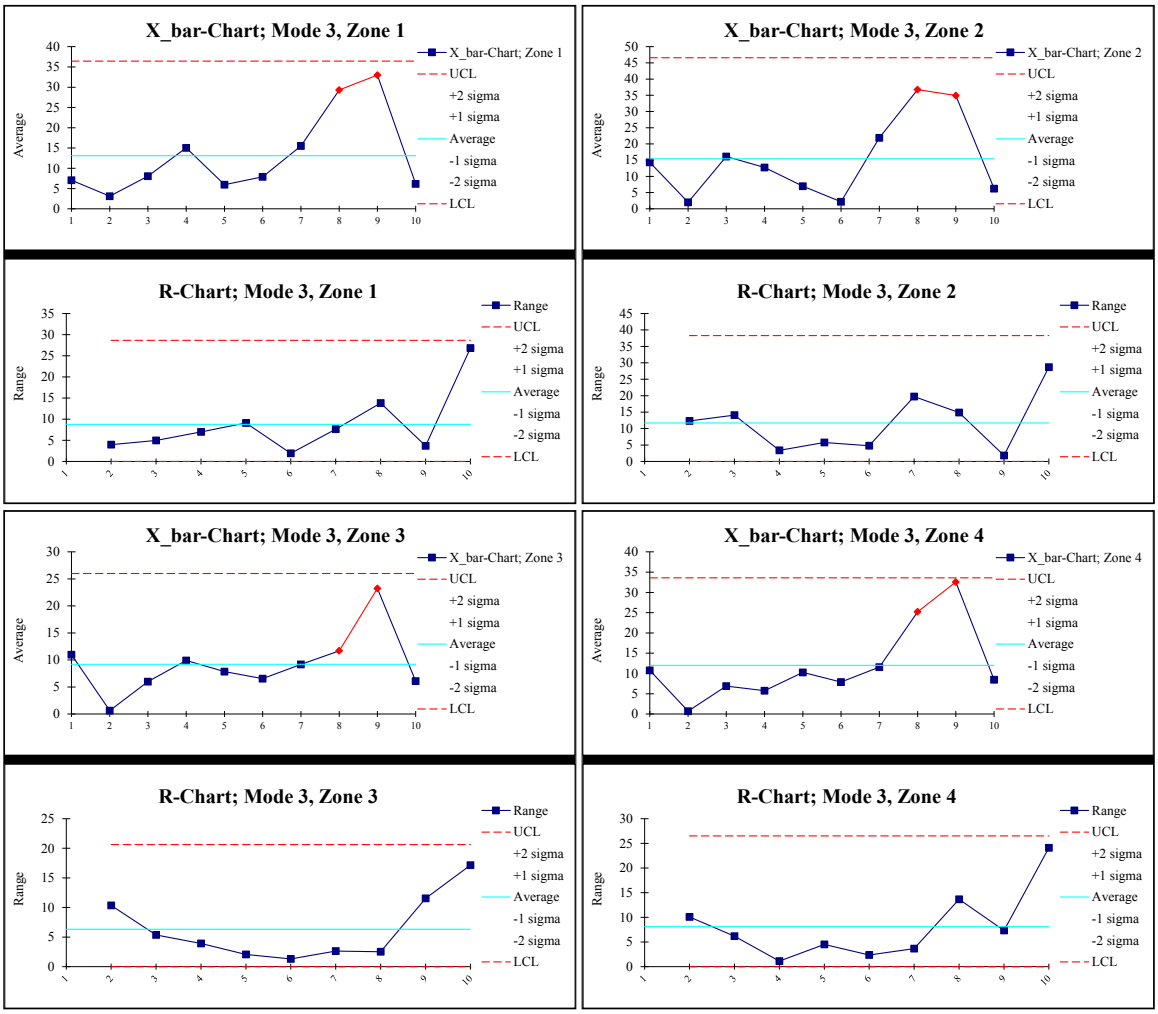
X_bar-Chart; Mode 3, Zone 1
X_bar-Chart; Zone 1
UCL
+2 sigma
+1 sigma
Average
-1 sigma
-2 sigma
LCL
Average
X_bar-Chart; Mode 3, Zone 2
X_bar-Chart; Zone 2
R-Chart; Mode 3, Zone 1
Range
R-Chart; Mode 3, Zone 2
X_bar-Chart; Mode 3, Zone 3
X_bar-Chart; Zone 3
X_bar-Chart; Mode 3, Zone 4
X_bar-Chart; Zone 4
R-Chart; Mode 3, Zone 3
R-Chart; Mode 3, Zone 4

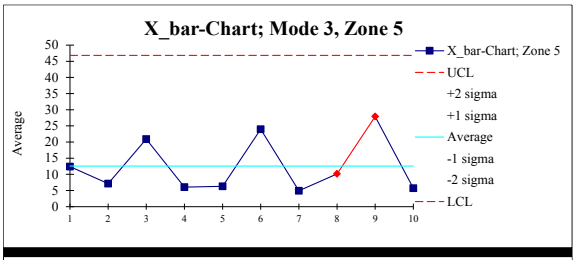
X_bar-Chart; Mode 3, Zone 5
Average
X_bar-Chart; Zone 5
UCL
+2 sigma
+1 sigma
Average
-1 sigma
-2 sigma
LCL

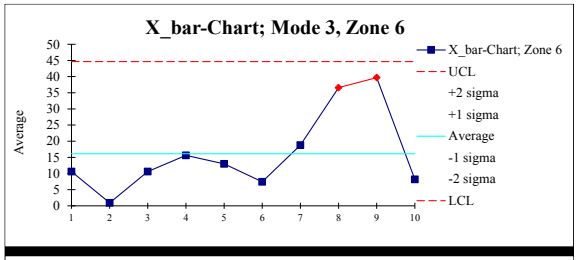
X_bar-Chart; Mode 3, Zone 6
Average
X_bar-Chart; Zone 6
UCL
+2 sigma
+1 sigma
Average
-1 sigma
-2 sigma
LCL

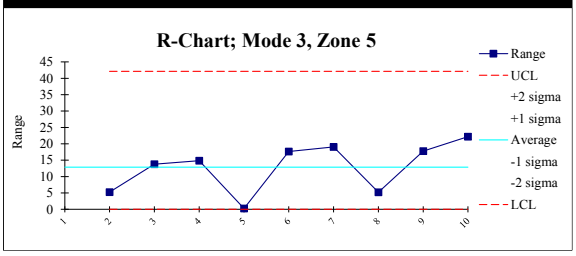
R-Chart; Mode 3, Zone 5
Range
Range
UCL
+2 sigma
+1 sigma
Average
-1 sigma
-2 sigma
LCL

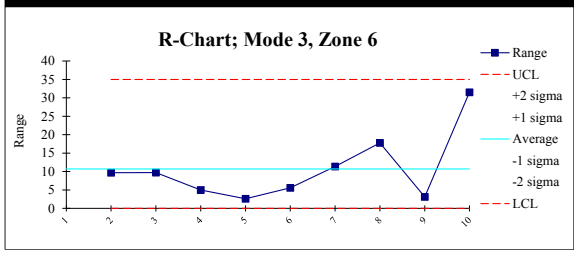
R-Chart; Mode 3, Zone 6
Range
Range
UCL
+2 sigma
+1 sigma
Average
-1 sigma
-2 sigma
LCL

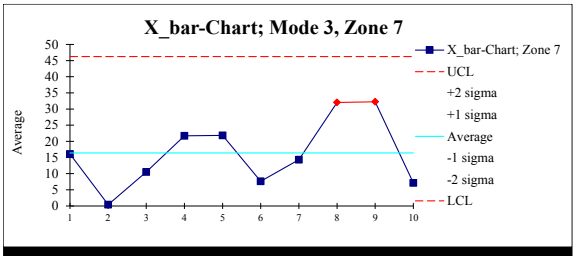
X_bar-Chart; Mode 3, Zone 7
Average
X_bar-Chart; Zone 7
UCL
+2 sigma
+1 sigma
Average
-1 sigma
-2 sigma
LCL

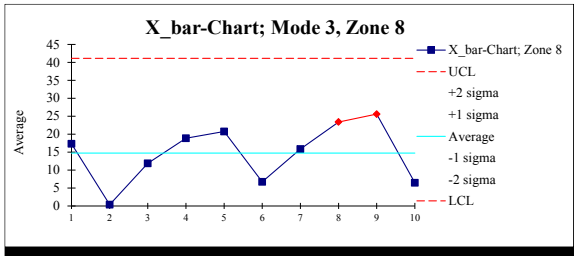
X_bar-Chart; Mode 3, Zone 8
Average
X_bar-Chart; Zone 8
UCL
+2 sigma
+1 sigma
Average
-1 sigma
-2 sigma
LCL

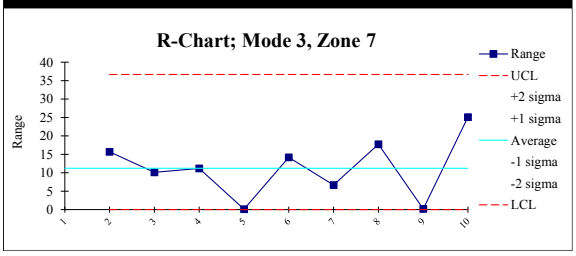
R-Chart; Mode 3, Zone 7
Range
Range
UCL
+2 sigma
+1 sigma
Average
-1 sigma
-2 sigma
LCL

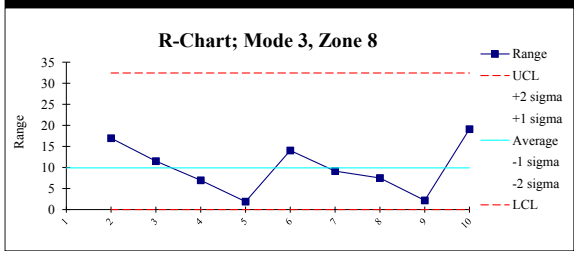
R-Chart; Mode 3, Zone 8
Range
Range
UCL
+2 sigma
+1 sigma
Average
-1 sigma
-2 sigma
LCL

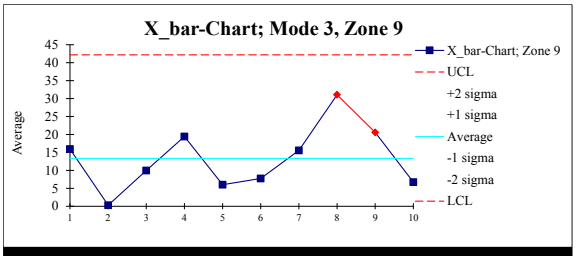
X_bar-Chart; Mode 3, Zone 9
Average
X_bar-Chart; Zone 9
UCL
+2 sigma
+1 sigma
Average
-1 sigma
-2 sigma
LCL

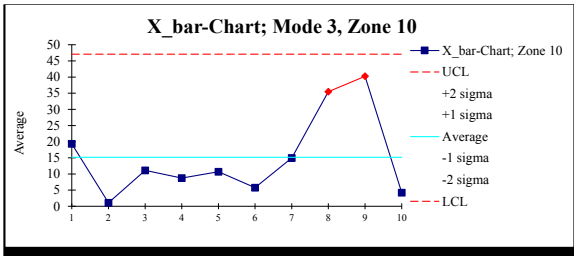
X_bar-Chart; Mode 3, Zone 10
Average
X_bar-Chart; Zone 10
UCL
+2 sigma
+1 sigma
Average
-1 sigma
-2 sigma
LCL

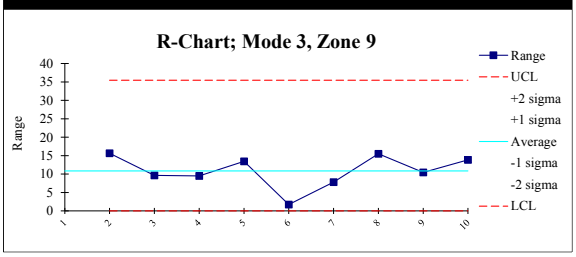
R-Chart; Mode 3, Zone 9
Range
Range
UCL
+2 sigma
+1 sigma
Average
-1 sigma
-2 sigma
LCL

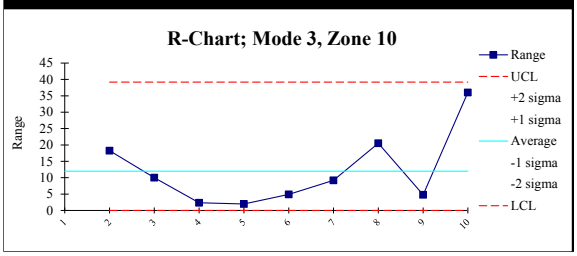
R-Chart; Mode 3, Zone 10
Range
Range
UCL
+2 sigma
+1 sigma
Average
-1 sigma
-2 sigma
LCL

H. VIBRATION FIXTURE DESIGN

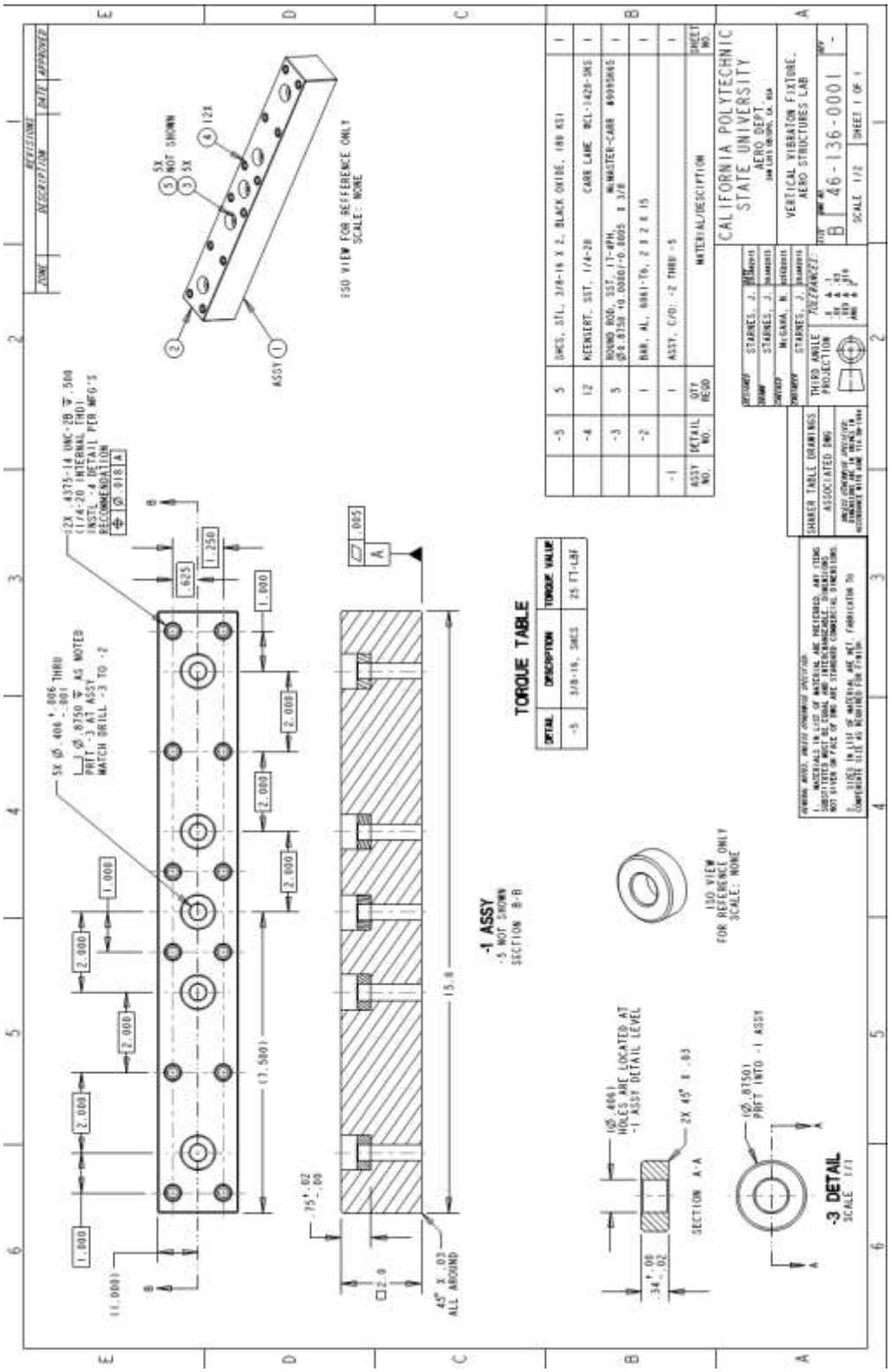

Initial design calculations of vibration fixture using MathCAD:

Designing Stiffness VS Strength: Values and equations are referenced from *Machine Design for Product Reliability course.*

Constraints: Fixtrue to be tested at 2000Hz
Tested Device is cubical 1 X 1 X 1 in for simplicity
Table attachments (worst case) are 12 in apart.

Assumptions: Ignore attachments stiffness of device
Ignore attachment stiffness of the table/fixture
Device must be completely supported over the entire width
Fixtrue attachments are considered simple supports
Bar is 15 in long

Parameters:

$Fn := 2000Hz$	Testing Frequency
$W := 1lbf$	Weight of tested device
$l := 12in$	Span between bolts
$b := 2in$	Bredth of fixture (width)

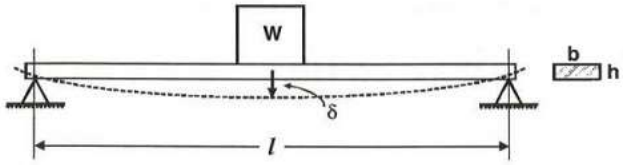

Aluminum Material Properties:

$E := 10 \cdot 10^6 psi$ $\gamma := 0.0975 \frac{lbf}{in^3}$

Calculate the Thickness:

First Calculate the Static Deflection:

$$\delta = \left(\frac{1}{48}\right)\cdot\left(\frac{W\cdot l^3}{E\cdot I}\right) \qquad \text{Where: } I = \frac{1}{12}\cdot b\cdot h^3$$

Static defelection is related to entire weight of load, not just the tested device.

$$W_{eff} = 0.49\cdot W_{fixture} \qquad \text{Where: } W_{fixture} = V_{fixture}\cdot\gamma \qquad \gamma = \text{Specific Weight of beam}$$
$$V_{fixture} = b\cdot h\cdot l$$

Combine the equations and get total weight:

$$W_{tot} = W_{eff} + W$$

Substitution gives the static deflection:

$$\delta = \left(\frac{1}{48}\right)\cdot\left(\frac{W\cdot l^3}{E\cdot I}\right) = \frac{(W + 0.49\cdot b\cdot h\cdot i\cdot\gamma)\cdot l^3}{48\cdot E\cdot\left(\frac{1}{12}\cdot b\cdot h^3\right)} = \frac{(W + 0.49\cdot b\cdot h\cdot i\cdot\gamma)\cdot l^3}{4\cdot E\cdot b\cdot h^3}$$

Too many unkowns present, so eliminate variables to solve for required height:

Static defelctoin: $Fn = \frac{1}{2\pi}\cdot\sqrt{\frac{g}{\delta}}$ Solving for Delta: $\delta = \frac{g}{4\cdot\pi^2\cdot Fn^2}$

Setting the two equations equal to each other:

$$\frac{g}{4\cdot\pi^2\cdot Fn^2} = \frac{(W + 0.49\cdot b\cdot h\cdot i\cdot\gamma)\cdot l^3}{4\cdot E\cdot b\cdot h^3}$$

Simplifying and regrouping exposes a cubic polynomial:

$$E\cdot b\cdot g\cdot h^3 - 0.49\cdot\pi^2\cdot Fn^2\cdot b\cdot h\cdot l^4\cdot\gamma - \pi^2\cdot Fn^2\cdot W\cdot l^3 = 0$$

Note: Now the equations contain two unkown variables, E (modulus of elasticity) and h (height). E is known for aluminum, therefore h is what remains to be unsolved.

Let h = x

$$p(x) = (E\cdot b\cdot g\cdot x)^3 - 0.49\cdot\pi^2\cdot Fn^2\cdot b\cdot l^4\cdot\gamma\, x - \pi^2\cdot Fn^2\cdot W\cdot l^3$$

$p(x) := 7.72\cdot x^3 - 3.91x - 68.2$ Reducing terms

$$v := p(x)\ \text{coeffs} \rightarrow \begin{pmatrix} -68.2 \\ -3.91 \\ 0 \\ 7.72 \end{pmatrix} \qquad r := \text{polyroots}(v)$$

$$r^T = (-1.074 - 1.72i \quad -1.074 + 1.72i \quad 2.149)$$

The graph of the polynomial p(x) and its roots are shown:

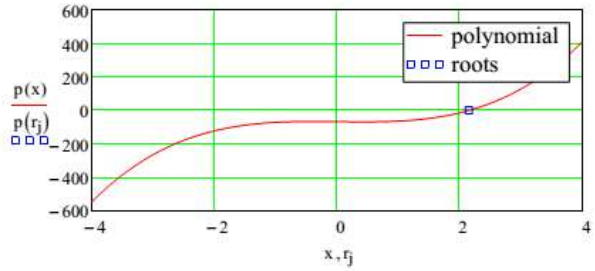

Note: Where the line passes the y-axis (the dot) shows the optimal height for the fixture. Thus, for an aluminum bar measuring 2 X 2 X 15 inches (bredth X height X length) satisfies the 2000Hz requirement using the minimum fasteners available(the two outside fasteners).

If all fasteners are used, the stiffness will be greater.

Stress in the beam

$$\sigma = \frac{M \cdot c}{I} = \frac{3 \cdot F \cdot l}{2 \cdot b \cdot h^3}$$

Where:

$M = \frac{F \cdot l}{4}$ Bending Moment

$c = \frac{h}{2}$ Distance from neutral axis

$I = \frac{1}{12} \cdot b \cdot h^3$ Moment of inertia

Dynamic force at calculated G's: [4][10]

Where:

$h := 2\text{in}$ 2 in is chosen for height becasue it is the closest standard size of aluminum to purchase.

$W_{tot} := W + 0.49 \cdot b \cdot h \cdot l \cdot \gamma$ Total Weight (weight of test object + weight of fixture)

$F := 2200\text{lbf}$ Shaker generated force rating

$W_{arm} := 22\text{lbf}$ Weight of shaker table aramture assmebly

$W_{sum} := W_{tot} + W_{arm}$ weight of moving components: armature+wt of test fixtrue+wt of test item

$G_{input} := \frac{F}{2 \cdot W_{sum}} = 43.49$ Gravitational acceleration mulitplier (peak-to-peak) *note: should be lower than shaker rating*

$G_{input} \cdot g = 16790.973 \cdot \frac{\text{in}}{\text{s}^2}$ Gravitational acceleration produced by shaker table (peak-to-peak)

$F_{dyn} := G_{input} \cdot W_{tot}$ $F_{dyn} = 143.221 \cdot \text{lbf}$

Therefore, the calculated stess is:

$$\sigma_{calc} := \frac{3 \cdot F_{dyn} \cdot l}{2 \cdot b \cdot h^2} \qquad \sigma_{calc} = 322.247\,\text{psi}$$

Note: The stress should be low.

The yeild strength of 6061-T6 Aluminum is 42,000psi, leaving a factor of safety to be very large (shown below):

$$FS := \frac{42000\text{psi}}{\sigma_{calc}} \qquad FS = 130.335$$

Vibraiton Fixture Estimated Frequency of Shaker Head UP/DWN: Values and equations are referenced from *Machine Design for Product Reliability course.*

Preliminary:
Bolts are assumed to be simply supported at the shaker tables bolt circle.
Beam/Plate has simply supported edges.

Find:
Lowest natural frequency expected

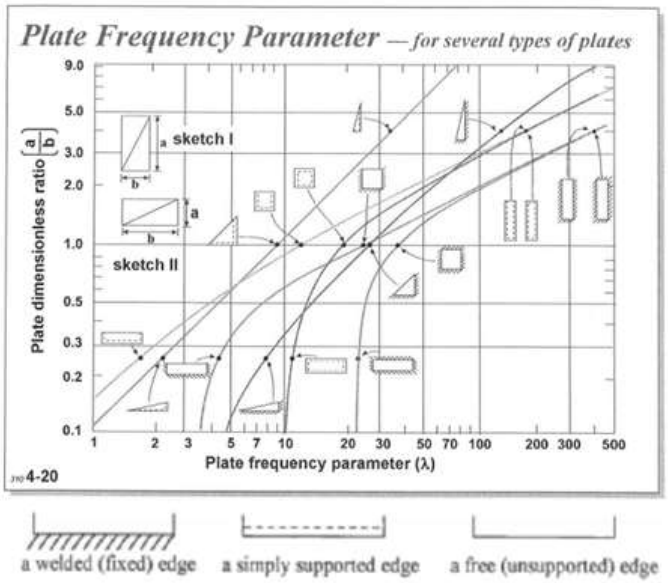

Table 4-20 from *Machine Design for Product Reliability*

$t := 2$ Thickness (in)

$a := \frac{15}{2}$ Lenght of fixture, divided by 2 (in)

$\lambda := 14Hz$ Plate Frequency Parameters

$b := \frac{12}{2}$ Width between outermost fasteners, divided by 2 (in)

$\frac{b}{a} = 0.8$ Plate Dimensionless ratio

Plate Resonant Frequency:

$$f_{n\_Plate\_freq} := 9.65 \cdot 10^3 \cdot \frac{\lambda \cdot t}{a^2}$$

$f_{n\_Plate\_freq} = 4803.556 \cdot Hz$

Note: Assumes bottom face of fixture is entirely touching the shaker table.

Preliminary Determination of Deflection in Loaded fixture:

- Values and equations are referenced from *Machine Design for Product Reliability course.*

Note: 1) does not include the weight of the fixture.
2) simply supported using fasteners

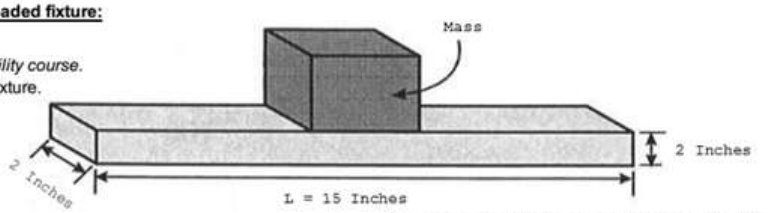

Figure from *Machine Design for Product Reliability*

$m := .097lbf$ Mass of test item

$l := 15in$ Length

$h := 2in$ Thickness of fixtrue

$b := 2in$ Width of fixture

Material Properties: Aluminum

$E := 10.2 \cdot 10^6 \frac{lbf}{in^2}$ Youngs Mod.

Static Deflection of Beam:

$I := \frac{1}{12} \cdot b \cdot h^3$ $I = 1.333 \cdot in^4$ Moment of Inertia

$\delta := \frac{m \cdot l^3}{48 \cdot E \cdot I}$ $\delta = 5.01494 \times 10^{-7} \cdot in$ Static Deflection

Resonant Frequency of combined with fixture:

$$f_{n\_beam} := \frac{3.13 \frac{\sqrt{in}}{s}}{1.2\sqrt{\delta}}$$

$f_{n\_beam} = 3683.243 \cdot Hz$

Note: Mounted on each bolt surface on shaker head. (Acts as pendulum at first mode.) "2" is a factorial ratio

$$f_{n\_beam} := \frac{3.13 \frac{\sqrt{in}}{s}}{\sqrt{\delta}}$$

$f_{n\_beam} = 4419.892 \cdot Hz$

Note: Mounted on flat surface.

Maximum Deflection Load:

$G_{input} = 43.49$ Input accel.

$Q := 30$ Resonant Magnification

$$\delta_{MAX} := \frac{386 \frac{in}{s^2} \cdot G_{input} \cdot Q}{(2 \cdot \pi)^2 \cdot f_{n\_beam}^2}$$

$\delta_{MAX} = 9.403 \times 10^{-4} \cdot in$

Pound-force that would cause defelction in fixture:

Rearange Static Defelection equation...

$$F := \frac{48 \cdot E \cdot I \cdot \delta_{MAX}}{l^3}$$

$F = 181.879 \cdot lbf$

Pound-force that would cause defelction in fixture:

Rearange Static Defelection equation...

$$F := \frac{48 \cdot E \cdot I \cdot \delta_{MAX}}{l^3} \qquad F = 126.305 \cdot lbf$$

BOLT CONNECTION: Values and equations are referenced from *Machine Design for Product Reliability course.*

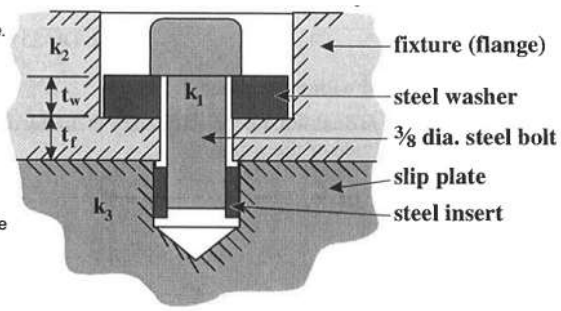

Figure from *Machine Design for Product Reliability course*

To determin the correct bolt diameter:

$m_{load} := 20lbf$ Est.load that is being tested

$a_{gs} := G_{input}$ Max acceleration (in g's)

$N := 5$ Number of bolts used

$F := m_{load} \cdot a_{gs}$ $F = 869.799 \cdot lbf$ Load **ONE** bolt will experience

F is divided by N to match the number of bolts in the bolt pattern:

$$F_{per\_bolt} := \frac{F}{N} \qquad F_{per\_bolt} = 173.96 \cdot lbf$$

Are the bolts stiffer than material being clamped?

IF YES...

Total bolt load force = pre-load + external load

Therefore, choosing 3/8-16 SHCS (commonly used to bolt to shaker table):

$F_{rated} := 9300lbf$ Rated force bolt can handle in tension [4]

$F_{preload} := 7533lbf$ Pre- load at 0.6 yeild [4]

$F_{total\_per\_bolt} := F_{rated} + F_{preload}$ $F_{total\_per\_bolt} = 16833 \cdot lbf$

Note:
Comparing this value with the bolt's rated force value, it shows a 3/8-16 bolt can withstand the force per bolt requirement of 3333.33 lbf.

Joint : Determine the area of fixtrue material required to prevent crushing, the diameter of the load washer and the thickness of the washer, when a 3/8-16 steel bolt is used in 6061-T6 alumin alloy plate. Values and equations are referenced from *Machine Design for Product Reliability course.*

Area of Fixture:

$F_{yeild} := 12555lbf$ Preload of 3/8 bolt at yeild

$C_1 := .8$ Aditional dynamic load factor for Aluminum

$\sigma_{cy} := 35ksi$ compression yeild for Aluminum

$$A := \frac{F_{yeild}}{C_1 \cdot \sigma_{cy}} \qquad A = 0.448 \cdot in^2$$

Outer Diameter of Loaded Washer:

$d := .466in$ Inner Diameter of hole in fixture material (d is sized to provide a press fit for washer flange)

$$D := \sqrt{\frac{4}{\pi} \cdot (A) + d^2} \qquad D = 0.888 \cdot in$$

Note: Used 7/8 diameter stainless steel rod because it was easier to purchase.

Thickness of Washer

$d_{bolt\_dia} := .375in$ Bolt Shank Diameter for 3/8-16 bolt

$d_l := d_{bolt\_dia} \cdot 1.33$ $d_l = 0.499 \cdot in$ Effective bolt head diameter. (Its an accepted common assumption that the outer diameter of the bolt head is 1.33 times the shank diameter.)

$$t_w := \frac{D - d_l}{2} \cdot \tan(60deg) \qquad t_w = 0.337 \cdot in$$

Required Thickness of washer. Rounded up to .340 inches to make machining easier.

Key Insert Pullout load from 6061-T6 Aluminum for one bolt:

$F_{su} := 27ksi$ Ultimate Shear Strength for Aluminum [8]

$INS\_ENG_{250} := .284in^2$ Shear engagement area of 1/4-20 Insert *(CarrLane [6])*

$K_{allowable\_pullout} := INS\_ENG_{250} \frac{F_{su}}{4}$ $K_{allowable\_pullout} = 1917 \cdot lbf$ **Note:**

Key inserts will hold the allowable loads with a factor of safety of 4, which is a commonly used FS for aerospace work holding systems.

Insure that pre-load torque does not exceed 1917 lbf at the bolt head. The following page is a reference to understanding pre-load torque and fastener stresses. Be advised, creating your own bolt analysis tool is suggested.

Bolt Characteristics Solver: Torque allowable for key inserts before pullout (red circle). Most likely only 10 ft-lb or less will be necessary.

Description	Sym	Equation	Value	Units	Input	Override	Output
Nominal Bolt Diameter / Grip	D		*0.4375*	in	*0.75*	L Grip in	
Pitch / Modulus	n	0.0714	*14*	thds/in	*29,000,000*	E psi	
Strength of bolt - Ftu	P_m	***SHCS-Stl-ASTM A574 <1/2***	*180000*	psi	*153000*	Yield psi	Pry Factor
Factor of Safety / Percent of Strength		FSu	*3*	*42.7%*	*2*	FS_y	1.5
			µ max	**µ mean**	µ min	**σ sigma**	
Friction - Mean / Friction Variance	µ	***Dry, No Lube***	0.414	*0.278*	0.142	*0.0454*	
Friction Coefficient Collar	Kc		0.234	0.157	0.080		
Friction Coefficient Threads	Kt		0.247	0.173	0.100		
K value T=K*D*P	K	Kt + Kc	0.480	0.329	0.180		
Pitch Diameter	PD	D-2*.38H	0.391	in			
Minor Diameter - Bolt / Internal Thd	Dm	D-2H+H/6	0.324	in	Di =D-2H	0.360 in	
Height of thread	H	cos 30*1/n	0.062	in	I	0.00090 in^4	
Tensile Stress Area	A	π/4*(D-0.9743/n)^2	0.106	in^2	Dia	0.3679 in	
Shear Load	Ps		***1415***	lbf < <	0	<< Enter Shear Load	
Effective Load	Pe	Bolt Ftu*A/FSu	***1971***	lbf < <	1971	<< Enter Effective Load	
Clamping Load / Preload	P	Pe*1.01 Kmax*P/K Kmax*P/Kmin	***1991***	***2902***	***5310***	lbf	
Torque	Tk	T=K*D*P		***418***	in-lbf +/-	***29***	Tol 7%
		T/12		35	ft-lb +/-	2	
Bolt Stretch - Spring Constant	y	y=P/kb	***0.00169***	in	***4,110,000***	kb AE/L	
Pitch Angle	λ	atan(1/n*πPD)	0.05807	Rad	3.33	Deg	
Half the Thread Angle	b	UN = 60/2	0.52360	Rad	*30.00*	Deg	
Angle of turn of the nut			*9*	Degrees	*7.00E-06*	CTE ΔT °F	*322*
Min Length of Thread Engagement	Le	***AL 6061-T6***		Shear - Fs	*23940*	8*P/5π*Di*Fs	***0.410***
Flange - Material / Properties		***AL 6061-T6***		Ftu	*42000*	psi	
Modulus / Bearing Ult / Shear Ult R4	E_c		*10,100,000*	Fbru=1.5*Ftu	*63000*	Fsu	*23940*
Clearance Hole - Diameter	Da	D*1.06	0.281	< <	0	Actual	
OD Screw Head / Washer	Db	D*1.5	0.65625	< <	0	Thickness Lw	0
Area Under Washer / Bolt Head	Ac	pi*(Db^2-Da^2)/4	0.276	in^2	0.484375	t =(L+Lw+Di2)/2	
Deflection to resist Load P	yc	yc=P/kf	***0.00120***	in	***5,790,000***	kf lbf/in R2	
Area - Shear - Flange	A_T	(Db+Da)/2*π*(L/cos30)	1.275	in^2	1.41	kf/kb	**MS**
Bearing Stress - Under Head		P/Ac	***25149***	psi	6378	A*Pmi/Fsu	***1.505***
Bearing Stress - Hole		Ps/D*Grip	***4311***	psi	18726	PRR	***4.553***
Shear Stress - Flange		P/A_T	***5448***	psi	27296	psi	***3.394***
Bolt Stress - Load µ min * / Tensile Stress	Pt	P+FSy*(Pe/(1+kf/kb)] R3	***6947***	lbf	***65346***	psi	***1.341***
Combined Stress - Mohr's Circle		P/A+√((P/A)^2 +(FSy*Ps/A)^2)			***74812***	psi	***1.045***

Finite Element Analysis Plot if mounted on flat surface:

Mode 1, top view:
4590.8 Hz twist about middle

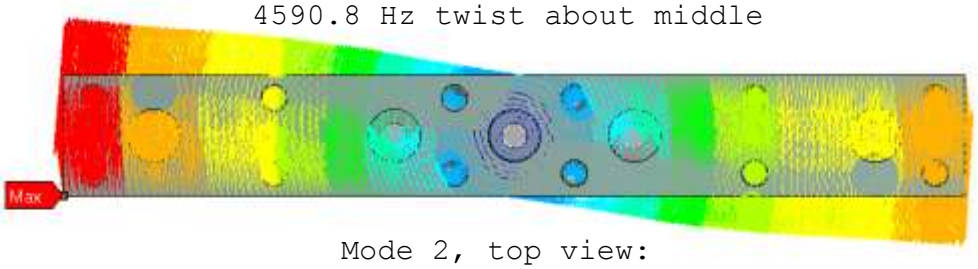

Mode 2, top view:
4737.3 Hz flutter about middle

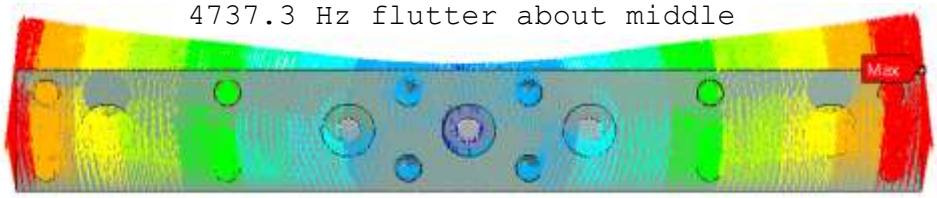

Mode 3, top view:
5217.5 Hz twist about L-R fastener

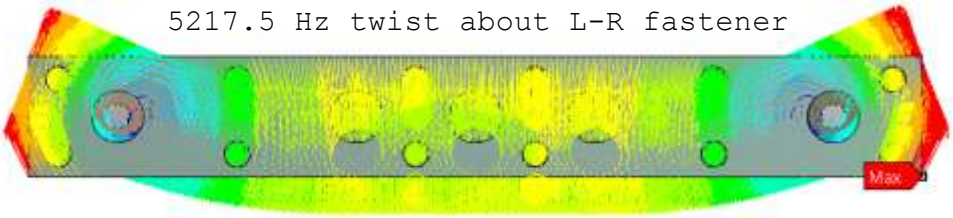

Mode 4, side view:
5363.5 Hz L to R shift with dive

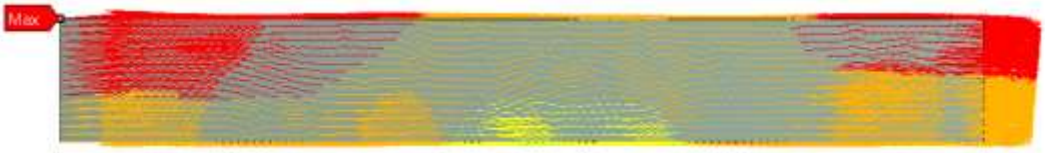

Mode 5, top view:
5564. Hz L to R shift with dive

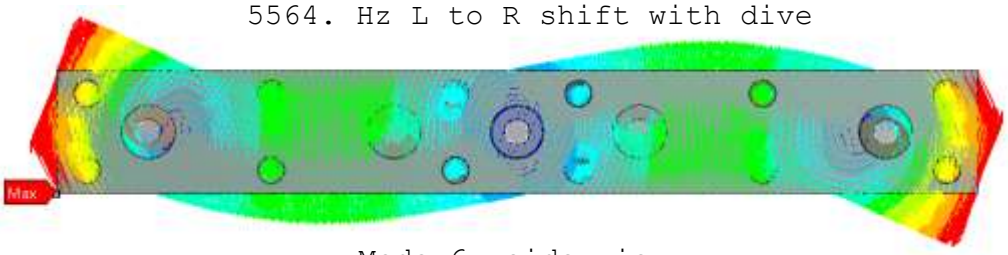

Mode 6, side view:
8044.3 Hz shift inward to outward

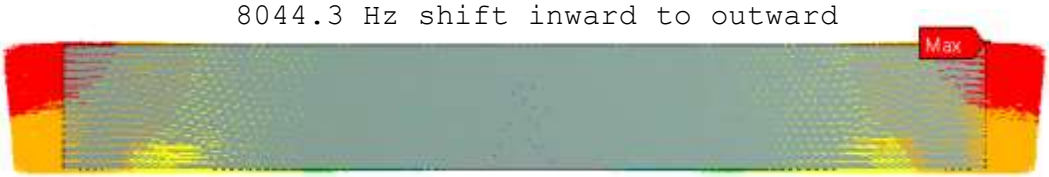

Finite Element Analysis Plot if mounted on shaker head:

Mode 1, side view and 30deg side veiw:
2209.9 Hz roll, fwd and backward

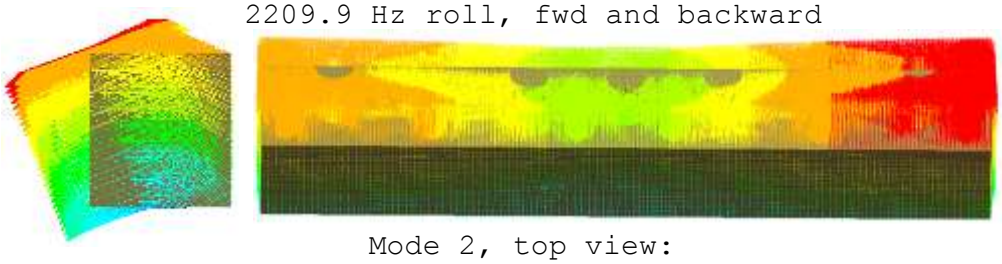

Mode 2, top view:
4166.6 Hz twist about middle

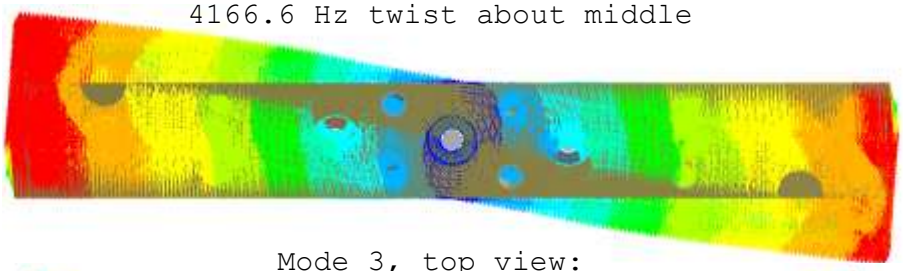

Mode 3, top view:
4834.1 Hz twist about L-R fastener

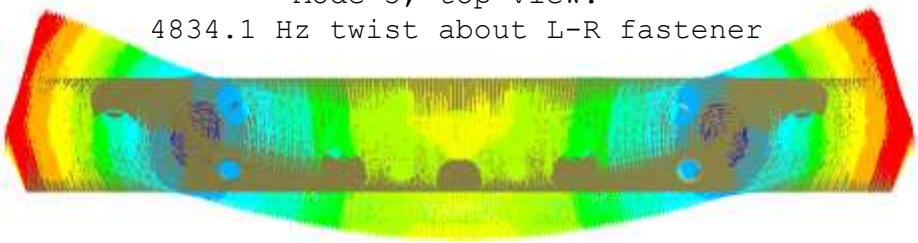

Mode 4, side view:
5271.5 Hz L to R shift

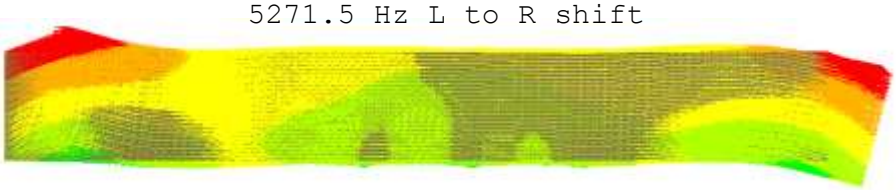

Mode 5, top view:
7376.5 Hz L to R shift with dive

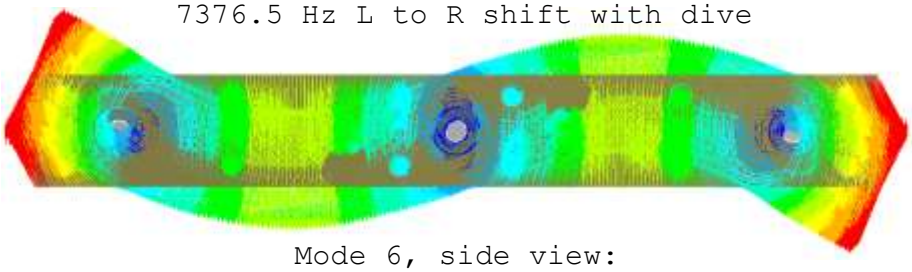

Mode 6, side view:
8044.3 Hz shift inward to outward

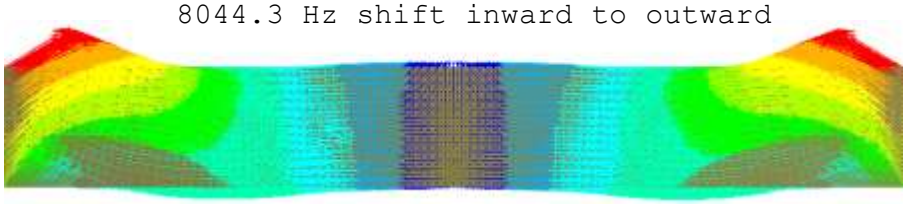

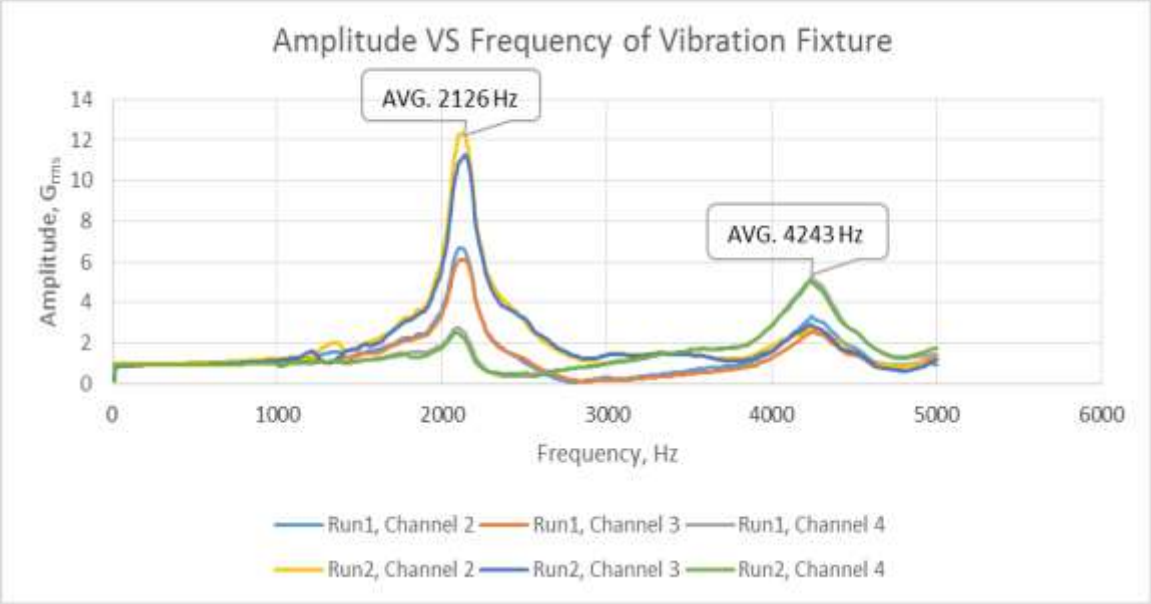

Vibration fixture natural frequency test data when testing on Unholtz-Dickie shaker head vertically, ramped to 5,000 Hz. All data points are overlayed on one graph. The average frequency for each peak is noted. This verifies that which freqencies to avoid when testing composite laminate plates.